ESPOO 2008 VTT PUBLICATIONS 698

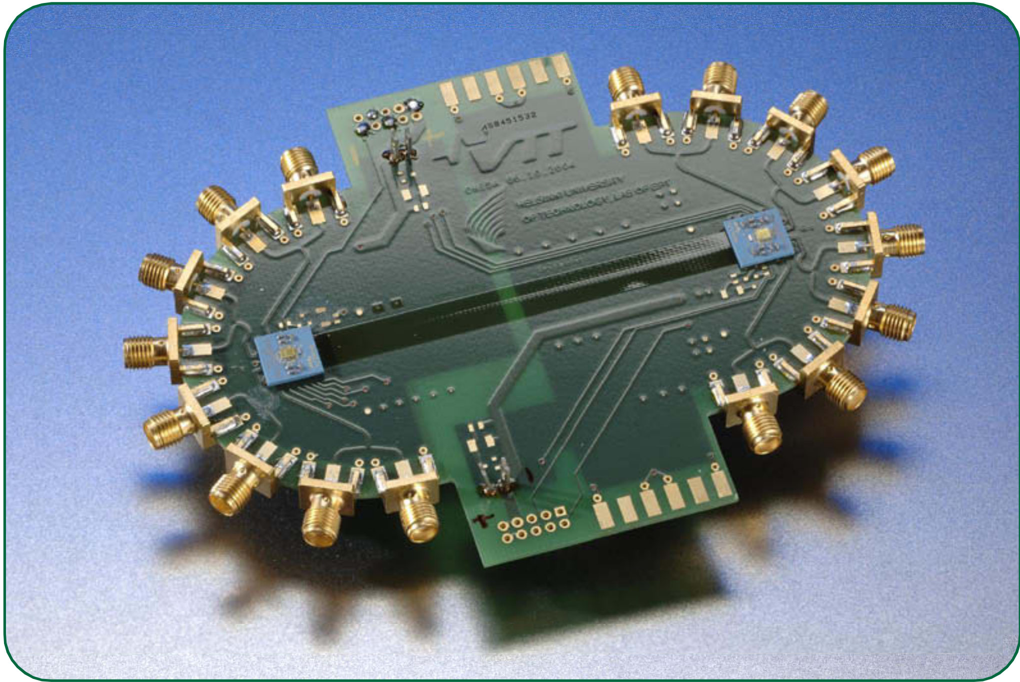

Mikko Karppinen

High bit-rate optical interconnects on printed wiring board

Micro-optics and hybrid integration

Infotech Oulu

VTT

VTT PUBLICATIONS 698

High bit-rate optical interconnects on printed wiring board

Micro-optics and hybrid integration

Mikko Karppinen

Dissertation for the degree of Doctor of Science in Technology to be presented with the assent of the Faculty of Technology, University of Oulu, for public discussion in Raahensali (Auditorium L10), Linnanmaa, on 28th November, 2008, at 12 o'clock noon.

ISBN 978-951-38-7127-7 (soft back ed.)
ISSN 1235-0621 (soft back ed.)

ISBN 978-951-38-7128-4 (URL: http://www.vtt.fi/publications/index.jsp)
ISSN 1455-0849 (URL: http://www.vtt.fi/publications/index.jsp)

Copyright © VTT Technical Research Centre of Finland 2008

JULKAISIJA – UTGIVARE – PUBLISHER

VTT, Vuorimiehentie 5, PL 1000, 02044 VTT
puh. vaihde 020 722 111, faksi 020 722 7001

VTT, Bergsmansvägen 5, PB 1000, 02044 VTT
tel. växel 020 722 111, fax 020 722 7001

VTT Technical Research Centre of Finland, Vuorimiehentie 5, P.O. Box 1000, FI-02044 VTT, Finland
phone internat. +358 20 722 111, fax +358 20 722 7001

VTT, Kaitoväylä 1, PL 1100, 90571 OULU
puh. vaihde 020 722 111, faksi 020 722 2320

VTT, Kaitoväylä 1, PB 1100, 90571 ULEÅBORG
tel. växel 020 722 111, fax 020 722 2320

VTT Technical Research Centre of Finland, Kaitoväylä 1, P.O. Box 1100, FI-90571 OULU, Finland
phone internat. +358 20 722 111, fax +358 20 722 2320

Technical editing Anni Repo

Edita Prima Oy, Helsinki 2008

Karppinen, Mikko. High bit-rate optical interconnects on printed wiring board. Micro-optics and hybrid integration. Espoo 2008. VTT Publications 698. 162 p.

Keywords data transmission, optical interconnects, printed wiring boards, micro-optics, multi-channel optoelectronics, optical transmitters, optical receivers, optical waveguides, microlens arrays, micro-mirrors, LTCC, hybrid integration

Abstract

Optical interconnects are foreseen as a potential solution to improve the performance of data transmission on printed wiring boards (PWB). Optical interconnects carry data signals as modulation of optical intensity, for instance through an optical waveguide, thus replacing traditional electrical interconnects.

The aim of the research work was to study and develop board-level optical interconnection technologies that would be suitable for volume manufacturing with typical electronics production processes, such as surface-mount assembly and board manufacturing. More precisely, the work focuses on the hybrid integration of multi-channel optoelectronics transmitters and receivers, which are equipped with micro-optical structures enabling coupling to board-embedded optical waveguides. The presented integration schemes are based on the use of low-temperature co-fired ceramic (LTCC) circuit boards with high-precision alignment structures.

Two experimental set-ups were designed and implemented to study the feasibility of the proposed integration schemes. The first set-up enabled evaluation of three different kinds of optical coupling schemes, which are based on microlenses, micro-ball lenses and butt-coupling respectively. The other demonstrator is a parallel optical interconnect integrated on a standard PWB. The optical coupling is based on microlens arrays and a micro-mirror, which, together with four polymer multimode waveguides on the PWB, form the interconnections between the surface-mounted 4-channel transmitter and receiver components.

The optical performance of the demonstrated structures is studied by modelling and characterisation. With the proposed improvements, the presented technologies are suitable for implementation of high bit-rate interconnections between ceramic-packaged integrated circuits or multi-chip modules on PWB.

Preface

This thesis is a result of the series of research projects studying and developing optical interconnection technologies at VTT Technical Research Centre of Finland in Oulu. The author became acquainted with the topic in 1998, but already earlier there had been some related work at VTT. This thesis is mainly based on the work and results of the OHIDA project (Optics on future circuit board for high-speed data transmission), which was a joint research project funded by Tekes – the Finnish Funding Agency for Technology and Innovation, industry and VTT, and was carried out between spring 2002 and summer 2005. Other contributing projects were VTT's strategic initiatives OTECO (Optical technologies for wireless communications) during 2000–2002 and MINARES (Key technology action on micro- and nano-technologies) during 2003–2004. Valuable work has been carried out in other projects as well, such as VTT's strategic project OPCO during 1999 and in some contract projects for industry.

I would like to acknowledge my supervisors, Professors Risto Myllylä and Harri Kopola, for their support and guidance. I also thank all those colleagues at VTT whose expertise and contribution have made the presented research work and results possible. I especially wish to emphasise the contribution of Prof. Pentti Karioja, who engaged me in this research topic and whose commitment has enabled and supported me to work on it in several projects, and to emphasise the productive contributions from Mr. Teemu Alajoki to all the experimental work, from Dr. Kari Kataja and Mr. Jukka-Tapani Mäkinen to the optical modelling, from Mr. Kari Kautio to the LTCC technology, and from Mr. Antti Tanskanen to the electrical design.

The fruitful co-operation with several project partners of VTT has been important to the research work as well. Especially, the contribution of Mrs. Marika Immonen and Prof. Jorma Kivilahti at the Helsinki University of Technology was crucial in implementing the presented experimental results.

I am grateful to the Graduate School of Modern Optics and Photonics for supporting my studies. I also acknowledge the Academy of Finland, the Infotech Oulu, the Finnish Cultural Foundation, the Nokia Foundation, and the Tauno Tönning Foundation for financial support during my research career.

Finally, I wish to apologise to my family for all the inconvenience this work has caused them, and express my greatest thanks to Piia for her long-lasting patience.

October 2008, Oulu

Mikko Karppinen

Contents

Abstract ... 3

Preface ... 4

List of abbreviations and symbols ... 9

1. Introduction ... 13
    1.1 Background and motivation ... 13
    1.2 Research problem ... 16
    1.3 Contribution of the thesis ... 19

2. State of the art and challenges ... 21
    2.1 Optical signalling in electronic equipment – history ... 21
    2.2 Evolution of board-level optical interconnects ... 23
        2.2.1 Fibre-based optical interconnects ... 23
        2.2.2 Optical interconnects overlaid on PWB ... 25
        2.2.3 Inter-chip interconnects with board-embedded waveguides ... 25
        2.2.4 Free-space optical interconnects ... 28
    2.3 Component technologies ... 29
        2.3.1 Light sources ... 29
        2.3.2 Characteristics of VCSELs ... 31
        2.3.3 Photodetectors ... 34
        2.3.4 Electronics ... 35
        2.3.5 Optical waveguides on PWB ... 37
        2.3.6 Micro-optical coupling elements ... 39
    2.4 Integration and packaging ... 43
        2.4.1 Optical alignment ... 43
        2.4.2 Hybrid integration ... 43
        2.4.3 Flip-chip bonding assembly ... 44
        2.4.4 LTCC substrates for photonics modules ... 45
    2.5 Conclusions and comparison to electrical interconnects ... 47

3. Design aspects and methodology ... 50
    3.1 System specifications and their implications ... 50
        3.1.1 Optical specifications ... 51

3.1.2 Reliability issues ... 52
3.2 High-speed issues ... 52
3.2.1 Bandwidth of waveguides ... 53
3.2.2 Link power budget ... 54
3.3 Coupling to multimode waveguides ... 55
3.3.1 Basic principles and trade-offs ... 56
3.4 Optical design methodology ... 57
3.4.1 Ray-trace modelling ... 58
3.4.2 Tolerance analysis for optimisation and yield estimation ... 59

4. Optical coupling to waveguides on board – comparison (Case study I) ... 60
4.1 Optical design and analysis ... 60
4.1.1 Butt-coupling scheme ... 60
4.1.2 Coupling with a double microlens array and a mirror ... 61
4.1.3 Coupling with micro-ball-lenses and a mirror ... 62
4.1.4 Comparison of coupling schemes ... 64
4.1.5 Simulation of ball-lens-based interconnect ... 67
4.1.6 Simulation of double microlens array-based interconnect ... 70
4.1.7 Alternative coupling schemes with double microlens array ... 72
4.2 Implementation of test assembly ... 80
4.2.1 Overview of the system ... 80
4.2.2 Electronics design and implementation ... 81
4.2.3 Fabrication of the test assembly ... 83
4.2.4 Optical waveguides ... 84
4.3 Characterisation of butt-coupling ... 86
4.4 Experiments on ball-lens-based coupling optics ... 88
4.4.1 Assembly ... 88
4.4.2 Characterisation of the coupling component ... 89
4.4.3 Characterisation of transmitter-to-waveguide coupling ... 90
4.5 Experiments on microlens-based coupling optics ... 92
4.5.1 Microlens array ... 92
4.5.2 Assembly ... 94
4.5.3 Characterisation of the transmitter ... 96
4.5.4 Characterisation of the coupling efficiency of the receiver ... 99
4.6 Comparison of coupling schemes ... 100

5. Parallel high bit-rate interconnect integrated on board (Case study II) 103
5.1 Overview of the demonstrator 103
5.2 Design 105
5.2.1 Electronics and device selections 105
5.2.2 Optical coupling components and packaging design 107
5.2.3 Optimisation of coupling structure 111
5.2.4 Final tolerance analysis of the implemented structure 113
5.3 Manufacturing of components for demonstrator 114
5.3.1 Module substrate manufacturing and characterisation 114
5.3.2 Board with optical waveguide layers 120
5.3.3 Micro-optical elements 124
5.4 Assembly 126
5.4.1 Assembly of Tx and Rx electronics 126
5.4.2 Assembly of microlens array on LTCC 129
5.4.3 Assembly of micro-optics on O/E-PWB 131
5.4.4 BGA assembly of Tx and Rx modules to O/E-PWB 132
5.5 Characterisation 133
5.5.1 Coupling loss due to the micro-mirror 134
5.5.2 Coupling efficiency and mounting tolerance of Tx module .. 135
5.5.3 Summary of the link budget and mounting tolerances 138
5.5.4 Data transmission performance 139

6. Discussion and recommendations 143

7. Summary and conclusions 147

References 150

List of abbreviations and symbols

List of abbreviations

2D	two-dimensional
3D	three-dimensional
APD	avalanche photodiode
BER	bit error-rate
BGA	ball-grid-array
CML	current mode logic
CMOS	complementary metal-oxide-semiconductor
CTE	coefficient of thermal expansion
DBR	distributed Bragg reflector
DC	direct current
DCA	Digital Communications Analyzer
DFB	distributed feedback (laser diode)
EDC	electronic dispersion compensation
EMC	electromagnetic compatibility
EMI	electromagnetic interference
FP LD	Fabry-Perot laser diode

FR4	Flame Retardant 4 (a PWB base material)
GI	graded-index
HBT	heterostructure bipolar-transistor
IC	integrated circuit
ISI	inter-symbol interference
LAN	local area network
LED	light-emitting diode
LTCC	low-temperature co-fired ceramics
MCM	multi-chip module
MM	multimode
MSM	metal-semiconductor-metal (photodiode)
MT	Mechanical Transfer (fibre ferrule)
NA	numerical aperture
O/E-PWB	optical–electrical printed wiring board
PIN	p-i-n photodiode
PRBS	pseudo-random bit sequences
PWB	printed wiring board
RC-LED	resonance-cavity light-emitting diode
ROC	radius of curvature

RSSI	signal detect output voltage
Rx	receiver
SI	step-index
SMD	surface mountable device
SPA	smart pixel array
TIA	trans-impedance amplifier
VCSEL	vertical-cavity surface-emitting laser (diode)
VLSI	very-large-scale integration
WDM	wavelength division multiplexing
TIR	total internal reflection
Tx	transmitter
UV	ultraviolet

List of symbols

A_f	area (of waveguide core)
A_s	area (of source)
B	brightness (i.e. luminance)
c	speed of light in vacuum
L	length (of waveguide)

n_{clad}	refractive index of waveguide cladding
n_{core}	refractive index of waveguide core
Δt	time delay
Ω_s	solid emission angle (of source)
Ω_f	solid acceptance angle (of waveguide)

1. Introduction

1.1 Background and motivation

Optical interconnection refers to a kind of data transmission in which the data signal is transmitted as a modulation of optical carrier wave (i.e. light) through an optically transparent media, such as an optical fibre, planar optical waveguide or air. Typically, the intensity of the light source, such as a laser diode, is modulated and the transmitted optical signal is converted back to the electrical domain by the use of a photo detector. For comparison, the more conventional electrical interconnect usually transmits data as a modulation of voltage through an electrically conductive media, such as copper wire. Regardless of the term *optical*, almost all optical data links actually function at the near-infrared wavelength range between 800 and 1600 nm.

Often, the use of the term *optical interconnect* is assumed to deal with data transmission inside an electronic device or system – that is, it is typically used when the transmission distance is short. This can be compared to the term *optical communications*, which refers to optical data transmission between distant and independent systems. However, the term optical interconnect is sometimes used when referring to optical communication links as well. Optical communications through fibre has long been the technology of choice for high-speed long-distance data links. Gradually, as the capacity requirements have increased, the optical links have emerged into shorter distance applications, such as fibre-to-the-home, local area network (LAN), and even into fibre-optic interconnects between boards and cabinets inside electronic equipment – i.e. into what are to be referred as 'optical interconnects' in this thesis. It is predicted that this trend will continue and, eventually, optics will perhaps be used to interconnect integrated circuits (IC) on a board or even to be used in intra-chip interconnects. That is, electrical interconnects, which have dominated since the infancy of electronics, are likely to be replaced with optical interconnects in some cases. Although there is no thorough distinction between the terms optical communications and optical interconnects, this thesis is clearly about the latter. This is because the technologies to be discussed are intended for relatively short-distance interconnections – less than 1 meter – and only to be used inside electronic equipment.

In general, the interest in studying and promoting optical interconnects to be used inside electronic equipment arises from the great challenges met when trying to further improve the performance of today's electrical interconnects. This happens due to the physical obstacles of the copper-based signal transmission, which typically uses striplines on a printed wiring board (PWB). These obstacles may result in a situation in which the performance of the whole system becomes limited by the interconnect capacity – a situation often called 'interconnection bottleneck'. An example of such a case is illustrated in Figure 1, which compares the development of the processor clock rate to the clock rate of the interconnection between the processor and the memory. The off-chip I/O capacity is more and more lacking the internal performance of the IC.

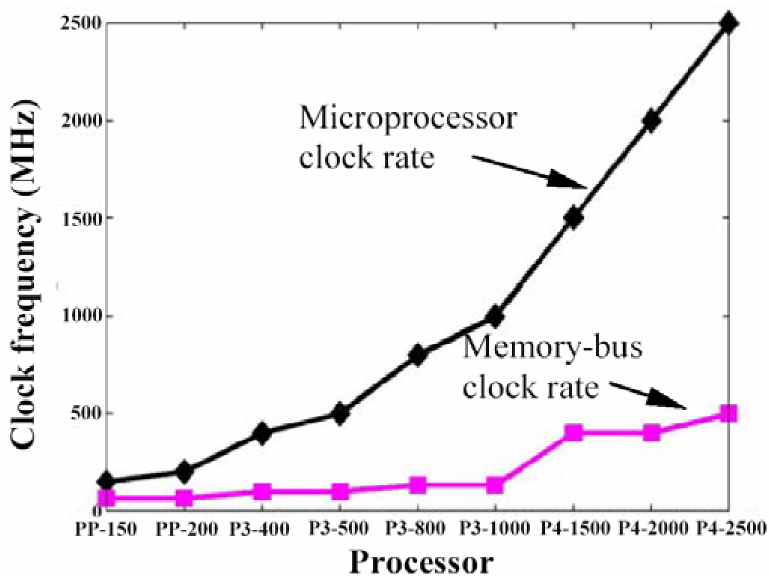

Figure 1. Comparison of clock frequencies of Intel Pentium processor ICs and their memory buses (iNEMI 2004).

Copper-based electrical interconnects are facing plenty of challenges. The high-speed signals can be distorted due to dispersion, reflections and ringing, as well as attenuation and its variation with frequency. The high attenuation of high-frequency signals results in a need to use high-power line-drivers, thus causing thermal management issues. Electromagnetic interference (EMI) causes noise and design constraints due to the need to fulfil electromagnetic compatibility

(EMC) specifications. Moreover, the performance of parallel links is limited by the crosstalk due to coupling from neighbouring traces and the signal skew caused by variations in the delay between different signal traces.

Optical interconnects, on the other hand, can have many advantages over conventional electrical interconnects, thus making it easier to achieve and maintain good signal integrity. These include lower signal dispersion, distortion, lower attenuation, lower skew and easier impedance matching of transmission lines, as well as immunity of the signal path to EMI. The latter enables reduced signal crosstalk, easier EMC design and the possibility for higher interconnection density in parallel links. Furthermore, an optical interconnect can be seen as an architectural enabler: for instance, the low attenuation of the high-speed signal path would allow placing the processor and memory farther from each other. The value of the aforementioned advantages, of course, depends on the application and all other constraints involved in the design and implementation of the system. The fundamental physical reasons for favouring optical interconnects over electrical ones are summarised, for instance, in Miller (1997).

Despite the significant progress achieved in the intensive research carried out by many groups worldwide, optical interconnects are not much used inside commercially available electronics products. Only fibre-based interconnects are in use to some extent. One reason is perhaps that the introduction of optical interconnects would represent a significant technological step in the design and production of electronic equipment. Such a step would require a major R&D investment from the industry. In addition, the historical aspect plays an important role. Even if optical interconnects were to demonstrate superior performance over the electronic alternative, technology transfer is not necessarily guaranteed due to the fact that the experience with materials, design procedures and manufacturing processes of electronic interconnects is well known and established. The logical conclusion is that in order to ease transfer to a novel technology with the high bit-rate optical interconnects, the needed technological step should be made as small as possible – in other words, the novel technology has to be developed based on existing technology instead of developing a completely new one. Consequently, on board-level interconnects, the technologies should be made compatible with the conventional circuit board processes and assembling practices. Moreover, there are at least two obvious prerequisites for the introduction of optical interconnects in commercial

applications: the costs per interconnect capacity should be competitive with copper-based ones in mass-production, and the required PWB area or volume may not exceed that of equivalent copper solutions.

1.2 Research problem

The aim of the research work presented in this thesis was to study novel technologies to enable implementation of high bit-rate optical interconnects on the board level. The technologies developed were targeted to be compatible with manufacturing processes and assembly technologies that are already in use in the electronics production industry. This was to ease the potential adoption of the developed interconnection technologies into commercial products.

In addition to the above-mentioned application oriented targets, the research work had more general objectives to study the design and implementation technologies for hybrid integration of micro-optics and photonics with electronics. Hybrid integration using multi-layer ceramic substrate technology – more precisely, low-temperature co-fired ceramics (LTCC) – was especially studied.

To give a more general picture of the research problem, a structure of a typical optical data link is illustrated in Figure 2. The electrical signal is converted into optical using a source, usually a laser diode, which is modulated with a current source. As an alternative to a directly modulated source, one can use an external optical modulator together with a continuous-wave source, which is common in high-speed long-haul optical communications. The light is coupled to the receiver through an optical medium, where a receiver converts the optical modulation back to electrical form using a detector, typically a photodiode, and a preamplifier, such as a trans-impedance amplifier (TIA). Often, there is also some digital pre- and post-processing of the transmitted data: binary data may be coded for the optical transmission, for instance, to avoid many consecutive ‘zeros’ or ‘ones’; a parallel data stream may be serialised into one optical channel; and the clock signal is often carried within the data and may need to be extracted.

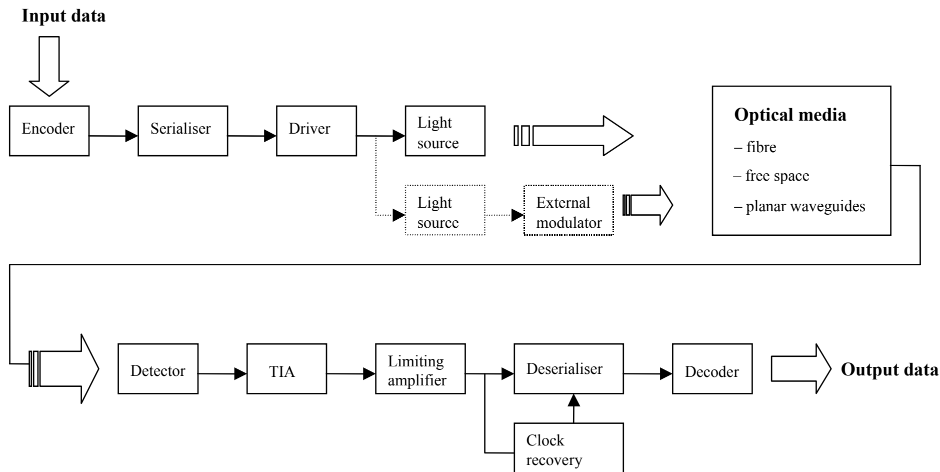

Figure 2. Schematic block diagram of an optical data link.

Interconnections are often classified using the international packaging level hierarchy (Tummala & Rymaszevski 1989), which is based on the type of interconnected components and their typical interconnection distances as follows:

0.	Chip level (intra-chip)	0...10 mm
1.	Multi-chip-module level (intra-MCM or chip-to-chip)	1...100 mm
2.	Board level (MCM-to-MCM or chip-to-chip)	10...300 mm
3.	Backplane level (board-to-board)	0.1...1 m
4.	Cabinet level (rack-to-rack)	0.3...5 m
5.	System level (cabinet-to-cabinet)	1...100 m.

In this thesis, the emphasised technology is the board-level interconnect (Level 2). The primary target is to interconnect at the PWB level using optical waveguides, which are potentially polymer-based and integrated into optical layers of PWB. Most of the work is useful for backplane interconnections (Level 3) as well, although board-to-board connectors, i.e. optical coupling between waveguides on different boards, are not addressed at all. In this thesis, these targets are approached by studying the lower level packaging technologies, especially module level packaging (Level 1).

Perhaps the most attractive optical solution proposed to overcome the interconnection bottleneck at the board and module level is the interconnection based on low-loss integrated waveguides (Chen et al. 2000, Krabe et al. 2000). This stripline-like optical waveguide approach with polymer waveguides embedded into the board as additional optical layers has a potential to fulfil the compatibility requirements of the existing PWB technology. The resulting hybrid optical–electrical printed wiring board (O/E-PWB) concept is illustrated in Figure 3. Such optical channels could also enable design techniques analogous to the ones used for wiring electrical signals on the board. In particular, PWBs made of conventional low-performance base materials, such as FR4 (Flame Retardant 4 – the most common PWB base material), are seen as the most attractive substrates for the O/E-PWB technology. This would enable equipping the low-cost, widely used technology basis with very high-speed interconnects.

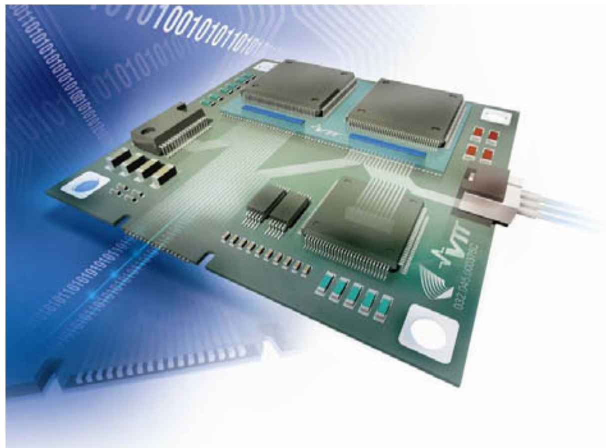

Figure 3. A vision of an optical–electrical printed wiring board.

One of the biggest challenges hindering the introduction of optical interconnects at the board level is the need to implement a feasible and reliable optical coupling between the optoelectronic transmitter/receiver and the optical waveguide. High coupling efficiency is required due to the rather limited loss budget (typically around 10…15 dB) of the high bit-rate transceivers based on VCSEL (vertical-cavity surface-emitting laser) diodes – a technology enabling high density integration. On the other hand, to achieve compatibility with conventional electronics manufacturing processes, all components (including optical ones) should be suitable for surface mounting or bare-die mounting

procedures and all materials should withstand the reflow soldering temperatures. Consequently, it is not suitable to use the so-called ‘active alignment’ technique, which is common in the manufacturing of fibre-optic modules and means that the optical power is monitored during the assembly to maximise the coupling efficiency; instead, ‘passive optical alignment’ is required.

The scope of this thesis is limited to the hardware-related physical layer technologies of the interconnections. The research presented is mainly based on the experimental case studies where an essential role is given to the design studies using optical modelling techniques, implementation studies using electronics production technologies, and characterisation studies using laboratory set-ups. More precisely, the thesis mainly deals with the design and implementation issues of hybrid integration and packaging. The presented work mostly concerns the module level (Level 1) packaging, but some board assembly and manufacturing (Level 2) issues are also included and the main targets are defined by the board interconnect (Level 2) challenges. The design and characterisation of micro-optical coupling structures have an important role as well. However, the fabrication of micro-optical components and optical waveguides are only commented on to the extent necessary from the point of view of integration. The manufacturing of electronic or optoelectronic devices is not studied. The modulation method and level of the optical signal is mentioned, but otherwise the electronic interfaces are only commented on very briefly considering the logic levels. No protocol or coding issues on the physical layer or on the higher levels of the data link are studied, or discussed.

1.3 Contribution of the thesis

This thesis demonstrates that the presented set of design, processing and packaging technologies enable the implementation of optoelectronic transmitters and receivers for high bit-rate, short-range optical interconnects. In particular, they are suitable for board-level interconnects based on planar optical waveguides as an interconnection medium.

The thesis especially provides evidence that LTCC substrate technology and surface mounting can be utilised for implementing transmitter and receiver modules with optical alignment between the optoelectronic devices and the

optical media. To the author's knowledge, no similar kind of coupling structure based on the via holes on the LTCC substrate and the use of top-emitting flip-chip-bonded VCSEL devices has been presented before. From a more general perspective, there are only a small number of publications where waveguide-based optical interconnections between surface-mounted components or modules have been studied experimentally. This thesis also demonstrates and analyses optical coupling structures not previously presented in the same kind of application: coupling based on micro-ball lenses and beam deflection using discrete micro-mirror components.

As a conclusion, the thesis presents some pros and cons of the different kinds of technologies studied. The feasibility and performance of the presented technologies are analysed both by simulating the optical and opto-mechanical systems and by characterising the implemented systems.

In addition to optical interconnection applications, the work provides novel information that is more generally applicable to the integration of micro-optics and optoelectronics in electronics components and sub-systems. This includes information on the capabilities and limitations of LTCC technology in the integration process.

Papers presented in the thesis and published or jointly published by the author are Karppinen et al. (2004a, 2004b, 2006a, 2006b, 2007), Immonen et al. (2005b, 2007), Karioja et al. (2006), and Keränen et al. (2005).

The author has also published or contributed to several other papers, which either have some overlap with this thesis work or some impact on it through a closely related topic. These include Karppinen et al. (2000, 2001a, 2001b, 2002), Alajoki et al. (2007), Guo et al. (2005), Heikkinen et al. (2007), Immonen et al. (2003, 2005c), Keränen et al. (2004), and Vervaeke et al. (2006).

2. State of the art and challenges

In this chapter, the status of the research and development on optical interconnects is briefly reviewed. The emphasis is on the technologies that are closely related to the work presented in this thesis. First, the founding of optical interconnects is summarised, showing the historical perspective. Next, the state of the art and some future prospects for the technology are illustrated, including device and packaging technologies as well as the system demonstrations. The focus is on the board-level chip-to-chip interconnection technologies. The purpose is also to specify the challenges and the gap in the existing knowledge in order to prove the novelty of the work to be presented in the thesis. Finally, the state of the art of the electronic interconnects are briefly described and compared to optical solutions.

2.1 Optical signalling in electronic equipment – history

The use of an optical carrier for interconnecting two ICs inside electronic equipment was suggested by Gilleo and Last (1963) from Amelco Semiconductor (today Teledyne Semiconductor). They demonstrated optical signal transmission between two p-n junctions, a LED and a photodiode, using a glass-based rod as a light guide. The paper also discussed the issues of device selection, optical coupling, optical media and hybrid and monolithic integration – all of which are still under active research. It is interesting to cite the commentary remark given in the paper:

> "GIANT STEP? Reliability, simplicity and economy can all be expected from better methods of interconnecting microcircuit groups. The method described in this article has been only a topic of conversation until recently. Now that optical interconnection has been accomplished it has nowhere to go but in the direction of further improvement and refinement. Understanding the problem and utilizing recent discoveries has produced a successful experiment. It looks more like a quantum jump than an incremental advance."

After more than 40 years, it is easy to notice that the prediction about "quantum jump" has not yet come true. However, the sentences are worth consideration,

especially if one knows that they were written by an outstanding pioneer of microelectronics: Dr. Jay T. Last had co-founded Fairchild Semiconductor, where he had directed the development work resulting in the commercialisation of the first digital ICs in 1961, which began the success of the silicon IC technology.

Although the optical interconnects did not appear in microcircuit applications, the development of optoelectronics devices had started and many other applications were presented – for instance, the optical-electrical-optical conversion appeared useful in electronics circuits in the form of an optocoupler (Biard et al. 1964). Moreover, the age of optical data transmission had begun. Soon, the emergence of optical fibres and semiconductor laser diodes boosted the research and development on the optical data transmission technologies. Thanks to the very low attenuation and huge bandwidth of optical fibre, it was rapidly found to be a superlative technology to enable high bit-rate long-haul communications. During the 80s and 90s, the development of wavelength division multiplexing (WDM) technology overcame the bandwidth limitation of the transceiver electronics and, thus, better exploited the huge data transmission capacity of a fibre. Consequently, fibre-optic data links have become the enabling technology, onto which the whole global Internet is constructed. Optoelectronics have also become a common technology in many other application areas.

Although most of the research work on photonic data transmission-related technologies has targeted communications applications, there has been continuous interest in optical interconnects inside electronic equipment as well. The topic started to become more popular in the late 80s after the paper by Goodman et al. (1984) that discussed the potential of optical interconnects in modern VLSI (very-large-scale integration) systems. Today, a search of the Inspec bibliographic database (by Institution of Electrical Engineers) with the key word “optical interconnect” for subject, title or abstract of a publication results in more than twelve thousand matches, of which almost five thousand are journal articles (whereas a search for “optical communication” results in more than 65 thousand matches).

2.2 Evolution of board-level optical interconnects

Here, the different kinds of optical interconnection solutions proposed, demonstrated or produced for applications, where the dominant interconnection technology is laminate-based PWB, are reviewed.

Since the benefits of optical interconnects increase with increasing interconnection length, it is obvious that the backplanes, i.e. typically large boards interconnecting daughterboards, are seen as the most attractive application for board-level optical interconnects. The existing and proposed *optical backplane* solutions are often classified into “three generations”: fibre-based interconnects, interconnects based on fibre laminates and/or shuffles, and board-integrated optical channels. The latter solution can be further classified into several sub-categories, from overlaid optical pathways to board-embedded waveguides, as will be described in the following sections. All the above-mentioned interconnects are based on a guided-wave optical transmission. In addition, there is also a fourth category, the free-space optical interconnects, which will be introduced in Section 2.2.4. It is the media and structure of the optical path, i.e. the opto-mechanical packaging solution, in which the categories differ from each other. On the other hand, the optoelectronics devices and electronics circuitry of the transmitters and receivers used are essentially of a similar kind in all categories.

2.2.1 Fibre-based optical interconnects

Today, fibre-optic data links are used inside electronic systems to interconnect between backplanes, racks and cabinets. That is, at longer distances than the backplane level, the optical alternative to conventional interconnects is to replace copper cables with fibres. In addition to high transmission capability and reduced EMI issues, the advantage of fibre is its lightness compared to bulky and heavy high-bandwidth electrical cables. Similar kinds of fibre-based links can also be used to interconnect daughterboards in electronic equipment – that is, to form a kind of optical backplane with high bit-rate point-to-point links.

Parallel optical links based on fibre-ribbon cables allow very high aggregate data rates with a relatively high integration level, thanks to multi-channel transmitters and receivers. The highest integration level is achieved with transmitters based

on VCSEL sources, mainly thanks to their low power consumption with high-speed direct modulation. Graded-index multimode (GI MM) fibre technology is favoured because it allows high enough bandwidth for short-distance interconnects and the module technology is cheaper to implement than single-mode fibres due to the easier optical alignment. Using industry-standard fibre-ribbon cables and multi-fibre connectors, typically with an MT (Mechanical Transfer) ferrule, as well as VCSEL and PIN photodiode arrays, commercially feasible multi-channel data links can be implemented with very high aggregate data rates. Typically, 12 parallel optical channels are used, and data links have been presented with channel bit-rates up to 10 Gb/s (Kuchta et al. 2004). Even higher channel counts are possible using 2D VCSEL arrays and 2D fibre-ribbon connectors – for instance, a 36-channel parallel optical link with a 3.3 Gb/s/channel rate has been demonstrated (Cook et al. 2003). In optical backplane systems, flexible fibre laminates and optical shuffle components are utilized in order to handle several fibres and fibre ribbons in a narrow space, as well as to ease implementation of cross-connections.

Polymer fibres allow a much smaller bending radius than silica fibre. Thus they have been proposed and demonstrated to be used as optical backplanes or intra-board interconnects – for instance, a fibre-ribbon concept for parallel chip-to-chip interconnects is presented in Wittmann et al. (1999) and Steenberge et al. (2004). Furthermore, it is also possible to embed MM silica fibres into an FR4 PWB to form intra-board optical interconnects (Schneider & Kühner 2006), as illustrated in Figure 4. Silica fibres provide negligible attenuation and high reliability; however, the cleaving of embedded fibres is difficult.

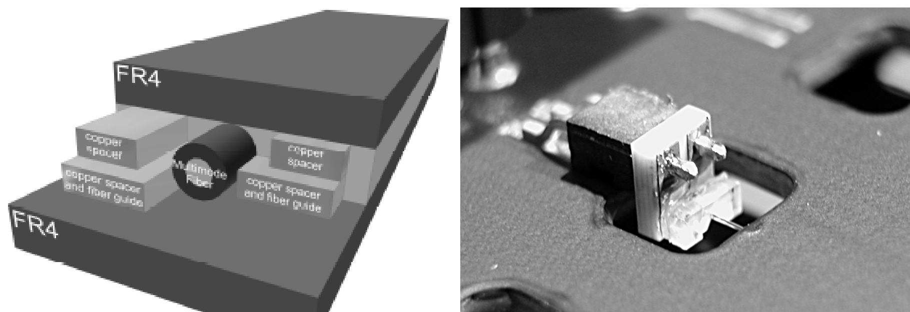

Figure 4. Board-embedded glass fibre concept for board-level interconnects (Kühner & Schneider 2007): left) cross-section of PWB with embedded fibre; right) coupling element mounted on PWB embedded fibre.

Nevertheless, fibre-optic links are unattractive for board-level interconnects due to the fact that the packaging density is limited due to the fibre connectors/pigtails, the bend radius of the fibres is limited, and system assembly is not easily automated. In addition, fibres cannot exploit the planar fabrication technologies that are utilised to reduce packaging costs in electronics manufacturing. To conclude, higher integration density is probably needed before optical interconnects may become widely used in board-level and shorter interconnects.

2.2.2 Optical interconnects overlaid on PWB

Various technologies have been studied to implement board-level interconnects using some kind of separate optical pathway component that is placed and used in parallel with the electronics PWB or perhaps overlaid on it. The component can be an optical plate or sheet including beam steering refractive or diffractive elements. For instance, an optical backplane bus demonstrator with a holographic plate was presented in Kim et al. (2000). (Such a plate is not clearly a guided-wave component and thus the system could also be categorised as a free-space interconnect.) Another kind of pathway component widely proposed is a foil with integrated optical waveguides. An example is the polymer foil technology with integrated waveguides that was used in the overlaid configuration to demonstrate a fully assembled optical backplane system (Liu et al. 1996). A major benefit of a separate optical pathway component is that it does not need to be compatible with all the PWB manufacturing and assembly processes – for instance, materials that do not withstand lamination or soldering temperatures can be used.

2.2.3 Inter-chip interconnects with board-embedded waveguides

Several different approaches have been proposed to construct a chip-to-chip interconnect based on an optical waveguide integrated on/in the PWB. One of the earliest demonstrators (Jelley et al. 1992) was based on the simple structure shown in Figure 5: a board-mounted edge-emitting laser diode was butt-coupled to an optical ridge waveguide on top of the board, and the output from the waveguide was deflected towards the active surface of the photodiode with a laser-ablated mirror surface.

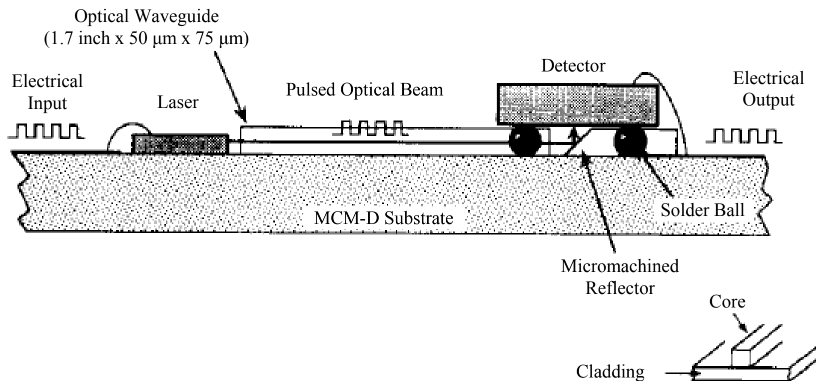

Figure 5. Optical interconnect on MCM substrate using edge-emitting laser and polymer waveguide (Jelley et al. 1992).

Later on, most of the research interest has focused in the use of VCSEL sources and board-embedded waveguides. In such cases, 45° deflection of the optical beam is often required both at the transmitter and receiver parts, as illustrated in Figure 6. In addition, rather than using a chip-on-board type mounting, it has been seen favourable to mount the optoelectronic transmitter and receiver components into a device package, possibly with the IC, as shown in Figure 3 and Figure 6. In that case, it is often necessary to utilise micro-optical components, such as lenses, to enhance coupling efficiency, as shown in Figure 6. Such optical interconnect systems have been demonstrated by several papers, the earliest including Chen et al. (2000), Krabe et al. (2000), and Ishii et al. (2001).

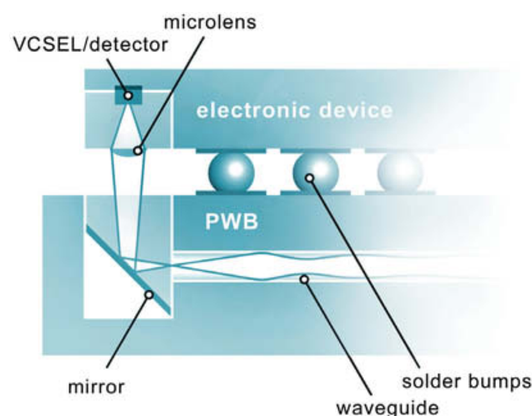

Figure 6. Illustration of a potential transmitter/receiver part of a board-embedded optical interconnect system with optoelectronics devices mounted in a surface-mounted electronic component package.

An example of a potential fabrication process for a fully board-embedded optical interconnect is presented in Figure 7. In addition to waveguides, the thinned VCSEL and photodiode chips are embedded. The waveguides are deposited on top of the components and directly aligned with the emitter/detector active areas. An optical interconnection layer is added to the board in the final laminating stage using the standard build-up PWB process. Even though the assembly process is simplified, the main problems are related to the thermal management and handling of the thinned components.

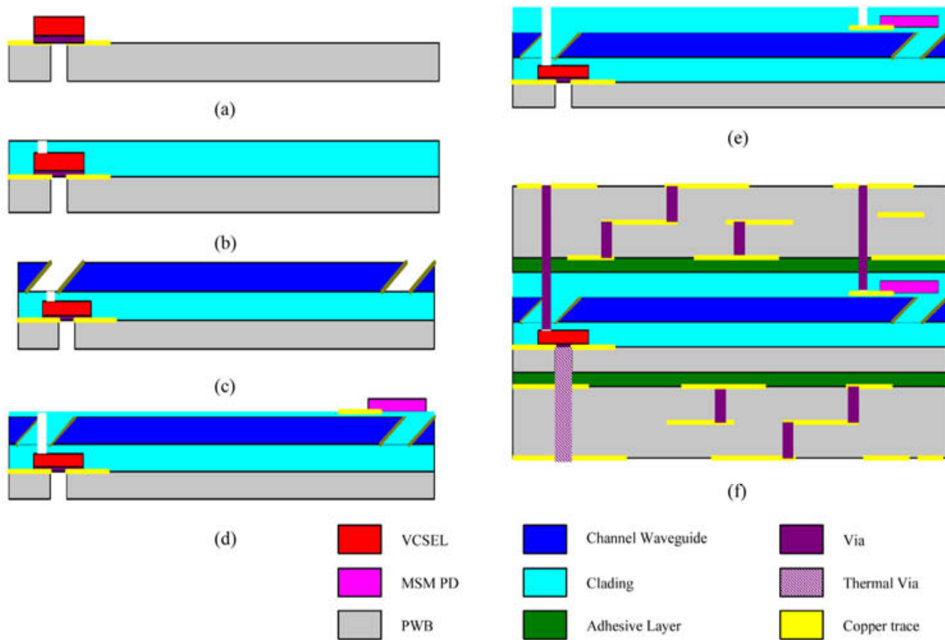

Figure 7. Process steps in embedded optics on a board concept proposed by Chen et al. (2000).

Coupling from board-to-board, such as from an embedded waveguide to another, allows the implementation of more complete optical interconnect systems. Board-to-board interface couplers have been published, for instance, in Luniz et al. (2001) and an optical backplane technology was demonstrated to transmit 2.5 Gb/s through backplane interface couplers and 1-m-long board-integrated waveguides. Board-to-board connections are not studied in this thesis.

Optical waveguide layers can be processed on the PWB or laminated inside the board. The advantages of the latter, i.e. the embedded solution, are that the surface area of the board is completely left to the pads and components and the waveguide layers are shielded from ambient environment and mechanical stresses, thus improving reliability (Immonen et al. 2005a, 2007). Moreover, multilayer optical waveguides would enable higher interconnect capacity and density as well as ease signal routing, especially if optical vias are implemented.

2.2.4 Free-space optical interconnects

The term "free-space optical interconnect" refers to the system where light is directed, or actually imaged, from the transmitter towards the receiver using optical components, such as lenses and mirrors, or there is just a transparent media between the transmitter and the receiver. This is in contradiction to the guided-wave optical transmission where the light is guided in a media based on total internal reflection phenomenon. In free-space interconnects, the light-guiding media between the transmitter and receiver can be air or another transparent material. A lot of research has been carried out on the free-space optical interconnects; mostly for very short distances, like intra-chip and intra-MCM (i.e. chip-to-chip) interconnects, but also for board-level and board-to-board applications, where ICs can be connected using massive parallel interconnects based on 2-dimensional laser and detector arrays, as demonstrated by Plant et al. (2001). However, no commercially feasible solutions have resulted yet.

There are major challenges hindering the feasibility of high bit-rate free-space optical links for board/backplane-level interconnection applications. First, it is extremely difficult to achieve the required optical alignment accuracy, especially when aiming to parallel interconnects with dense pitch. This is because, typically, the mechanics of the standard PWB technologies are not designed to provide alignment accuracies required by high bit-rate parallel optics – that is, the PWBs are not rigid and not forced to be straight on the racks. In addition, for the board-to-board application, the alignments between daughtercards are not very accurate, and for the board-level application the alignment tolerances of the components and parts are only in the order of 50…200 µm, which is not high considering dense parallel interconnects. Secondly, the long-term reliability of a free-space optical link is questionable since the electronics are typically not in an

isolated environment and, consequently, a cabinet eventually becomes dusty inside and in many applications the cabinet may be exposed to high humidity and large ambient temperature changes as well as mechanical stresses and vibrations. The challenges and possible solutions have been discussed by many authors and reviewed, for instance, by Tooley (1996) and Plant and Kirk (2000). In intra-board applications, the alignment tolerances between components are reduced and it may be feasible to implement a chip-to-chip interconnect, as presented by Thienpont et al. (2001) and Vervaeke et al. (2006) in describing a system with optical beams propagating inside a prism-shaped component.

The feasibility of board-to-board free-space optical interconnects has also been studied by the author (Karppinen et al. 2001). The optical implementation of two different kinds of interconnect topologies, a unidirectional ring bus and a star network based on beacon-type links, was mainly designed and characterised by the use of ray-trace simulation methods. The results of the study highlighted the significant path loss required to achieve misalignment-tolerant optical coupling. Consequently, very high bit-rate interconnects are difficult to implement without significant changes to the backplane systems.

2.3 Component technologies

Here, the electronic, photonic and optical component technologies' potential for high-speed short-distance optical interconnection applications are briefly reviewed, with a focus on the board-level interconnect.

2.3.1 Light sources

A light-emitting device is one of the key components of any optical data link. The structure and characteristics of the emitter have a significant role in the design of the transmitter, especially affecting the choice of optical coupling and packaging scheme. To enable feasible integration of the optical interconnect into electronic system, the emitter has to fulfil several requirements, such as small size, low power consumption (i.e. high electrical-to-optical conversion efficiency, even >50%), high modulation bandwidth (when a direct modulator is used), emission characteristics that enable efficient optical coupling, and low fabrication

costs. The costs would preferably be in the order of (or less than) the costs of the other devices in the system. Also, the possibility to fabricate as 1-dimensional or even 2-dimensional emitter arrays is important in order to enable implementation of dense parallel interconnects and thus achieve high aggregate transmission rates.

Of the currently available light emitter technologies, only semiconductor devices fulfil the requirements of optical interconnection applications, such as very small size and high conversion efficiency. There are two types of semiconductor emitters: light-emitting diodes (LED) and laser diodes (LD). They can also be classified as surface-emitting and edge-emitting devices, depending on how the emitted light exits from the die.

VCSEL is commonly promoted as the most attractive optical source for the short-distance optical interconnections. It is a laser diode in which the gain medium is surrounded by Bragg mirrors in such a way that the laser emits in the direction perpendicular to the surface of the die. VCSELs have many advantageous properties that are especially valuable in short-distance interconnects, such as low threshold current, low drive current, low operation voltage, high direct-modulation bandwidth, low temperature sensitivity (as compared to edge-emitting lasers), circular output beam with rather small divergence (allowing easy coupling to waveguide), suitability for high-density integration as monolithic arrays, compatibility with wafer level testing and screening (reducing manufacturing costs). A particularly attractive choice is the 850-nm VCSEL array that has already become a mature technology in parallel fibre-optic links. This is due to the fact that 850 nm is the local attenuation minimum of a silica fibre and, thus, commonly used in short-reach fibre-optic links.

The suitability of LEDs for optical interconnects is hindered by their rather slow direct modulation bandwidth, which is limited by the spontaneous recombination rate of the charge carriers. Typically, the maximum bandwidths of datacom-optimised LEDs are in the order of a few hundred MHz, and the smallest rise and fall times are in the order of 2...3 ns. However, it is possible to modify the LED structure to get higher bandwidth; at least, up to 1.7 GHz has been demonstrated (Akbulut et al. 2001). LEDs also have two other features that hinder their applicability as optical interconnects. First, typical output powers of high bandwidth LEDs are only in the order of 100 µW or less. Secondly, the output beam pattern has high divergence (approximately Lambertian source)

making it difficult to achieve high optical coupling efficiency with waveguides. The more advanced device construction, a resonance-cavity light-emitting diode (RC-LED), has a number of advantages over conventional LEDs, such as improved directionality (making optical coupling easier), spectral purity and enhanced external efficiency and better temperature stability. Nevertheless, just like a conventional LED, RC-LED also suffers from a limited modulation rate due to the lifetime of spontaneous emission (Schubert et al. 1996).

The conventional type of edge-emitting laser is a Fabry-Perot laser diode (FP LD), which comprises a semiconductor optical amplifier providing gain and front and back mirrors around the gain medium forming a laser resonator. The more advanced edge-emitting laser types, the distributed feedback (DFB) laser and the distributed Bragg reflector (DBR) laser, allow for single-mode operation, which is advantageous in long-haul fibre communications as chromatic dispersion is minimal but not seen as a significant advantage in short-distance interconnects. Although edge-emitting LDs are very common in fibre-based data links, they are less attractive for board-level interconnects. This is because they have difficulties meeting the cost/performance requirements, especially as a multi-channel source, due to the inherent way the device chips have to be processed, diced, cleaved and assembled. In addition, the edge-emitters are not able to compete with VCSELs in power dissipation, which is a key property when aiming at dense-packaged interconnects. Moreover, the output beam of edge-emitting lasers is asymmetric with high divergence (30...50º) perpendicular to the pn-junction, which often complicates coupling into waveguides.

An option technology to construct a high-speed source is to use an external optical modulator in combination with a continuous-wave-emitting laser diode or LED source. With this technology it would be possible to use a single emitter as a source of several transmission channels by dividing the power of the emitter among several modulators. The disadvantage in the use of an external modulator is that the integration and optical coupling structures become more complicated.

2.3.2 Characteristics of VCSELs

VCSELs can be manufactured for several different wavelengths (Koyama 2006). Today, devices emitting at around 850 nm represent the most mature high-

speed-optimised VCSEL technology. This is because they have been widely adopted as a standard in short-distance fibre-optic interconnects. The wavelength matches with the so-called 'first transmission window' of the silica fibres. VCSELs operating at wavelengths below a micrometer are based on GaAs/AlGaAs-based process technology. Another VCSEL wavelength range which has gained interest within optical interconnect demonstrators is 980 nm. One reason is that, since GaAs is transparent at 980 nm, it is possible to fabricate devices emitting from the rear of the device (i.e. through its substrate).

During the recent years there has been a significant development effort towards VCSELs operating at a wavelength range of 1200…1600 nm, i.e. to the wavelengths used in single-mode fibre communications. It seemed challenging to produce VCSEL structures using the InP-based process technology required for that wavelength range, but today the devices are emerging for commercial use and are replacing directly modulated FP LDs in some short-haul communications applications (Cheng et al. 2005).

Thanks to the small device size and the low power dissipation, dense arrays of VCSELs, both 1-dimensional and 2-dimensional, can be fabricated and are feasible for high-speed links. The commercially available VCSEL arrays typically have a pitch of 250 μm because that matches with the standard pitch used in fibre-ribbon cables and connectors. However, even much smaller pitches are possible as the die area required by VCSEL device is typically only in the order of 10…20 μm in diameter. For instance, a 110-channel VCSEL array with a 20-μm pitch has been demonstrated (Koyama 2006).

Recent advances in VCSEL technology are also promising higher data rates in the near future. Transmitter operation even up to 25 Gb/s (error-free at 85 °C with bias current of 7 mA) has recently been demonstrated using a 1070-nm InGaAs VCSEL (Suzuki et al. 2006). Also, monolithic 2D VCSEL arrays for parallel optical interconnects have been shown to operate up to 20 Gb/s/channel (Schares et al. 2006). Moreover, novel VCSEL-like devices, where an electro-absorption modulator is monolithically integrated above the VCSEL cavity, have shown much higher modulation bandwidths, even up to 60 GHz, with low drive currents (Paraskevopoulos et al. 2006).

VCSELs are typically emitting a 'volcano crater'-shaped beam, whose divergence is rotationally symmetric, but the intensity distribution has significant variation due to the multimodal operation. As an example, we see here the measured beam characteristics of a commercial 850-nm high-bandwidth VCSEL (ULM850-10-TT-A0112B by Ulm Photonics Gmbh), which was used in some of the experimental studies in this thesis (in Chapter 4). Beam divergence was determined with a knife-edge laser beam analyser (Melles Griot BeamAlyzer). The differences in beam characteristics between the transverse and lateral direction, as well as between laser diodes in the same array, were small, as seen in Figure 8, which presents a comparison between three VCSELs. Figure 9 shows the far-field intensity distributions of one the VCSELs at three different bias currents. The measurements showed that the full-angle $1/e^2$ beam divergence varied between 20…25° depending on the current and VCSEL.

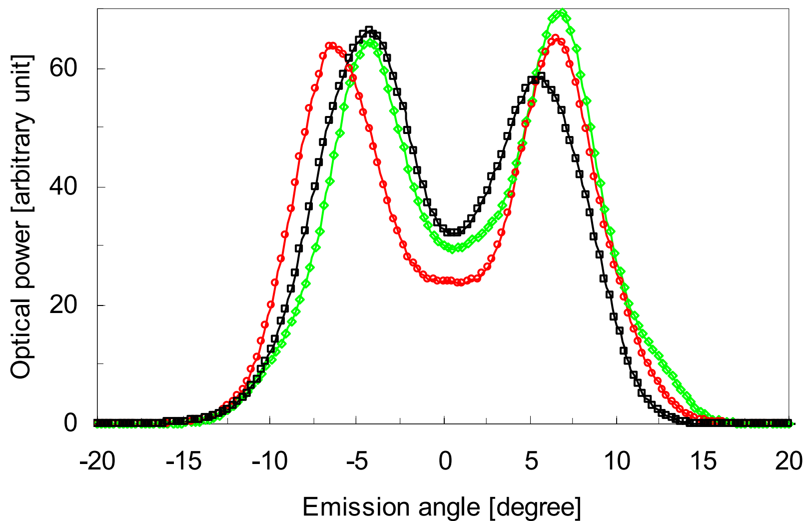

Figure 8. Farfield distribution of three different VCSELs (at 5 mA bias).

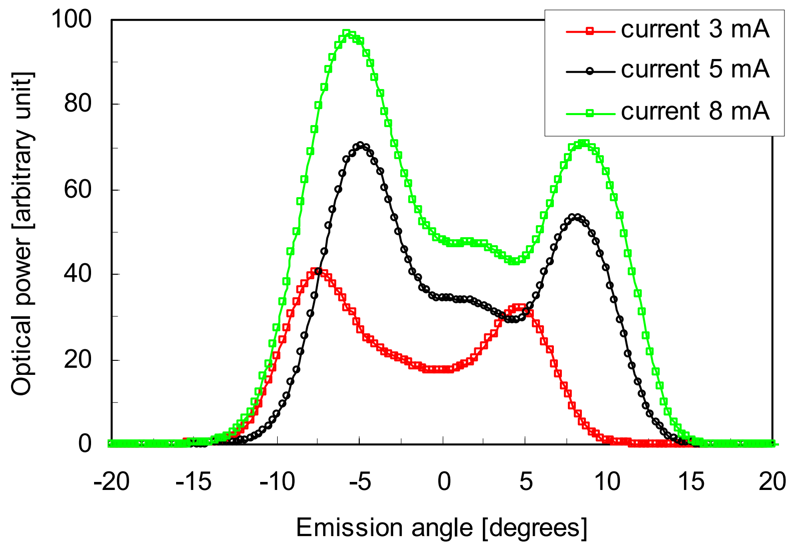

Figure 9. Farfield distribution of a VCSEL by Ulm at different bias currents.

2.3.3 Photodetectors

The detector to be used in optical interconnection applications should provide high bandwidth, high sensitivity (at the operation wavelength), a large photosensitive surface area (to ease optical coupling), and the possibility for high-density multi-channel integration. There are three types of semiconductor photodetectors that may fulfil these requirements: p-i-n photodiodes (PIN), metal-semiconductor-metal photodiodes (MSM), and avalanche photodiodes (APD). PINs are the most commonly used in short-distance fibre-optic links. MSM is a low-capacitance device enabling high-speed operation with a larger active area than PIN. For instance, a 12-channel MSM array with 10 GHz bandwidth and 80 µm active area diameter has been presented (Hurm et al. 2002). Nevertheless, the responsivity of MSM is typically lower than of PIN due to the top electrode structure that absorbs part of the incident power. Although APD provides the highest responsivity thanks to the internal gain, it is not considered attractive for board-level interconnects due to the requirement of high-bias voltage and rather complicated, i.e. expensive, fabrication processes.

The optimisation of the photodiode for high speed and high sensitivity with easy optical coupling is a trade-off: in order to ease alignment and optical coupling between waveguide and detector, as large an active area as possible would be preferred. But, on the other hand, when the area of the detector increases, so its capacitance increases, which results in decreased receiver bandwidth and increased pre-amplifier noise. This is also means that when the channel rate is increased, the optical coupling to the detector becomes more challenging. As a reference, PINs operating up to 10 Gb/s at 850 nm typically have an active area diameter of 60…75 µm, and, for instance, in Schares et al. (2006) it was demonstrated that the 3-dB bandwidth of the InGaAs PINs increased from 13 GHz to 30 GHz as the diameter was reduced from 60 µm to 30 µm respectively.

In practice, all commercially available high-speed photodiodes are optimised for fibre-optic applications today. This is a kind of shortcoming in demonstrating board-level optical interconnects as it is not always possible to find a photodiode with the optimal area. Fortunately, the high bit-rate fibre-optic links based on VCSELs use GI MM fibres that have an effective core diameter of 50 or 62.5 µm, which is also in the order of the preferred waveguide core diameter for board-level interconnects. In addition, the availability of photodiode arrays is limited to the pitch of 250 µm that is commonly utilised in parallel links based on fibre-ribbon cables and MT ferrules.

GaAs is a suitable material for photodiodes at wavelengths up to 850 nm, and Si is sufficient at wavelengths up to 1 µm. Both Si and GaAs photodiodes are used in fibre-optic links at around 650 and 850 nm wavelengths, but GaAs is more popular in high-speed applications. In longer wavelengths up to 1.7 µm, an InGaAs material system on InP substrates is commonly used, also in fibre-optic communications using 1.3-µm and 1.55-µm transmission windows. Another interesting detector material is Ge, because of its potential to monolithically integrate PINs on Si-based integrated circuits. However, discrete Ge photodiodes are not used in data transmission applications.

2.3.4 Electronics

The data rate of the high-speed board-level optical interconnect is typically limited by the bandwidth of the optoelectronic circuit and devices rather than the

bandwidth of the transmission channel. Therefore, similar to the fibre-optic links, it is favourable to use binary intensity modulation techniques, especially on-off keying with a non-return-to-zero pulse, and to have the bit-rate equal (or very close) to the symbol rate.

The data signals following a standard logic level, such as the current mode logic (CML) at high bit-rates, are not suitable to drive the LD directly. The laser requires a certain bias level and, to achieve a high extinction ratio, the voltage swing must be sufficiently large. Therefore, a laser driver circuit, typically an IC, is used to do the impedance matching and transform the logic signals into the appropriate modulation of the laser current. In addition, for proper biasing of the LD, it is often necessary to ensure the data steam is DC balanced and does not contain too long sequences of subsequent 0's or 1', e.g. by the use of 8B/10B encoding of the data. At the receiver side, a preamplifier is needed to amplify the small photocurrent and, typically, a post/limiting amplifier is also used to adjust the preamplified signals to match the logic level. Also, a bias is required for the photodiode.

The emergence of monolithic multi-channel driver and receiver ICs has enabled high integration of parallel transceivers. Due to the layout restrictions of high-speed traces it is very difficult to implemented a high channel count with discrete electronics and ICs. It is also important to note that in order to maximize the high-speed performance of the receiver, a preamplifier, which is usually a transimpedance amplifier (TIA), should be integrated very close to the photodiode, thus minimizing parasitic impedances. So far, up to 12 x 10 Gb/s receiver ICs have been built, e.g. by Schild et al. (2003). Today, 10 Gb/s/channel driver and receiver ICs with, at least, up to 4 channels are used in commercially available fibre-ribbon links.

A research trend is to implement driver and receiver ICs using standard CMOS (complementary metal-oxide-semiconductor) processes, as they promise lower costs and low power consumption. For instance, a 4 x 10 Gb/s transceiver based on quad CMOS ICs and VCSEL and PIN arrays has been shown to consume only 100 mW in total (Kromer et al. 2005). Moreover, even a low-power 25 Gb/s TIA has been demonstrated using the CMOS process (Schow et al. 2006).

To further increase integration, the monolithic integration of a photodiode on a TIA/receiver IC is aimed at. In the highest speed applications this is possible with heterostructure bipolar-transistor (HBT) processes. CMOS technology is also suitable, e.g. a 10 Gb/s integrated photodiode and TIA with low power consumption (Afzalian & Flandre 2006), though the responsivity is rather low.

To minimise the need of additional electronics due to optical interconnects, a research target is to connect the optoelectronic devices directly to the logic circuits. That is, the VCSELs would be driven bias-free directly with logic gates and the detectors would directly drive the logic gates. This means a trade-off in performance, but may be feasible if the link budget does not need to be maximised.

Another technology to potentially improve the link bandwidth is the electronic dispersion compensation (EDC) that has been proposed to increase the data rate of multimode fibre links recently. This means the inter-symbol interference (ISI), which limits the channel bit-rate, is compensated by adaptive equalisation circuitry in the receiver after the TIA (Zhao & Choa 2002).

2.3.5 Optical waveguides on PWB

Optical waveguide is another key component of the interconnection. The accuracy of the PWB manufacturing and SMT assembly processes suggest that convenient cross-sectional dimensions of the waveguides are in the order of 50…100 µm – that is, they are highly multimodal waveguides (Griese 1999). Therefore, it would actually be more precise to speak about *lightguides* instead of waveguides, but the latter has become a much more commonly used term and it is also used in this thesis.

The waveguide in board-level interconnects has to exhibit many challenging properties. The interconnection length can be centimetres or even dozens of centimetres. Therefore, very low attenuation is a must, requiring both a low-loss optical material and very low surface roughness of the waveguide core in order to minimise scattering losses. (This significantly differs from the typical centimetre-length scale of the integrated optics devices that are widely used today's fibre-optic communications networks.) One of the major challenges in achieving low attenuation is the high roughness and irregular surface of the

common PWBs. For instance, FR4 is an epoxy-based substrate that is re-enforced with glass fibres, which form a weave that increases the rigidity of the board.

Other important optical parameters of the waveguide are numerical aperture (NA), refractive index and shape, all which should match with the properties of the source and detector, as well as the coupling optics. In addition, the embedded waveguide should provide good thermal and mechanical compatibility with the PWB material, including good adhesion. Moreover, the waveguide has to maintain good optical properties with high stability against environmental stresses during the electronics assembly processes and in the operating environment. For instance, the waveguide has to survive the reflow soldering process, typically at temperatures around 250 °C.

Several different kinds of potential waveguide manufacturing technologies have been presented, such as photolithography, hot embossing, moulding, printing, ion-exchange, laser direct writing, and laser ablation. Of these, UV lithography with direct patterning of the optical polymer layer is probably the most common technology. Perhaps the ‘simplest’ version is the lithographic waveguide fabrication using direct waveguide-core photo-patterning and rib cladding process, which is depicted in Figure 10. The cladding and core layers are commonly deposited by spin-coating if the substrate is small. However, screen-printing or spray-coating methods are also suitable for industrial PWB processes with large panel sizes.

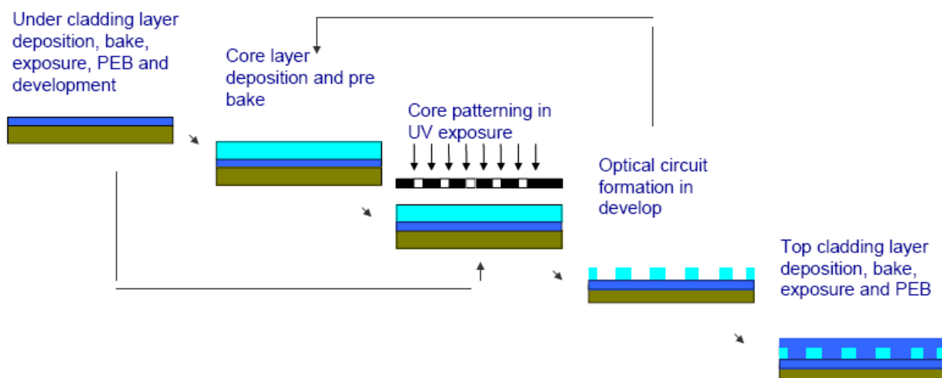

Figure 10. Optical waveguide process based on direct patterning of the core layer (drawing by M. Immonen / Helsinki University of Technology).

To achieve compatibility with PWB materials, polymer materials are favoured for the board-integrated waveguides. There have been numerous publications describing the different types of waveguide material systems, including acrylates, polyimides, cyclic olefins, siloxanes and silsesquioxanes (Zhou 2001). Recent advances in low-loss materials development have resulted in propagation losses of a number of polymers below or in the order of 0.1 dB/cm. The lowest waveguide losses have been achieved with acrylic and polysiloxane material systems, for instance in McEwan et al. (2002) and Moynihan et al. (2005) respectively. The papers have also presented good compatibility with PWBs and stability. Losses in polyimide- or epoxy-based materials are slightly higher, but they offer good temperature resistance in return.

It is also possible to fabricate passive waveguide components, such as bends, splitters and crossings. Bends are essential for signal routing on the board. Compared to copper traces, a disadvantage of optical waveguides is that they suffer from optical loss if the bending radius is small. For instance, the results in Moynihan et al. (2005) suggested that with a waveguide index contrast of 0.03 and core width of 50 μm, the board designs can realize a bend radius of 20 mm or higher without incurring any significant additional loss. On the other hand, crossings with low cross-talk and excess loss increases the possibilities for signal routing on a single layer. Splitters enable fan-out circuits. Nevertheless, they are only applicable if the link budget is high enough to tolerate the splitting loss as well as the possible excess loss of the passive component. For example, in Moynihan et al. (2005), 1 x 4 splitters were demonstrated with insertion losses of 8 dB or less.

2.3.6 Micro-optical coupling elements

One of the key challenges of the OE-PWB technology is to provide efficient and robust optical coupling between the waveguide and the laser diode or the detector. Micro-optical elements are often utilized to enhance the optical coupling efficiency and possibly also to loosen the mechanical alignment tolerances. For instance, the expanded beam method offers a viable solution to loosen the alignment tolerances in some locations along the light path. In practice, this means that optical elements, typically lenses, are applied to expand the light beam into a collimated beam between the elements, which are

challenging to accurately align. The expanded beam method has been demonstrated, for instance, both with single lenses to loosen the alignment tolerance of a daughter-board-to-backplane connector (Guttman et al. 1999) and with microlens arrays to loosen the alignment tolerance of a ball-grid-array (BGA)-mounted component (Ishii et al. 2001) (Figure 11). Although additional packaging complexity is generated from the lenses, the expanded beam connector allows lateral, vertical and longitudinal misalignments, for instance, up to several hundred micrometres for a minimal additional loss of less than 1 dB (Guttman et al. 1999). A drawback of the expanded beam method is that it sets a lower limit on the density of channels in parallel interconnects.

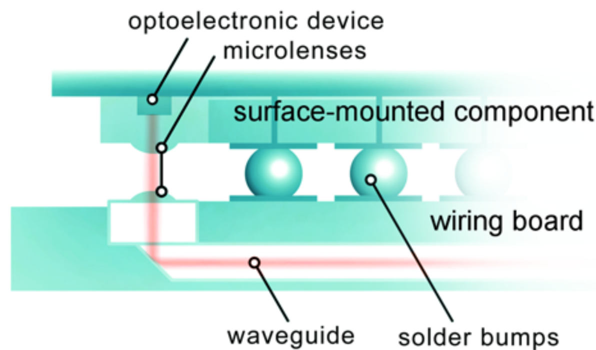

Figure 11. Coupling between photonic device and board-embedded waveguide using microlenses in an expanded beam configuration, as well as a waveguide-integrated micro-mirror.

In many proposed and demonstrated packaging implementations the VCSEL and detectors are facing towards the waveguide, thus the optical beams have to be turned through 90°. The beam can be turned with a discrete mirror component. Different kinds of mirrors have been presented so far, such as a flip-chip bondable micro-mirror device (Robertsson 2004) and a surface-mountable micro-optical element (Erps et al. 2006). The challenge in the use of discrete micro-mirrors is that one must first form a cavity on the waveguide layer in order to expose the waveguide facet, and that facet should also be of good optical quality, i.e. not cause too much scattering. Recently, there has been a lot of research interest in integrating the mirror directly onto the optical waveguide layer by shaping the waveguide end to form a 45° tilted facet with high reflectivity achieved by metallization or a total internal reflection (TIR) effect.

Various fabrication technologies have been proposed and demonstrated; for instance, laser beam ablation (Steenberge et al. 2004), wedge dicing with a 45° angled blade of a wafer saw (Hikita et al. 1999), hot embossing (Lehmacher & Neyer 2000), tilted-beam reactive-ion-etching (Gan et al. 1999), tilted-beam X-ray lithography (Kim & Kim 2004), and direct-patterning with inclined UV-exposure (Immonen et al. 2005c), which is presented in Figure 12.

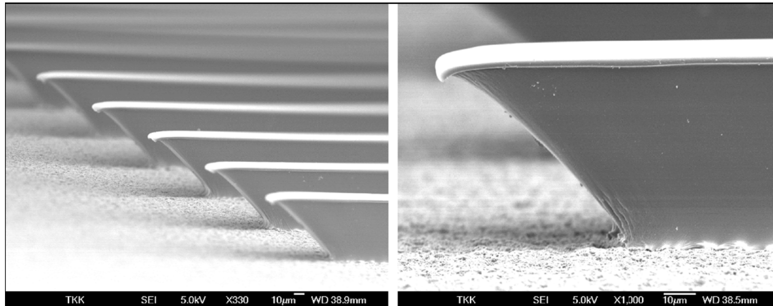

Figure 12. SEM image of waveguide cores (dimensions 100 x 85 μm) with 45° rectilinear TIR mirror planes in the waveguide ends. The structures were patterned using inclined UV-exposure of SU8 polymer (Immonen et al. 2005c).

Microlenses are often proposed for hybrid-integrated optical interconnects and have been used in many demonstrations. The microlens arrays are especially advantageous for parallel optical interconnects. Today, microlenses are customarily volume fabricated as 1D or 2D arrays on the wafer level for many applications. Various manufacturing technologies are possible, including even roll-to-roll-type continuous mass fabrication (Chang et al. 2006). Microlens arrays have been used in many hybrid-integrated multi-channel optical interconnects demonstrators, e.g. by (Ishii et al. 2003). Microlenses enable enhancing optical coupling, extending the separation between components and loosening the required alignment accuracies.

Alternatively to microlenses, the coupling between the o/e device and the waveguide with mirror facet can be enhanced with an integrated vertical light guide, possibly having a pillar shape (Bakir et al. 2004). Since the use of free-space lens optics is avoided, coupling with optical pillars, as presented in Figure 13, may enable very dense interconnects to a flip-chip-mounted o/e device. Moreover, when fabricated from a polymer material that is flexible

enough to enable bending of the pillar without deformation, the optical pillar may also compensate for small displacements in a flip-chip-mounted device (Glebov et al. 2006).

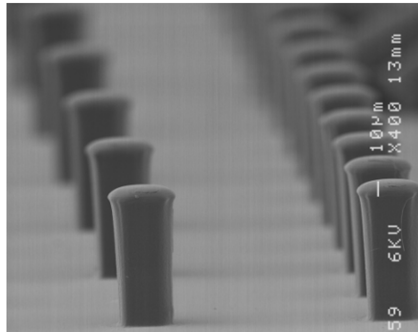

Figure 13. SEM image of an optical pillar array. Pillar height is 100 μm and diameter ca. 28 μm. (Karppinen et al. 2007.)

Another element that can be used to couple light into and out of the waveguide is a diffractive grating coupler. Various grating coupler concepts have been presented and studied. For instance, 35% in-coupling efficiency was demonstrated by pattering a tilted surface relief grating on the top surface of the multimode waveguide core (Chen et al. 2000). Nevertheless, it has appeared very challenging to implement high-efficiency couplers that would be feasible for board-interconnect applications based on multimode waveguides, surface-normal incidence and incompletely collimated beams without polarisation control.

An issue regarding the integration of micro-optics into electronics is the endurance of the materials during the assembly processes. Today, the micro-optical components are typically installed in the products after the electronics assembly phase. This is because the micro-optical components are often made of polymer materials, such as PMMA, that exhibit glass transition temperatures below 200 °C and thus do not survive the reflow soldering temperatures. On the other hand, such an assembly procedure is not acceptable (or at least not favourable) in the case of embedded board-level optical interconnects. Consequently, all optical components and adhesives should survive a normal reflow soldering process, which typically means peak temperatures in the order of 250 °C for around one minute. This means that only a small part of the polymer materials commonly used in micro-optics are applicable.

2.4 Integration and packaging

The implementation of board-level optical interconnects using today's photonics and electronics technologies requires hybrid integration of several different material and device technologies. On the other hand, there are many functions that have to be implemented through the integration and packaging, such as optical coupling, electrical interfaces, thermal management, shielding and protection. Therefore, integration technologies also play a key role in defining the costs of the overall solution and, thus, its feasibility.

2.4.1 Optical alignment

Today, the dominant factor in the subassembly costs of fibre-optic transceivers is the packaging and alignment process, and this is strongly dependent on the required alignment accuracy (Palen 2007). Until recently, photonic devices were mainly assembled manually, which led to poor productivity, low yield and high manufacturing cost. Before optical interconnects can be widely used in applications, the optoelectronic device packages have to be compatible with the current automatic electronic assembly process, i.e. surface-mountable device (SMD) technology. Active optical alignment is a time-consuming and costly process. Instead, a passive alignment technique has to be used. Passive alignment can be obtained by several different kinds of technologies, such as visual determination of the position (precision vision with pick-and-place), the use of fiducial marks on devices or substrates, mechanical stops or guides (micro-machined features on devices or substrates), solder force alignment, or a combination of the above. The high density of the multi-channel interconnects and small area of the high-speed photo-detectors set challenging requirements for the accuracy of the pick-and-place type of assembly. Another aspect to take into account is that angular tolerance control will be much tighter in optoelectronics than in the electronics packaging assembly.

2.4.2 Hybrid integration

In the very-short-distance optical interconnection applications, optoelectronic transmitters and receivers are typically constructed of discrete electronic IC and

optoelectronic devices, which are assembled onto a high-accuracy substrate (optical sub-assembly) using wire bonding techniques and alignment structures. However, such methods are not very suitable for cost-efficient assembly and require too much substrate area; thus the research trend is towards dense hybrid integration that would allow incorporating both photonic devices and micro-optical components into surface-mountable IC packages.

Here, the so-called smart pixel array (SPA) technology, studied for free-space optical interconnects, is especially worth mentioning. SPAs are arrays of transceiver components, each pixel including transmitter and receiver electronics, emitter and detector devices, and often also some micro-optics. An example of SPA was demonstrated in Liu (2002) by hybrid integration of a GaAs-based optoelectronic device array chip with microlenses onto a CMOS chip. VCSEL emitters and MSM detectors were used to demonstrate a large array suitable for massively parallel interconnects, e.g. with processor chips.

The high-alignment-accuracy hybrid integration of a microlens array with a VCSEL array was presented in Eitel et al. (2000). They achieved approximately 2 μm lateral alignment precision by the use of lithographically patterned alignment marks and precision-machined spacers.

Alternatively, refractive or diffractive microlenses can be fabricated on VCSELs or photodiodes by heterogeneous integration; either on top of the device, e.g. by UV casting (Gimkiewicz et al. 2004), or via wafer-bonding (Liu 2002), or on the rear of the chip if it has a transparent substrate such as 980-nm VCSELs have, e.g. by etching the substrate (Lin et al. 2007). Integrated lenses can facilitate optical coupling and ease the packaging alignment tolerances.

2.4.3 Flip-chip bonding assembly

For high-density interconnects, flip-chip mounting of VCSEL and photodiode arrays is favoured. A challenge in densely integrated parallel receivers is that channel-to-channel crosstalk induces a power penalty. This penalty can be a result of either imperfect optical coupling due to misalignment between the waveguides or fibres and the photodiodes, or due to electrical crosstalk between the electrical circuit signal lines either on-chip or through the substrate. One way

to reduce the electrical crosstalk, and thus increase integration density, is to use flip-chip interconnects instead of bond wires, as discussed in Park et al. (2005). Flip-chipping eliminates the wire-bond inductance between the driving or receiving circuits and the optoelectronic devices, which becomes problematic at data rates greater than 2.5 Gb/s (Krishnamoorthy & Goossen 1998).

Flip-chip bonding is also advantageous for optoelectronics packaging due to the very accurate positioning capabilities; even 0.5 μm accuracy is feasible with today's high-precision equipment. Nevertheless, there is a trade-off between the alignment accuracy and the mounting cycle time (i.e. the production rate). An example of the use of flip-chip bonding for optical alignment of VCSEL and photodiode arrays with multimode fibres through the substrate was presented in (Kuznia et al. 2003). Their technology was based on Ultra-Thin Silicon-on-Sapphire technology, where optoelectronic devices and CMOS ICs were mounted on a sapphire substrate allowing dense high-performance integration.

2.4.4 LTCC substrates for photonics modules

A versatile technology platform for implementing densely integrated optoelectronics micro-modules is a low-temperature co-fired ceramics (LTCC) substrate (Keusseyan et al. 2002), (Karioja et al. 2006). LTCC has proven a suitable integration technology for high-performance micro-modules, such as millimetre-wave modules, which can BGA-mounted on PWB (Heyen et al. 2003). The standard patch-type process for manufacturing LTCC panels is illustrated in Figure 14, and Figure 15 presents an example of an LTCC-based module including various integrated features. Thanks to the possibility to implement precision structures for optical alignment, LTCC allows the integration of photonic devices and electrical circuits into a ceramic wiring board. LTCC also enables high packaging density due to its multilayer structure and possibility for passive-component integration and bare-chip encapsulation. In addition, good high-frequency and thermal properties, as well as stability, reliability, and compatibility with hermetic sealing and cost efficiency, are advantageous for high-speed optoelectronics. Mechanical tolerances in the order of ten micrometers can be achieved in the alignment of the components and different layers with LTCC technology. The processing of 3D passive structures with ~3 μm tolerances has been presented for passive alignment of the photonic components. Thus the

mechanical tolerances are good enough for multimode optical waveguide applications with the use of passive alignment. Furthermore, the recent near-zero-shrinkage tape materials promise even better accuracy.

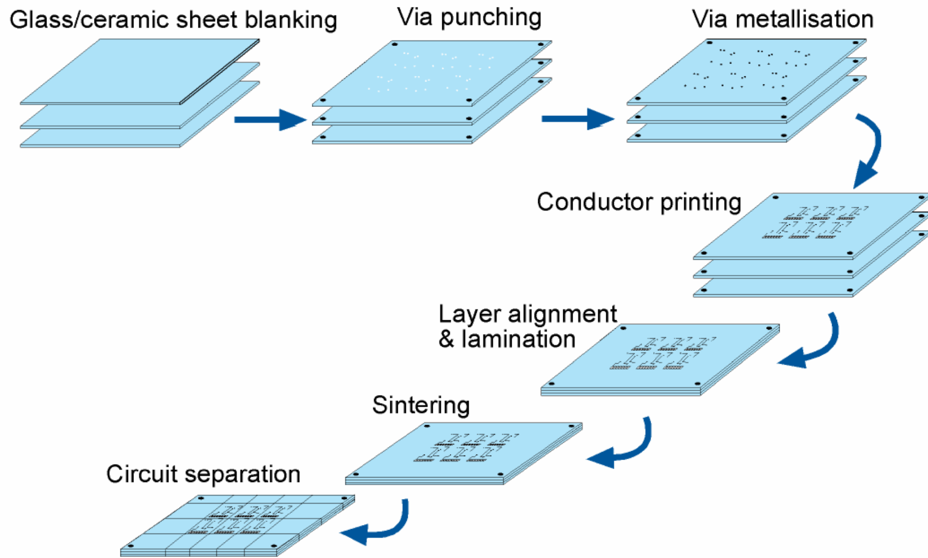

Figure 14. Manufacturing process of LTCC wiring boards.

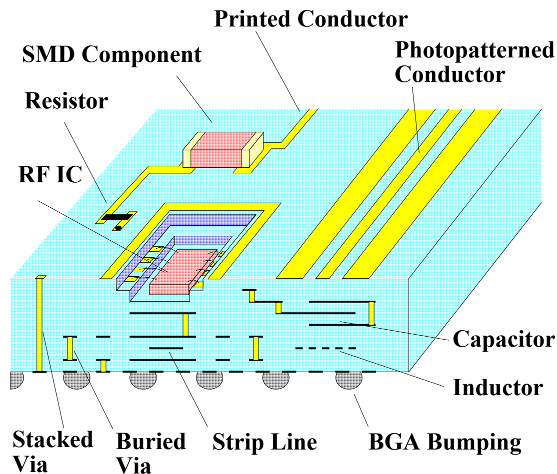

Figure 15. Schematics (cross-sectional view) of an LTCC multi-chip module illustrating various embedded capabilities.

To the best of the author's knowledge, we were the first ever to present the use of passive optical alignment of a fibre and a surface-emitting device based on an LTCC structure (Karppinen et al. 2001a). An arrayed transmitter structure was designed and demonstrated with fibre pigtails, flip-chipped VCSELs and driver electronics. An LTCC via a hole was used to provide the alignment structure for the fibre on the module substrate, as presented in Figure 16. It was demonstrated that, thanks to less than ±20 µm total alignment tolerances, LTCC is a potential technology for low-cost, small-sized, high bit-rate optoelectronic modules featuring passive alignment of MM fibres to surface-emitting devices. Later on, a similar structure has been used in two other VCSEL-based transceiver module demonstrators (Guo et al. 2005, Heikkinen et al. 2007), achieving a sufficient alignment accuracy to 50 µm MM fibres. The LTCC substrate material Dupont 951 was used in the aforementioned modules because it has proven to be suitable for implementing accurate structures for micro-optical alignment and also provides good enough electrical performance.

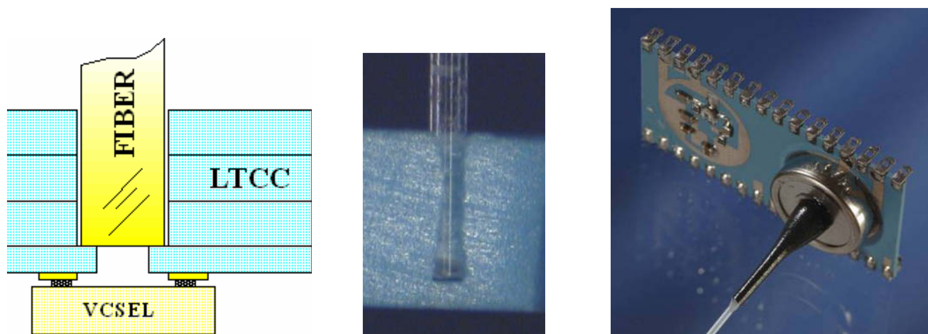

Figure 16. VCSEL-to-fibre passive alignment based on an LTCC via a hole: left) alignment structure; middle) cross-sectional micrograph of the fibre in the alignment hole; right) radio-over-fibre transceiver prototype based on the alignment structure (receiver part unshielded and without fibre).

2.5 Conclusions and comparison to electrical interconnects

To summarise the message of the previous chapters, there are several technology gaps still hindering the applicability of optical interconnects at the board level.

These include mass-producible micro-mirror technology and SMT-compatible hybrid integration of optoelectronics with coupling optics.

The fundamental difference between the electrical and optical interconnects is the power consumption of the electrical link scales according to square law versus interconnection length, due to the RC constant, whereas the power consumption of an optical interconnection scales linearly in length. Therefore, it is clear that the optical (fibre) data links are a superlative technology for high-speed long-haul communications. However, another fundamental difference in the technologies is that electrical-to-optical conversion is always needed in the transmitter and vice versa in the receiver since, so far, all signal processing happens in the electrical domain. These conversions are inevitable and cause some losses of energy, even if the interconnect is very short. Thus the optical interconnect has a minimum power consumption, only dependent on the conversion efficiency of the optoelectronic devices, whereas electrical interconnects do not have such a fundamental power consumption minimum. Consequently, it is generally stated that, at a certain high data rate, the power consumption of the electrical interconnect is smaller at short link distances and there is always a break-even distance above which the optical interconnect has lower power consumption.

A generic comparison between optical and electrical interconnects and analyses of break-even lengths is presented in Feldman et al. (1988). Later on, several other papers have presented comparisons based on different kinds of technological details and also applying somewhat different criteria. The challenge here are several somewhat independent figures of merit to be considered, such as channel bandwidth, power consumption, required board area/volume, interconnect density, manufacturing costs. On the other hand, the 'fair' comparison becomes even more vague due to the fact that there are no 'standard/typical' solutions of optical interconnects on the board, only approaches proposed for future applications. Recently, the previous comparisons were reviewed by Uhlig and Robertsson (2006), pointing out the only clear conclusion that the optical links outperform electrical links on power consumption above a certain breakeven link length at a given bandwidth. This is due to the skin effect and dielectric losses in electrical wires at high bandwidths, and is also the reason why fibres are clearly superior to copper cables in communication networks. However, whether this breakeven point will fall into

the distances and data rates of a board-level interconnect in the near future cannot be clearly shown. Uhlig and Robertsson (2006) also pointed out that, due to the crosstalk issues, the 10 Gb/s electrical wiring on the board requires an order of magnitude larger pitch than optical waveguides, i.e. optics can provide a higher interconnect density. On the other hand, it is still questionable whether there are significant benefits from board-level optical interconnects in overall performance (Svensson 2002).

3. Design aspects and methodology

One of the aims of the research was to demonstrate an optical interconnect technology that is competitive with the modern electronic interconnect technologies. In this chapter, the methods used and the selections made in designing the experimental structures of thesis are described and justified. These include the optical design and optimisation methodology, and device selections, as well as the integration and packaging-related selections. In addition, some analysis of the high-speed performance is presented.

3.1 System specifications and their implications

In order to be truly attractive for commercial applications, the optical interconnect is aimed at simultaneously outperforming, or at least matching with, the copper-based ones in all important performance-related parameters. These include total power consumption and costs per interconnect capacity, as well as required board area and volume. In addition to high performance, the manufacturability and the reliability issues are important. It was foreseen that the components and the technologies should not require excessive changes to the established manufacturing processes. Also, the new optical technologies should support the simultaneous use of existing technologies, i.e. the optical interconnects would be introduced as an additional technology to be used in parallel with the electrical interconnections. One consequence of the above is that an optical link should not complicate packaging significantly, for instance due to a local increase in heat dissipation, and, especially, active temperature control (i.e. cooling) of components should be avoided.

Based on the state-of-the-art technology status and foreseen needs of the optical interconnects as a future high-speed data bus, some technical targets were defined at the beginning of the work. The following features and specifications were then used as a guideline during the work:

– point-to-point data bus; simplex waveguide channels
– multi-channel (i.e. parallel optical link); high channel density (pitch 250 μm)
– maximum transmission distance (i.e. waveguide length) ~500 mm or longer

– transmission speed (i.e. symbol rate) 10 Gb/s/channel or higher
– bit-error-rate (BER) ~10^{-12} or smaller (without error correction)
– ambient operation conditions as in typical consumer or industrial electronics
– lower power consumption than in electrical interconnects.

3.1.1 Optical specifications

One of the key optical parameters of the data link is the operational wavelength. The optimal choice depends on the attenuation spectrum of the transmission media as well as on the emission wavelength and power of the available sources and sensitivity of the suitable detectors. The waveguide materials' potential for PWBs usually exhibit lowest attenuation at wavelengths below 1 µm down to visible range, but rather low loss may also be achieved at wavelengths around 1300 nm, as shown in Immonen et al. (2007). On the other hand, the availability of suitable sources, i.e. mature high-speed VCSEL technology, is currently limited to the 850 nm wavelength.

In the product development, one may have to consider the laser light eye-safety regulations as well. It is possible that the most stringent power limits do not need to be obeyed in an embedded optical interconnect application because there should be no possibility of laser beam exposure to the human eye under any operational conditions and, even if major damage would reveal the laser beams, it would probably also cause the laser current to turn off. If one has to conform to the safest regime, IEC Class 1, the maximum launch power can be approximately –1 dBm at 850 nm. However, if Class 1M is sufficient, meaning light is not harmful unless viewed with a magnification aid, the launch power can be almost +10 dBm (IEC 2001). Since 1300 and 1550 nm light sources are less damaging to the eye than sources at 850 nm, more power can be launched at those wavelengths while conforming to the eye-safety level. Nevertheless, this would not necessarily be beneficial because higher launch power would also mean higher power consumption by the transmitter.

3.1.2 Reliability issues

The introduction of optical interconnects must not compromise the reliability of the electronic system. This usually means that the developed solutions should operate reliably within a wide ambient temperature range (sometimes even up to –40...+85 ºC), tolerate moisture or dust in the ambient environment, and be robust against vibrations and mechanical shocks. The optical and optoelectronic components typically require even more care during packaging than bare electronics to ensure reliability. This is due to the fact that, in addition to conventional interconnect reliability and thermal management issues, the optical devices have sensitive surfaces to be protected against contamination, the optical path ways need to be kept clear, and the optical alignment needs to be maintained. These requirements have many consequences, which should be taken into account when designing the system and selecting the technologies. Some issues are pointed out here, though only briefly as the reliability studies were not included in this work and the demonstrated technologies were not particularly designed for high reliability.

An example of issues concerning reliability that may require special consideration are underfills under flip-chip and BGA-mounted devices with optical structures underneath. In addition to conventional joint reliability reasons, the use of underfill material may be preferred as it would prevent dust or moisture disturbing the optical channel. On the other hand, if an underfill is applied below an optically interconnected device, the underfill material should be optically transparent at the operational wavelength and should spread homogeneously, i.e. without air bubbles, to avoid deteriorating the optical path. Moreover, the underfill should then be taken into account in the optical design of the coupling structure.

3.2 High-speed issues

The aim is to maximise the aggregate data rate versus both power consumption and space occupied (i.e. board area and component volume). This can be achieved by increasing the bit-rate of individual optical channels or by increasing the density and number of parallel optical channels. In this section, some high-speed issues are presented in detail. The high-speed device technologies

were described in Section 2.3. A significant remark was that a large photodiode area is preferred to loosen the alignment tolerances in optical coupling, but in practice the area is limited by the trade-off in the receiver bandwidth and sensitivity due to the increased capacitance.

3.2.1 Bandwidth of waveguides

The bandwidth of a multimode step-index (MM SI) optical waveguide is mainly limited by the inter-modal dispersion, i.e. the differences between the propagation time of different modes through the waveguide. Dispersion causes inter-symbol interference (ISI) in the communication channel and thus increases BER. For a step-index waveguide, the inter-modal dispersion can be estimated with a differential time delay between the axial ray, which propagates along the optical axis of the waveguide (i.e. the mode having the highest group velocity), and the marginal ray, whose propagation angle has the largest deviation from the optical axis (i.e. the mode having the slowest group velocity). The differential time delay is given by

$$\Delta t = \frac{Ln_{core}}{c}\left(\frac{n_{core}}{n_{clad}} - 1\right), \tag{1}$$

where L is the length of the waveguide and c is the speed of light in a vacuum (Hecht 1987). This equation is just an approximation that may somewhat underestimate the total inter-modal dispersion of the waveguide because it does not take into account the skew rays, i.e. the rays propagating along a path that does not intercept the waveguide axis.

To estimate the bandwidth of a typical optical waveguide on a PWB, we use Truemode™ polymer as an example waveguide material here. A Truemode Backplane™ waveguide manufactured on FR4 has refractive indexes of $n_{core} = 1.540$ and $n_{clad} = 1.521$ (Immonen et al. 2005b). Substituting these values results in the differential time delay of 64 ps/m. This value is better illustrated as its inverse, which states that the estimated bandwidth–distance product of such a waveguide is 16 GHz · m. The bandwidth can be increased by decreasing the refractive index difference, but, with a small difference, the bending losses of the

waveguide will increase and the optical input coupling becomes more challenging. Therefore, a practical bandwidth maximum of a step-index MM polymer waveguide at the board-level can be estimated to be approximately 20 GHz · m (Uhlig & Robertsson 2006). Higher bandwidths could be achieved with graded-index waveguides but, so far, no manufacturing technology suitable for PWB-embedded has been presented. The launch condition, i.e. possible misalignment between the device and waveguide, and thus coupling of some specific VCSEL modes, can also affect the bandwidth.

3.2.2 Link power budget

The power budget of the link depends on the output power of the source, the sensitivity of the receiver and the path loss. The first two are both temperature- and bandwidth-dependent device characteristics, whereas the path losses are bandwidth-independent but may have some temperature dependence. Path loss can be roughly divided into three parts: coupling loss from the source into the waveguide, attenuation of the waveguide, and coupling from the waveguide to the detector.

To get some insight on the power budget, let us consider a 10 Gb/s/channel data link that can be fabricated with commercial device technologies today. The highest average output powers of high-speed VCSEL arrays are in the order of 1 mW per channel. Typically, multi-channel receiver ICs can provide approx. –15 dBm sensitivity when BER lower than 10^{-12} is required, see e.g. Primarion (2002b). Even with the state-of-the-art waveguide materials, the waveguide losses can reach ca. 5 dB on very large boards with ca. 50 cm dimensions. Assuming a 1 dB power penalty due to the transmitter extinction ratio, this leaves <10 dB for the coupling losses and the link margin. The latter is needed to allow excess losses due to potential misalignments, and power and sensitivity reductions due to temperature variations and aging, etc. Although it is not possible to give exact estimates as all these values are very much device and application-specific, it becomes clear that the coupling losses cannot be more than a few dB in total.

In practice, even lower BER may be needed in interconnects, thus further reducing the loss budget. One should also note that this is the BER limit of the

optical link itself, because error correction methods inside electronic equipment are not favourable due to the requirements of short latency and low power consumption.

As a consequence of the very limited optical power budget, it is difficult to implement point-to-multipoint interconnects; only a small splitting ratio (1-to-2...4) may be possible and even this will require very low waveguide attenuation or very short links (a few centimeters or less) – unless one also integrates optical amplification devices, as proposed by Uhlig and Robertsson (2006).

It is also necessary to leave some margin for all manufacturing tolerances, both in device characteristics and in packaging, as well as for performance degradation over time (i.e. aging). In practice, most single-VCSEL transmitters use a photodiode to monitor their output power through back-reflection of the light in order to maximise the power budget through the full operation temperature range and to overcome the effects of VCSEL ageing and detect failures. The monitor PD allows closed-loop control of the VCSEL current. However, the monitor photodiode increases the size and adds packaging complexity, especially in the case of a VCSEL array.

3.3 Coupling to multimode waveguides

High-efficiency optical coupling between the transmitter/receiver and the waveguide is a necessity, as emphasised above. Sufficient optical alignment, both lateral and angular, should be achieved by the use of pick-and-place assembly of the components in order to be compatible with automated electronics manufacturing. One challenge is that the tilts of devices, i.e. angular misalignments, have to be small with optics, but this aspect has not had much importance in traditional electronics assembly.

The waveguide technologies were reviewed in Section 2.3.5. The waveguides' potential for OE-PWB applications have cross-sections in the order of 50…100 µm and NA in the range of 0.2…0.3.

3.3.1 Basic principles and trade-offs

The coupled power from a source to a MM waveguide (or fibre) can be calculated using the formula (Keiser 2000)

$$P = \int_{A_f} dA_s \int_{\Omega_f} d\Omega_s B(A_s, \Omega_s), \tag{2}$$

where $B(A_s,\Omega_s)$ is the brightness (i.e. luminance) of the source and A_s and Ω_s are the area and the solid emission angle of the source respectively. The area of the waveguide core A_f and the solid acceptance angle of the waveguide Ω_f define the limits of the integrals. The coupling efficiency is the coupled power P divided by the total emitted power of the source. Often, the formula is used in a simplified form where the coupling efficiency depends on the NA of the waveguide and the divergence of the source. With a step-index waveguide, this is true. However, with a multimode VCSEL source one should actually integrate the luminance of the VCSEL over the acceptance angle and area.

Consequently, the emission characteristics of the source, especially the beam divergence, is an important parameter in optimising the coupling optics. Since the divergence of VCSEL is somewhat dependent on the drive current, i.e. emitted total power, it is sometimes possible to do some trade-off between the nominal power budget and the alignment tolerances and crosstalk; if the link power budget in the nominal case has a high margin, one may reduce the emitted power and, thus, the beam divergence.

There are also a couple of basic principles in the design of optical coupling in an O/E-PWB:

- In order to have optimized in-coupling efficiency, the emitter output angular properties need to be matched to the numerical aperture (NA) of the waveguide. Thus, if the emitter beam divergence is larger than the waveguide NA, the source has to be imaged to the input of the waveguide with a magnification larger than unity.
- In order to have optimized out-coupling efficiency, the optics has to match the waveguide output surface area to the detector area. Thus, if the waveguide output surface area is larger than detector area, it has to be imaged to the detector with a magnification smaller than unity.

These two principles lead to trade-offs in the optimization of the micro-optical system and the cross-sectional dimensions of the waveguide:

Most importantly, to loosen the alignment tolerances there is a trade-off between coupling a divergent laser beam to a waveguide and coupling the waveguide output beam to the relatively small active area of a high-speed detector. One method to partly overcome this trade-off is tapering of the waveguide ends (i.e. having a larger waveguide core at the transmitter and smaller at the receiver). In practice, this can only be used in one dimension (parallel to board) since it would be very difficult to vary the thickness of the waveguide layer in production. Nevertheless, the use of tapering is limited by the channel pitch in high-density parallel interconnects.

The expanded beam method enables loosening the tolerance requirements, e.g. between the package and the board. The method can be simply realised with two microlens arrays (see Figure 11). Nevertheless, the use of the method is limited in high-density parallel interconnects as well. This is because, in order to avoid optical crosstalk between channels, the width of the expanded beam has to be smaller than the pitch of the channels. In practice, the maximum alignment tolerance (without any crosstalk) is the pitch minus the beam waist between the lenses. For instance, if the pitch is 250 μm and the beam waist is 100 μm, one can expect to achieve ±75 μm alignment tolerance in an ideal case.

In addition, since the wafer surface is the active area in the suitable VCSEL and high-speed photodiode arrays, the beam of the source has to be bent through 90° to couple into the waveguide, and again the waveguide output has to be bent through 90° to the photodiode surface.

3.4 Optical design methodology

The optical systems presented in this thesis were studied and optimised by the use of ray tracing design tools. They enabled modelling the optical path losses as well as carrying out opto-mechanical tolerance analyses and optimisations.

3.4.1 Ray-trace modelling

The optical channel between the transmitter and receiver can be modelled by non-sequential Monte Carlo ray-trace software using a realistic 3D system model, as demonstrated by Karppinen et al. (2002, 2001b). These simulations result in total coupling efficiency, i.e. path loss, of the system. Although the ray-tracing approach is not as accurate as the wave propagation approach (Zaleta et al. 1996), it enables accurate analysis of complicated optical systems with such properties as multimode sources (e.g. VCSELs), scattering, and aperture clipping. Propagation through an MM waveguide can be modelled as well, although the simulations tend to become time-consuming due to the large number of reflections. Furthermore, the ray-trace approach enables analysis of the crosstalk can in multi-channel interconnections.

In the work presented in this thesis, most of the optical simulations were carried out using ASAP® (Advanced Systems Analysis Program), which is a non-sequential Monte Carlo ray-tracing software from Breault Research Organization, Inc. 3D optomechanical models of the demonstrated links were created. All surfaces of the optical components (except the photodiode) were defined without anti-reflection coatings, although AR coatings are preferred in real applications to reduce the coupling losses. 850-nm VCSEL sources were modelled with realistic beam characteristics. They can be defined into ASAP as circularly symmetric beams having angular distributions similar to measured VCSEL beams (Karppinen et al. 2001a).

The ray-trace propagation through the waveguide was included in the simulations in order to obtain more realistic characteristics of the waveguide output beam. The cross-section of the waveguide had two sharp (45°) and two rounded edges. The input and output facets of the waveguide were defined with light scattering properties (Gaussian distribution with a 5° scatter angle). The waveguide material was defined to cause 0.05 dB/cm attenuation.

In addition to waveguide losses, the ray tracing method allows analysis of the time jitter due to multi-path dispersion (Karppinen et al. 2002). In other words, the multi-path induced impulse response of the system can be calculated from the optical path lengths of the rays propagated through the system. Furthermore, the impulse response allows estimating, for instance, the inter-symbol interference

(ISI) and, thus, the maximum data transfer rate of the interconnect with the chosen modulation method.

3.4.2 Tolerance analysis for optimisation and yield estimation

In order to design an optical interconnect system that is insensitive to both component misalignments and manufacturing tolerances, two types of analyses are needed (Zaleta et al. 1996):

- In sensitivity analysis, each tolerance variable (xyz-displacements and tilts) is simulated separately and the most critical tolerances are found. Sensitivity analysis helps to optimize the optics. However, the root-sum-square and worst-case analysis that can be made from the sensitivity analyses of individual misalignment effects alone is not a sufficient method because it does not take into account the simultaneous interaction of all variables.
- In Monte Carlo analysis, the effect of all variables is simultaneously analyzed by creating a large number of randomly chosen perturbed systems (with misalignments). Thus statistical information on the system performance is obtained, allowing prediction of the manufacturing yield of the system. In addition, the correlation between the loss and the tolerance parameters reveals the parameters that most affect the total system performance.

During the work presented in this thesis, an opto-mechanical simulation tool for Monte Carlo tolerance analyses with ASAP was developed at VTT in order to enable more detailed optimisation with the manufacturing tolerances, as well as to predict the feasibility of optical coupling for mass production.

The method and tool have been used by Keränen et al. (2004) for the analysis of butt-coupling between an edge-emitting multimode laser diode and an MM GI fibre. For the two characterised modules with fibres having NA larger than 0.20, the simulated coupling efficiencies agreed well with the measured ones. Another case, where the method was applied and the result compared to an implemented VCSEL-based transceiver, was published by Guo et al. (2005).

4. Optical coupling to waveguides on board – comparison (Case study I)

In this chapter, a study of different optical coupling structures for on-board interconnects with embedded waveguides is presented. First, different coupling schemes are analysed and compared by optical modelling methods. Then, the implementation of a test assembly is described in order to experimentally study the fabrication challenges and the feasibility of the three different coupling structures. The characterisation results, mostly about the misalignment tolerances of the coupling structures, are presented and discussed at the end.

Most of the work and results presented in this chapter have been published earlier (Karppinen et al. 2004a, 2004b, Alajoki 2004).

4.1 Optical design and analysis

The aim was to develop and compare optical coupling structures for board-level interconnects between IC packages or multi-chip modules, as illustrated in Figure 3. Typically, the most inaccurate alignment phase in the production of this kind of electronic sub-system is the BGA board assembly. On the contrary, the tolerances of the chip-mounting methods, i.e. the alignment between the VCSELs and PDs, is much smaller. In practice, less than ±5 µm is rather easily achievable with well designed alignment marks and structures.

After a preliminary analysis of several different optical coupling schemes, three schemes were selected for more detailed analysis with optical simulations and tolerancing. The structures were designed and optimised in such a way that they were suitable for practical implementation in the planned test assembly. All simulations were made at the 850 nm wavelength, as were the experiments.

4.1.1 Butt-coupling scheme

The butt-coupling concept, with a potential implementation illustrated in Figure 17, was included in the analyses and the implemented test assembly for

comparison purposes. In butt-coupling, the nominal coupling losses can only be small if the devices can be placed close to the waveguide ends, the VCSEL output divergence is small compared to the NA of the waveguide, and the detector area is bigger than the cross-section of the waveguide. In addition, to minimize coupling loss, good quality waveguide end facets have to be made in the cavity formed on the optical layer PWB for the subassembly. Such cavities can be at least by laser ablation (Hendrickx et al. 2007).

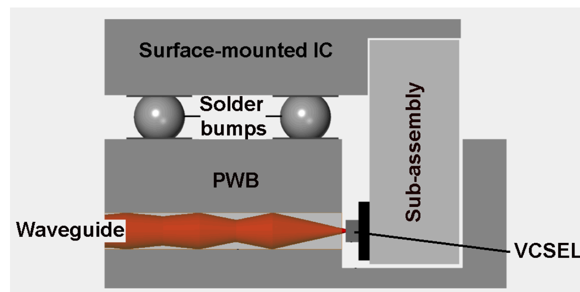

Figure 17. Illustration of the butt-coupling scheme realized with an optical sub-assembly attached to the optically interconnected device.

4.1.2 Coupling with a double microlens array and a mirror

The second coupling concept studied uses two stacked microlens arrays. The optical design and packaging principle of a transmitter is shown in Figure 18. A similar structure is suitable for both ends of the data link (Figure 19). The idea is that the first lens collimates the VCSEL beam and the second one focuses the beam on the waveguide, thus the design enables lengthening the distance between the device and the waveguide. In addition, a 45° mirror surface is needed to deflect light from the VCSEL into the waveguide. Correspondingly, at the receiver end of the system, the output beam from the waveguide is first deflected 45° by the mirror, then collimated by the lens and finally focused by another lens towards the detector. This kind of design principle enables the optimal distance between the lenses to be approximately the same at both ends, which can be an advantage in manufacturing and assembly.

In the simulation, the lens parameters used were: radius of curvature (ROC) 266 μm, lens array pitch 250 μm, lens aperture diameter 250 μm, surface profile

spherical, and front focal length in air 515 µm with point source. In the simulations, the refractive index of 1.51 was used for the microlens arrays. Two such microlens arrays were stacked and placed so that 1:1 imaging of a VCSEL to a waveguide would be achieved. The distance between the stacked lens arrays was 0.6 mm. The double microlens array can be realized by processing microlens arrays on both sides of a substrate or by joining the bottom surfaces of two microlens array substrates.

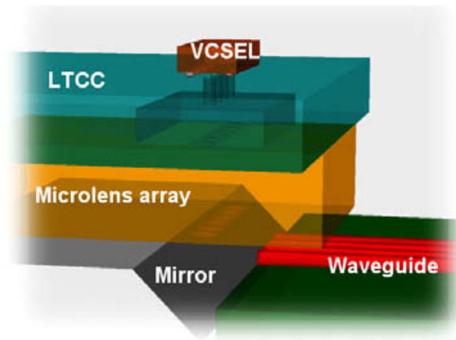

Figure 18. Schematics of the VCSEL-to-waveguide coupling using a double-sided microlens array and a mirror. The drawing also presents a potential packaging scheme using an LTCC module substrate.

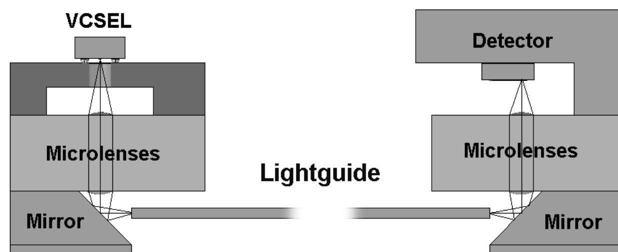

Figure 19. Schematics of the simulated optical path based on double-sided microlens arrays and mirrors. A potential packaging scheme is also presented.

4.1.3 Coupling with micro-ball-lenses and a mirror

The third selected coupling scheme was based on micro-ball lenses attached to a mirror surface, as illustrated in Figure 20. Two ball lenses per each optical

channel are used to image the source on the input of a waveguide (1:1 imaging) when a micro-mirror tilts the beam through 90° and vice versa at the receiver end (Figure 21). The resulting component is placed under the VCSEL or PD array chip and the whole transmitter or receiver module is positioned on the waveguide array. In the designed system, a ball lens diameter of 250 µm was used. This was to match the pitch of the optics to the pitch of the VCSEL and PD arrays. In the simulations, the lenses were assumed to be made of BK7 having an index of refraction of 1.51. It was also assumed that the lenses will be glued onto the mirror and that the adhesive, which is index matched to the BK7, will completely fill the space between the lenses and mirror. That is, refraction will only occur on one surface of the ball lens – i.e. on the two outer surfaces of the complete coupling component.

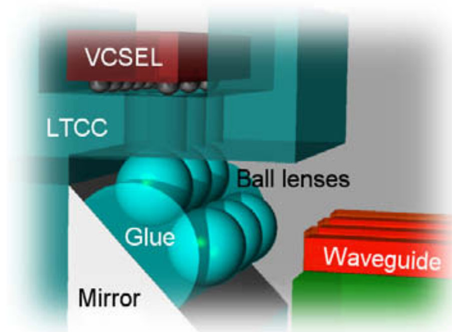

Figure 20. Schematics of the VCSEL-to-waveguide coupling scheme based on ball lenses attached to a mirror. A potential packaging structure using an LTCC module substrate is also presented.

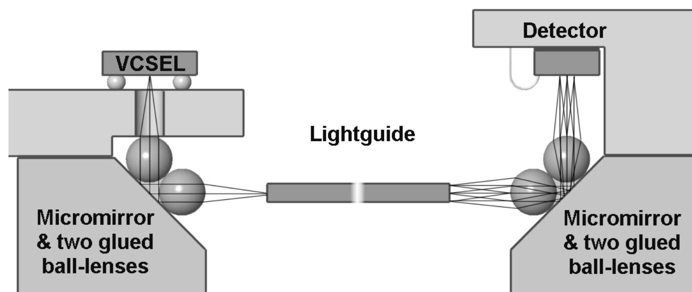

Figure 21. Schematics of the simulated optical path based on ball lenses attached to a mirror. Also, the implemented packaging scheme is shown.

4.1.4 Comparison of coupling schemes

First, a simplified path loss and Monte Carlo tolerance analysis was carried out for the three designed optical systems using the methods presented in Section 3.4. One thousand randomly generated tolerance sets (component misalignments) were generated to calculate the loss histograms for both the transmitter and the receiver ends. Further, the results were used to calculate the loss histograms of the complete link by convolution of both the transmitter and receiver end losses. However, no waveguide losses were included in the total losses. The simulations were performed using a Gaussian source, which is only an approximation of the VCSEL multimode output beam. The VCSEL emitting area diameter was defined to be 10 µm and the beam divergence (full width at 1/e) was set at 14°. The active area diameter of the photodiode was 65 µm. The waveguide had NA of 0.18 and a square cross-section of 100 µm x 100 µm.

Before comparison, both the microlens array and the ball lens-based systems were optimised by selecting the distances between the optical components in such a way that the VCSEL laser beam could be focused on the waveguide front facet and then the same configuration set for the receiver end. In the micro-ball system, the optimisation resulted in 200 µm separations between the lenses and the VCSEL, detector and waveguide ends. In the microlens array system, the separations became 200 µm between the lens systems and the waveguide ends, and 250 µm between the lens system and the VCSEL/detector. In the butt-coupling system, the separations between the waveguide ends and the VCSEL/detector were set at 200 µm. The tolerance values were set to match the expected alignment accuracy of the components in the test assembly, which was to be implemented later on.

The results of the tolerance analyses are presented in the graphs illustrated in Figure 22 for the three coupling schemes, and the results are summarized in Table 1. Table 1 also lists the tolerance values (maximum displacements) used in the modelling as well as the nominal losses of the three systems, i.e. the losses without any misalignments. The placement tolerances were assumed to follow the Gaussian distributions with 3σ values given in the table.

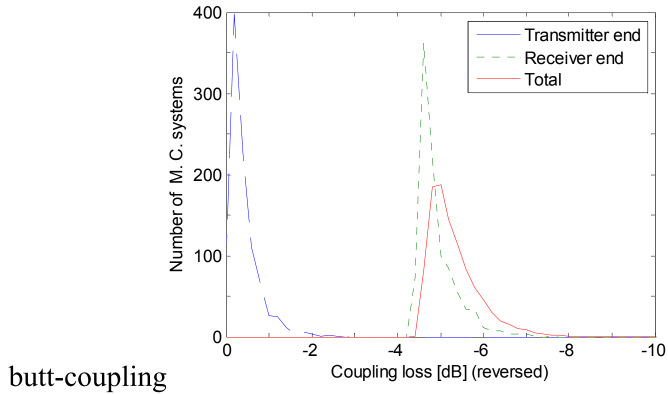

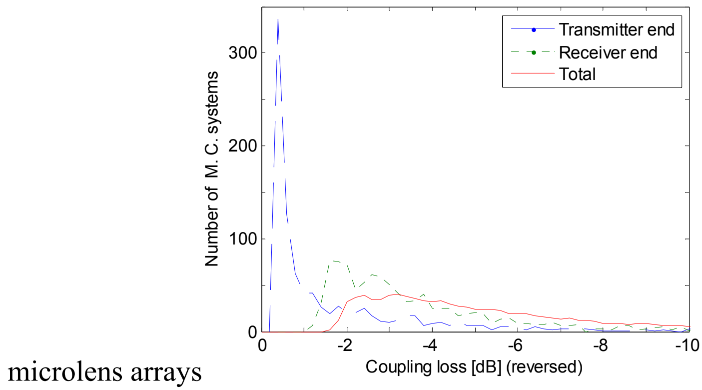

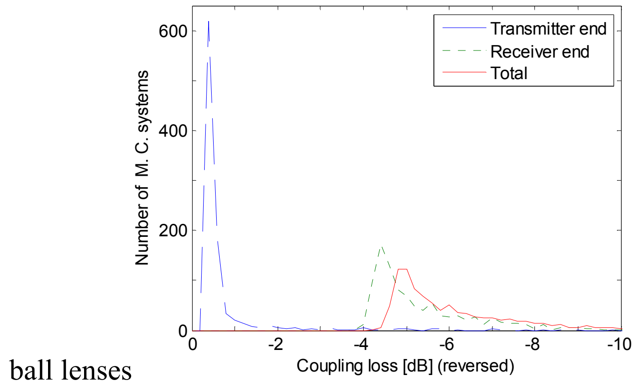

Figure 22. Coupling loss histograms of the transmitter and receiver ends (separately simulated in 1,000 cases at both ends) and of the combined system (calculated by a convolution of 1 million systems and scaled to 1 thousand): upper) butt-coupling; middle) coupling with double microlens array and mirror; lower) coupling with double micro-ball lenses and mirror.

Table 1. The statistical data from the Monte Carlo tolerance simulations (illustrated in Figure 22) of the three coupling schemes for both the transmitter and the receiver ends as well as the combined (convoluted) systems. Also, the maximum misalignments used in the simulation.

	Butt-coupling			**Microlens arrays**			**Micro-ball lenses**		
XYZ-displacements	±20 µm			±20 µm			±20 µm		
XYZ-tilts	±4°			±2°			±2°		
XYZ-tilts of mirrors	-			±1°			±1°		
Coupling	In	Out	Both	In	Out	Both	In	Out	Both
Nominal loss	-	-	4.5	-	-	1.6	-	-	5.0
Max loss	2.98	7.68	10.66	∞	21.32	∞	∞	15.11	∞
Mean loss	0.39	4.89	5.27	1.55	3.25	4.81	0.74	5.60	6.34
Min loss	0.06	4.44	4.49	0.34	1.23	1.58	0.40	4.39	4.79
Mode loss (peak loc.)	0.09	4.69	4.95	0.36	1.67	4.20	0.46	4.69	5.23

The simulation results show that the losses are considerably higher at the receiver than at the transmitter in all coupling schemes. This is mainly because of the relatively large waveguide cross-section (100 µm x 100 µm) compared to the 65-µm diameter of the circular active area of the detector. On the other hand, the low losses at the transmitter reflect the fact that VCSELs can be well imaged on the large waveguide facets. This suggests that, to optimise the systems, the losses at the receiver could be reduced by diminishing the waveguide cross-section area. This could be done up to a certain point without affecting the nominal losses at the transmitter. Nevertheless, the sensitivity to the misalignments would be simultaneously increased at the transmitter.

The highest nominal coupling efficiency is obtained with micro lens arrays. Nevertheless, the shape of the histogram reveals that there are several cases with much lower coupling efficiency, both in in-coupling and out-coupling, i.e. the variation in total loss is high with the used tolerance parameters. The ball lens system is less sensitive to alignment tolerances than the microlens system but the nominal and mean losses are higher. Also, there are some ball-lens systems in

which the transmitter side has very low coupling efficiency (that is not perceivable in Figure 22). The butt-coupling system is rather insensitive to misalignments with these parameters. This is mainly due to the large waveguide cross-section.

4.1.5 Simulation of ball-lens-based interconnect

The micro-ball-lens-based optical channel was also analysed using a more realistic complete path model, which is illustrated in Figure 21. This meant that the rays were propagated from the VCSEL to PD through the waveguide and that the ‘volcano crater’-shaped multimode output beam was used for the VCSEL. The structure was similar to the one implemented in the test assembly. The same dimensional parameters were used as in Section 4.1.4. The waveguide had a square cross-section, two corners were sharp but two corners were slightly rounded to get a waveguide model closer to a fabricated one. Material attenuation of the waveguide was set to 0.05 dB/cm, and the waveguide end facets were defined to have some roughness (Gaussian distribution with 5 degree scatter angle).

The simulated path loss along the nominal optical channel is shown in Figure 23 for two different sizes of the waveguide, with 50 µm and 100 µm edges of the squared profile (with two rounded corners). The coupling loss is practically the same at the transmitter end in both cases, but at the receiver end the loss is much less with the waveguide having 50 µm sides than with the one having 100 µm sides. This is because the optics cannot image the whole output beam of the thicker waveguide towards the detector. However, what is not seen is that the system with the thicker waveguide is less sensitive to misalignments. Also, the low losses at the transmitter reflect the fact that VCSEL can be well imaged to the waveguide facet in a nominal position.

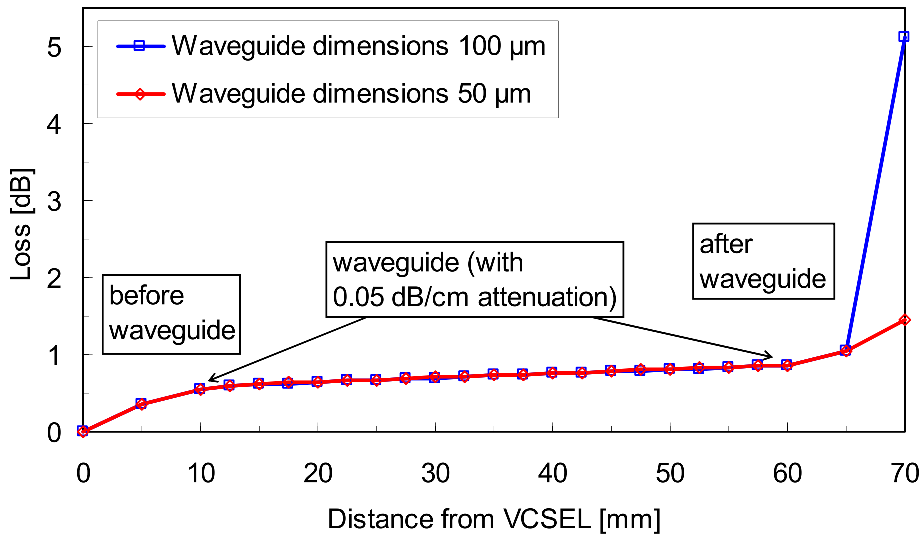

Figure 23. Simulated power path loss along the optical path of the ball-lens-based link when no misalignments.

The tolerance analysis of the full optical channel was made with the 50 µm-thick waveguide. The tolerance modelling parameters are listed in Table 2. The simulation was performed with two different sets of tolerance values, i.e. probability distributions of misalignment. The set A modelled the case called 'passive alignment', which is expected to be realizable using the proposed electronics assembly methods. The set B modelled the 'active alignment' case that is realizable in the laboratory, where the demonstrator can be assembled using precision translation stages while monitoring coupled optical power. The results of the tolerance simulation are presented in Figure 24. They reveal that with the tighter tolerance set most systems have a total transmission loss between 5.0 dB and 5.5 dB, i.e. the assembly tolerances only have a minor effect on the optical power budget. With the looser set, 55% of the systems have transmission loss below 6 dB, but there are also several systems with much higher losses; 3.5% have a higher than 14 dB loss. This implies that, although the performance of the optical channel is predicted to be satisfactory, the manufacturing yield is not expected to be high.

Table 2. Alignment accuracy parameters used in the tolerance analysis of the optical channel based on ball lenses.

Value set	Tolerance parameter	Tolerance value (maximum misalignment)				
		Lenses & mirror (Tx&Rx)	VCSEL	Tx module	Photo diode	Rx module
A passive align	Shift x,y,z	±10 µm	±5 µm	±15 µm	±5 µm	±15 µm
	Tilt x,y	±0.5°	±1°	±1°	±1°	±1°
	Tilt z	±1°	-	±0.5°	-	±0.5°
B active align	Shift x,y	±0 µm	±2 µm	±5 µm	±1 µm	±2 µm
	Shift z	±0 µm	±25 µm	±10 µm	±25 µm	±5 µm
	Tilt x	±0°	±0.5°	±1°	±0.5°	±1°
	Tilt y	±0°	±1°	±1°	±1°	±0.5°
	Tilt z	±0°	-	±1°	-	±1°

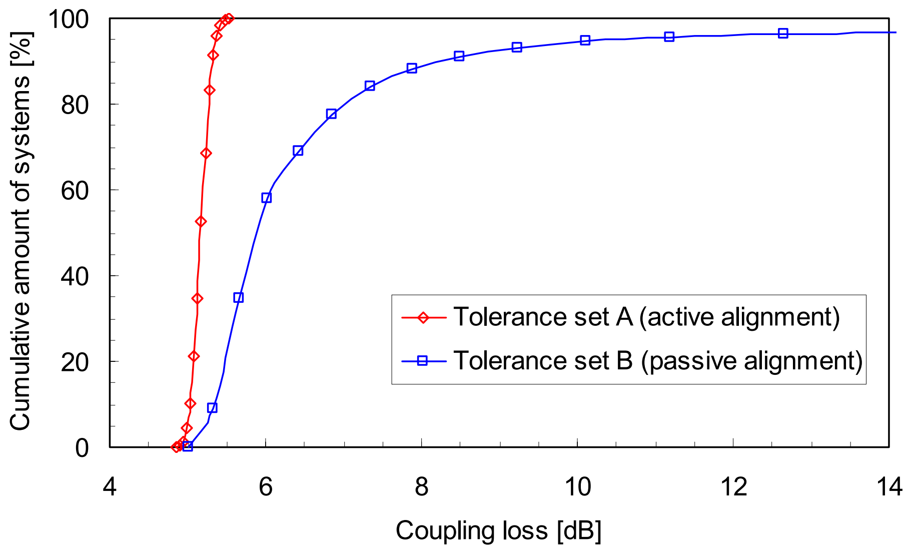

Figure 24. Cumulated loss histograms resulting from the Monte Carlo tolerance simulations of a ball-lens-based optical path with two different parameter sets.

4.1.6 Simulation of double microlens array-based interconnect

A ray-trace-based tolerance analysis with a multimode VCSEL beam was done for the microlens array system as well. The opto-mechanical system model was presented in Figure 19. The simulations also included propagation through a similar 50 µm waveguide as with the ball-lens system. First, the dimensions were optimised for the tolerance simulation. The selected dimensions were: VCSEL-to-1st lens 400 µm, 2nd lens-to-mirror 500 µm, mirror-to-waveguide 150 µm, waveguide-to- mirror 150 µm, mirror-to-3rd lens 400 µm, 4th lens-to-PD 500 µm.

When defining the tolerance parameters, it was assumed that the VCSEL will be flip-chip bonded, the PD will be die-bonded and the double microlens array will be realised by joining the bottom surfaces of two microlens substrates. A potential implementation of the transmitter module structure considered when defining the tolerance parameters is illustrated in Figure 25. It was also assumed that, first, the lens array and the VCSEL/PD chip are positioned and aligned to the LTCC substrate, and then the two modules, the mirrors and the waveguide are aligned with each other. The result of the Monte Carlo tolerance analysis in Figure 26 shows two cumulated loss histograms simulated with the tolerance parameters presented in Table 3. The only difference between the two parameter sets was the alignment accuracy of the microlens array stack. (That is, "lens-to-lens" stands for the alignment accuracy between the two merged lens arrays, and "stacked lens pairs" stands for the alignment accuracy of the double lens module in the optical system.) It can be seen that most of the links exhibit a rather low path loss; 50% of the systems have a loss below 3.5 dB or 5.5 dB, depending on the tolerance set. However, there are many links having unacceptable losses; for instance, 8% or 18% of the systems have a path loss higher than 14 dB – that is, most of the manufactured systems would perform well but the yield would not be very high.

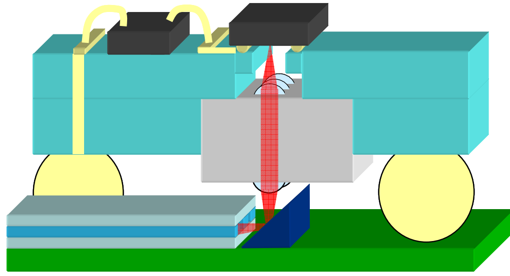

Figure 25. Schematics of the coupling structure based on a double-sided microlens array and a mirror.

Table 3. Alignment accuracy parameters used in the first tolerance analysis of the optical channel based on double microlens arrays.

Tolerance parameter	Tolerance value (maximum misalignment)				
	VCSEL & PD	Lens-to-lens	Stacked lens arrays	Tx & Rx modules	Mirrors
Shift x,y	±5 μm	±10 μm	±5/10 μm	±15 μm	±10 μm
Shift z	±5 μm	±10 μm	±10 μm	±15 μm	±10 μm
Tilt x,y	±1°	±0.1°	±0.5°	±1°	±0.5°
Tilt z	-	-	±1°	±1°	±0.5°

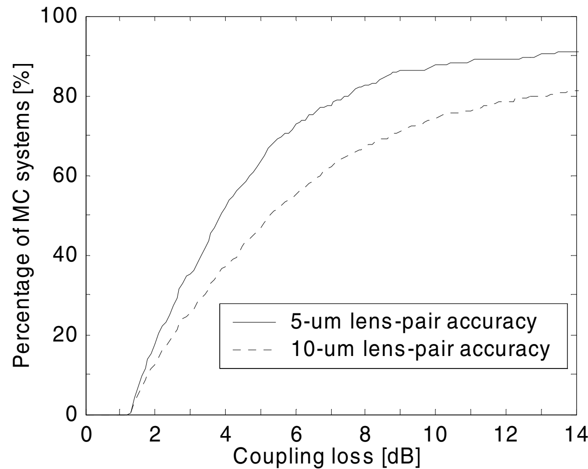

Figure 26. Cumulated loss histograms of the Monte Carlo tolerance simulation of the microlens array-based demonstrator with two different parameter sets.

4.1.7 Alternative coupling schemes with double microlens array

In addition, a comparison was made between the complete system simulated above and a system that is otherwise similar except that the two microlens arrays are attached on separated substrates and thus can have different alignment accuracies. Such a system is illustrated in Figure 27. It is called System 2, whereas the previous one is called System 1. In this case the packaging scheme could be such that the mirror and the other microlens array would be mounted on the board with the waveguide and the other microlens onto the transmitter/receiver module. Consequently, it was assumed that the alignment of the lower microlens array would be less accurate in respect of the VCSEL/PD and the other array, but more in respect of the mirror and the waveguide.

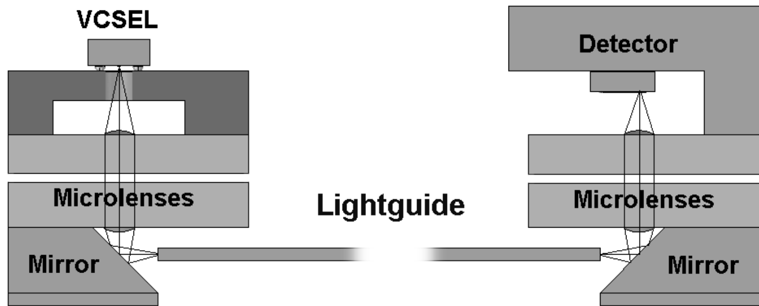

Figure 27. Microlens-based coupling system in which the substrates of the lens arrays are separated.

First, a preliminary optimisation of the system dimensions was done by studying the coupling losses as a function of the separations between the components, both at the transmitter and the receiver. The resulting loss graphs are presented in Figure 28 and Figure 29 for the system with stacked microlenses. The value labelling of the contours correspond to excess loss in decibels compared to loss in the nominal case. In the simulations, the distance between the centre of the mirror and the waveguide facet was fixed at 150 μm. The simulations were performed with two different values of lens ROC: 266 μm and 280 μm. The difference between the graphs was negligible and the results shown in the figures were obtained with 280 μm.

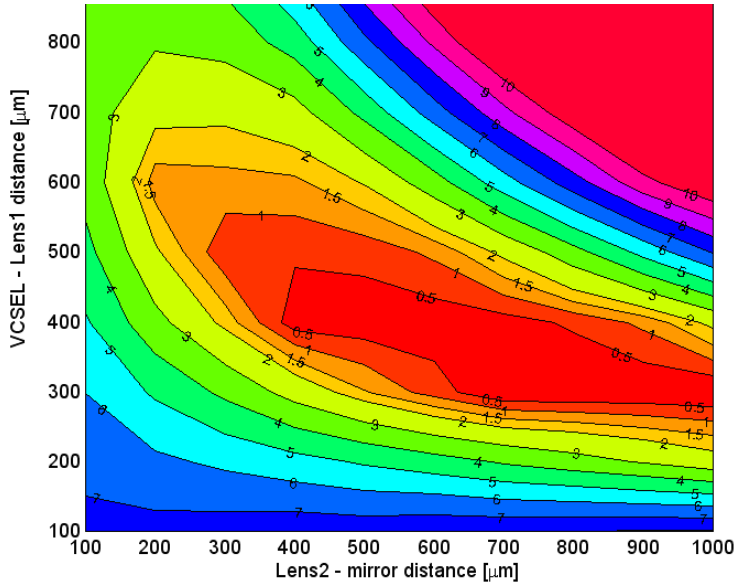

Figure 28. Sensitivity graph for preliminary optimisation of the component separations at the transmitter end in the system with stacked microlens arrays (ROC 280 µm).

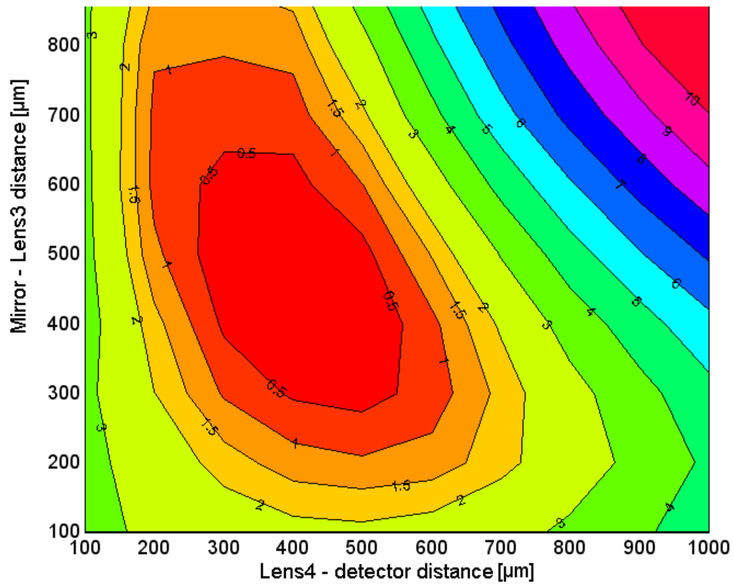

Figure 29. Sensitivity graph for preliminary optimisation of the component separations at the receiver end in the system with stacked microlens arrays (ROC 280 µm).

It should be noted that this kind of analysis and optimisation by sensitivity graphs can only be used as a preliminary study because it does not take the alignment tolerances of the components into account. Thus Figure 28 implies that the smallest loss would be achieved with the 2nd lens-to-mirror separation anywhere between 400…1000 µm (and even longer). However, one should note that if the angular misalignments were included, it is highly probable that the system with shorter separations is less sensitive to the misalignments. Consequently, when using this kind of graph we always chose the shortest separations, which gave the smallest loss, as the preliminary optimum.

From the graphs, 400 µm was tentatively selected for all dimensions: VCSEL-to-1st lens, 2nd lens-to-mirror, mirror-to-waveguide, waveguide-to-mirror, mirror-to-3rd lens, 4th lens-to-PD. In the case of the separate microlens arrays, the separations between the microlens array substrates were first fixed at 100 µm. The simulations resulted in almost similar graphs to the other system; only the optimal lens-to-PD separation had slightly shifted, so the optimum was around 100 µm larger. This is not surprising because the change in geometry is so small compared to the previous case and because in the transmitter the beam is approximately collimated between the microlens arrays around the optimal range. The small change required in the receiver side is because the waveguide output is a large area source (compared to VCSEL) and is not well collimated by the first lens. Consequently, with increased separation between the lenses, increased separation is needed after the second lens as well in order to focus the waveguide output on the PD. Anyway, the same preliminary dimensions were selected for the detailed tolerance analyses of both systems.

Furthermore, a third system (System 3) was also studied. It was identical to the one with the separated microlens arrays, i.e. System 2, except that the refractive index of the lenses was 1.82 (instead of the RI 1.51 of the others). The system with high RI is analysed here and included in the comparison because such a coupling scheme was also implemented and will be presented later in Chapter 5.

The sensitivity graphs for the preliminary optimisation of the separations between the lenses, mirrors and waveguide ends in the coupling system with large RI microlenses are shown in Figure 30, Figure 31 and Figure 32. It is clear that the optimal separations are smaller than in the previous cases. This is expected to be a significant advantage, at least because the excess losses due to

angular misalignments of the components will be reduced (when comparing systems with identical lens and PD diameters as well as with identical waveguides and devices pitches).

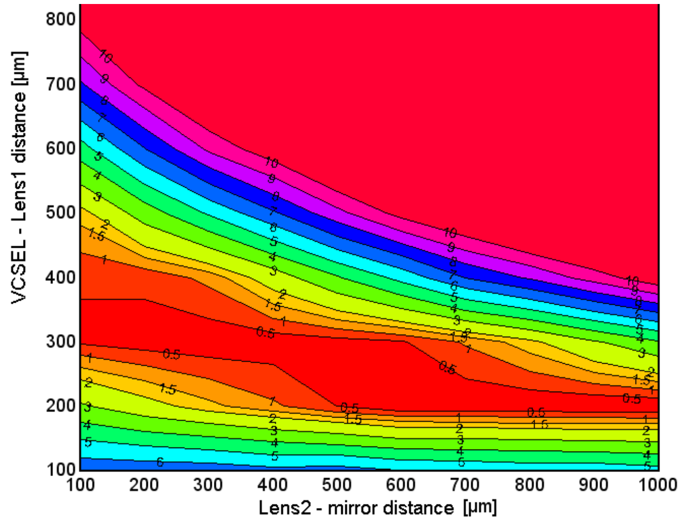

Figure 30. Sensitivity graph for preliminary optimisation of the component separations at the transmitter end in the system based on separate double microlens arrays (having an RI of 1.82).

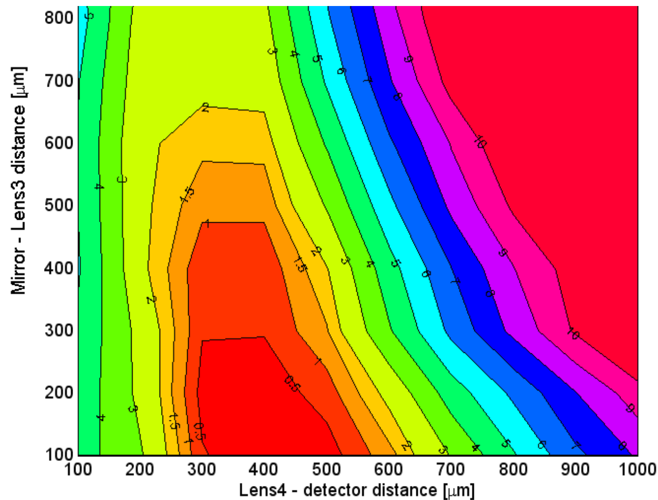

Figure 31. Sensitivity graph for preliminary optimisation of the component separations at the receiver end in the system based on separate double microlens arrays (having an RI of 1.82).

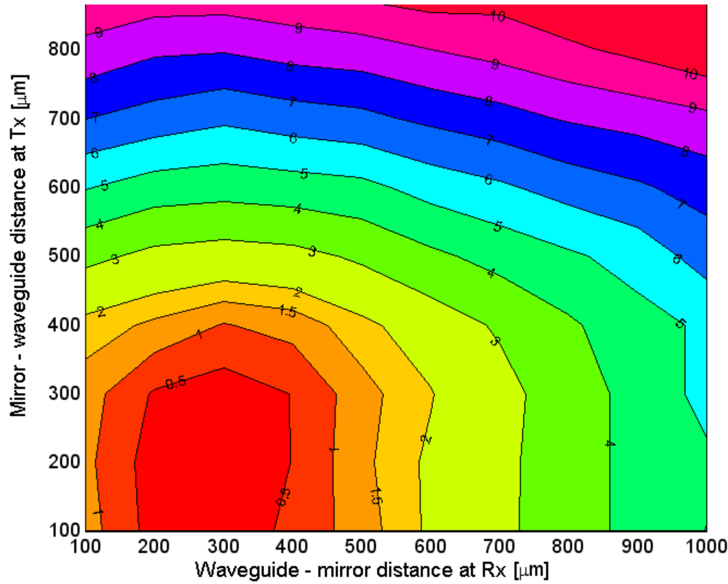

Figure 32. Sensitivity graph for preliminary optimisation of the mirror-to-waveguide separations at the transmitter and receiver ends in the system based on separate double microlens arrays (having an RI of 1.82).

The final optimisation and the comparison between the three designs were carried out by Monte Carlo tolerance analyses of both designs with several slightly different dimensions. The used alignment tolerance parameters are listed in Table 4, and the different system designs are listed in Table 5. The VCSEL-to-1st lens separation was 400 µm in all designs. The resulting loss histograms for the different systems are presented in Figure 33, Figure 34 and Figure 35. Each system was simulated with 300 different Monte Carlo tolerance sets.

Table 4. Alignment accuracy parameters used in the tolerance analysis when comparing optical channels based on double microlens arrays.

Tolerance parameter	Tolerance value (maximum misalignment)				
	Lens array	VCSEL & PD	Tx & Rx module	Mirror	Lens stack (only Sys 1)
Shift x,y,z	±10 µm	±5 µm	±20 µm	±10 µm	±5 µm
Tilt x,y	±0.1°	±1°	±1°	±0.5°	±0.5°
Tilt z	(± 0°)	(± 0°)	±1°	±0.5°	±1°

Table 5. Parameter sets of different component separations used in the tolerance analysis when comparing optical channels based on double microlens arrays. All values are in micrometers. In systems Monte1, Monte2 and Monte3 the mirrors had indefinite sizes, whereas in all other systems (Monte4 ->) square mirrors with 100 µm sides were modelled.

System	**Rlens**	**lens 2 – mirror**	**mirror – lens 3**	**lens 4 – PD**	**mirror – wg**	**wg – mirror**
Monte1_sys1&2	266	400	400	400	150	150
Monte2_sys1&2	266	300	300	400	150	150
Monte3_sys1&2	280	300	300	400	150	150
Monte4_sys1&2	280	400	400	400	150	150
Monte5_sys1&2	280	300	400	400	150	150
Monte6_sys1&2	280	400	400	500	150	150
Monte7_sys1&2	280	300	500	500	150	150
Monte8_sys1&2	280	300	500	400	150	150
Monte9_sys1	280	100	200	400	350	350
Monte9_sys2	280	100	300	400	350	350
Monte10_sys1	280	100	100	400	350	450
Monte10_sys2	280	100	100	400	350	550
Monte11_sys2	280	100	100	500	350	550

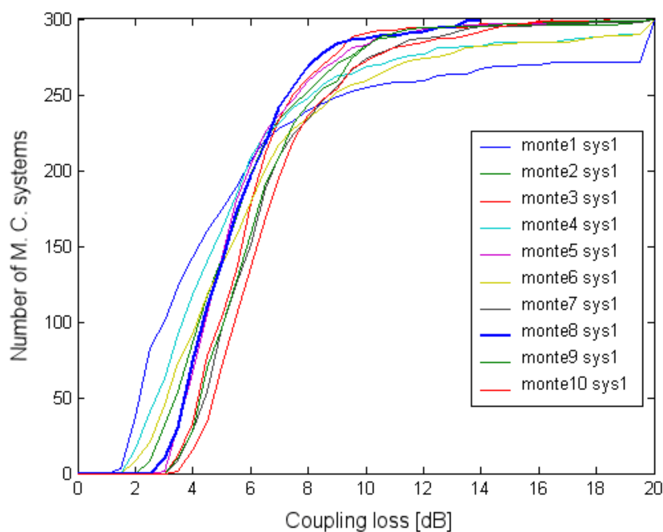

Figure 33. Cumulative path loss histograms from tolerance simulations of full optical path with coupling based on stacked microlens arrays.

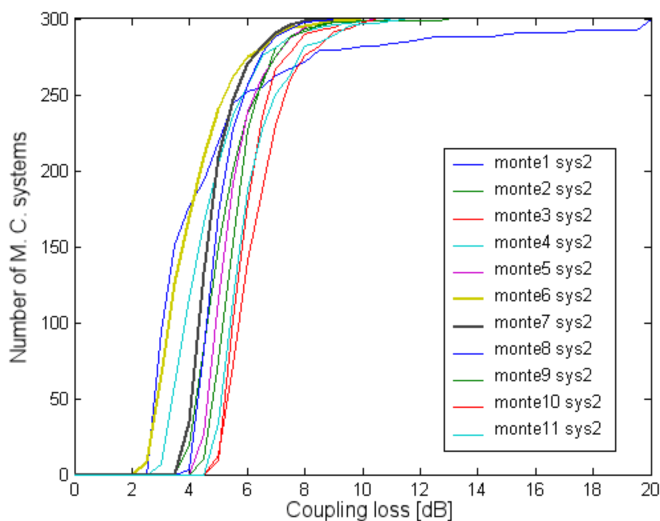

Figure 34. Cumulative path loss histograms from tolerance simulations of full optical path with coupling based on separate double microlens arrays (having an RI of 1.51).

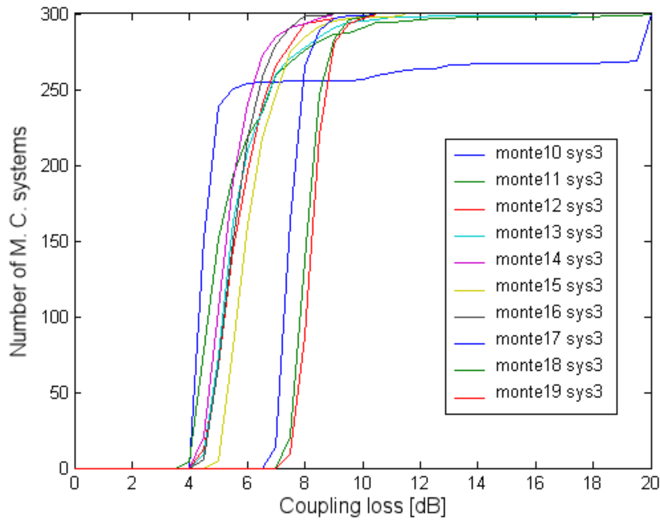

Figure 35. Cumulative path loss histograms from tolerance simulations of full optical path with coupling based on separate double microlens arrays (having an RI of 1.82).

In these simulations, System 1 has lowest minimum loss. However, the same system has also the widest histogram, i.e. its path loss is the most sensitive to misalignments; thus it is not a feasible choice.

In addition, this comparison clearly reveals the benefit of using the separate microlenses in such a way that the other one is mounted on the board. Moreover, the difference to the other solution is clear, even though the alignment of the module was assumed to be rather accurate.

In general, the high refractive index and rather small radius imply that when collimation of the VCSEL beam is aimed, the distance between VCSEL and lens becomes short, namely around 300 µm. This means that, at the lens plane, the diameter of the VCSEL beam will be much smaller than the diameter of the lens. Consequently, no aperture clipping of the VCSEL beam will occur and the alignment tolerances are relaxed. The latter happens because the collimated beam between the microlenses will also have a shorter diameter than the lenses; thus small transversal misalignments between the module and the PWB will have no effect at all. In addition, the rotational misalignments, i.e. tilts, have less effect with smaller distances.

4.2 Implementation of test assembly

A test assembly was designed and implemented to experimentally study the different optical coupling concepts. Its purpose was to serve as a platform that enables testing of both the performance of different concepts as well as studying the implementation and fabrication issues, such as substrate manufacturing tolerances, the assembly methods and their accuracies, as well as electronics implementation for high bit-rate, high-density parallel interconnects. The three optical coupling concepts chosen for the demonstrator were butt-coupling, coupling with double micro-ball-lenses on a micro-mirror, and coupling with double-sided microlens arrays. The optimisation of the optics was described in Section 4.1. The properties of commercially available micro-optical components set some constraints on the implemented structures. Each of the coupling schemes was realised as a four-channel parallel optical link with 10 Gb/s/channel electronics.

4.2.1 Overview of the system

The test assembly was realised as a modular system, which included three complete separate parts with no physical contact: a multi-channel transmitter, an optical waveguide board, and a multi-channel receiver. The structure of the test assembly is illustrated in Figure 36. The transmitter was constructed from an electrical PWB with coaxial input connectors and an optoelectronic front-end module BGA-mounted on the PWB. Identically, the receiver was constructed from an electronic PWB with connectors and a BGA-mounted LTCC-based optoelectronic front-end. A PWB with optical waveguides could then be placed between the transmitter and receiver parts. The optoelectronic front-end modules also included the micro-optic for coupling to waveguides. The input and output coupling structures were located on areas of the LTCC substrates that do have the PWB below them, thus bringing the edge of the waveguide board underneath the LTCC substrate in close proximity to the coupling structures.

The modular approach of realisation was adopted in order to obtain flexibility for characterization. Since the waveguide board is not attached to the transmitter or receiver, it is possible to change or move the board in order to couple an individual transmitter or receiver channel to different kinds of waveguides – that is, to characterise different combinations of transmitters, receivers and waveguides.

The mechanical structure also allows measuring the alignment tolerances with precise positioning using translation stages.

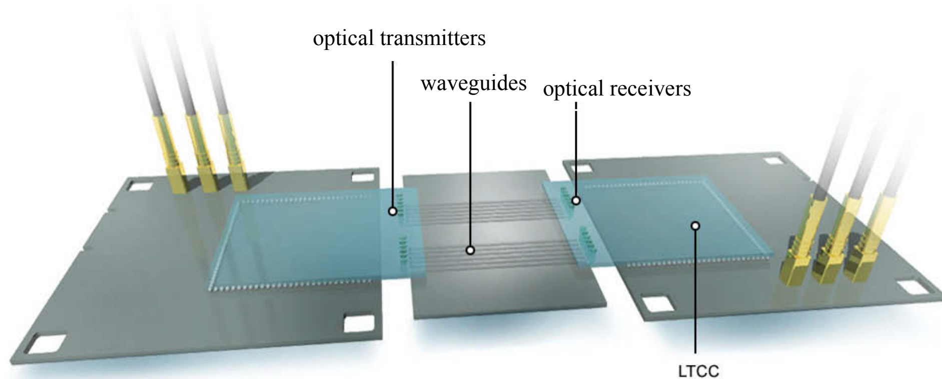

Figure 36. Schematic illustration of the modular test assembly.

4.2.2 Electronics design and implementation

Each of the three optical coupling schemes was implemented as a 4-channel parallel link based on monolithic VCSEL and PD arrays. However, the electronics of the individual channels were implemented with separate components, i.e. by the use of single-channel laser drivers, trans-impedance amplifiers and limiting amplifiers. All coupling schemes have identical schematics design but with slight variations in layout due to the different kinds of optical construction.

Bare die VCSEL arrays fabricated by Ulm Photonics Gmbh (ULM850-TT-A01x12B) were selected. They can show 8 GHz modulation bandwidth at a nominal 3 mW output power at the 850 nm wavelength. The emitting area diameter is 10 µm and the beam divergence (full width at 1/e) around 25°. Each chip included 12 VCSELs, but only four of them were connected to driver circuits in the test assembly. (In addition, conductor traces and pads were also fabricated for some of the remaining VCSELs in the array to enable testing them with a DC drive current.) Bare die laser driver ICs having 10 Gb/s maximum data rate by Maxim Inc. (MAX 3930) were used. The driver uses CML level signalling on both clock and data inputs. It is actually designed for edge-emitting

laser diodes, but it was selected because suitable 10 Gb/s VCSEL drivers were not commercially available at that time. Since edge-emitting lasers typically have lower series resistance and higher operation currents than VCSELs, the minimum modulation current of the driver, 20 mA, would have been too high for the VCSEL. Consequently, a termination resistor was used as a current bypass to protect the VCSEL from excessive drive current.

For the receiver, bare die InGaAs-based PIN diode arrays (PDCA04-65-0850-WB) by Opto Speed AG (today Albis Optoelectronics AG) were chosen. They included 4 PINs each having a 65 µm active area diameter, 9 GHz bandwidth, 260 fF capacitance, and 0.5 A/W responsivity at 850 nm. The chips were wedge bonded. The electronic circuit of each receiver channel was implemented with a TIA and limiting amplifier ICs, both by Maxim (MAX3970 and MAX3971).

The devices were specified to enable around 9 GHz of receiver bandwidth, and the receiver noise floor was around –27 dBm as calculated according to the data sheets. Thus, at the VCSEL nominal output power and 10^{-12} bit-error-ratio, the data link provides around 18 dB optical loss margin.

The top-layer layout design of the implemented test platform is depicted in Figure 37. The electronics were implemented on a single PWB, in which the left part was used for the transmitter assembly and the right part for the receivers. The receiver front-ends, i.e. LTCC-based modules, of all three optical coupling schemes can be mounted on the same PWB. However, there is only a place for one transmitter front-end on the board, so a separate board was assembled for the transmitter of each optical coupling scheme. (An LTCC substrate with all three transmitters would have become impractically large and would have caused reliability issues with the BGA joint.)

The limiting amplifiers and supporting electronics for the VCSEL bias and modulation current control, as well as supply filtering, were constructed on the PWB. This also contained the coaxial card-edge connectors for the inputs and output data and clock signals, as well as the strip lines for differential 10 Gb/s electrical transmission from the connectors to the optoelectronic front-ends. Rogers 4350 high-speed laminate was selected as the PWB material in order to ensure good transmission of 10 Gb/s signals. The boards were manufactured by Aspocomp Oy.

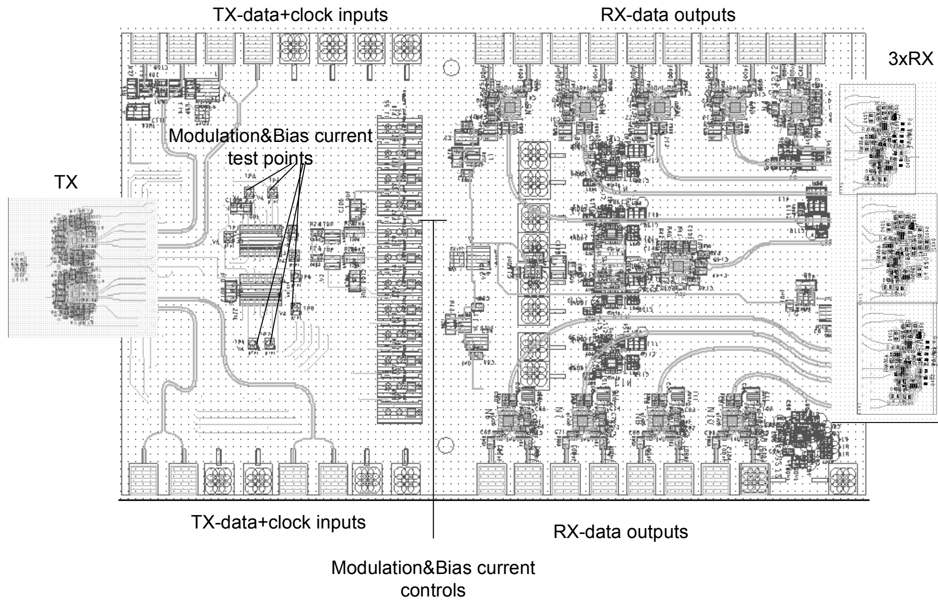

Figure 37. Layout design of the test assembly. The transmitter part with an optoelectronic front-end for one optical coupling scheme is on the left, and the receiver part with all three coupling schemes is on the right.

4.2.3 Fabrication of the test assembly

The LTCC substrates for the optoelectronic front-end modules were fabricated using VTT's pilot process line. The substrate material Dupont 951 was used (see Section 2.4.4), which provided good enough electrical performance. The 3D structures needed for all three optical coupling schemes could be implemented on two LTCC panels; one included substrates for all three different transmitters and the other included substrates for all three receivers.

The electronics was assembled as follows. First, the VCSEL array was flip-chip mounted using thermo-compression bonding, because it requires the highest process temperature. Next, the PD array and the ICs were die bonded and wedge bonded on the LTCC, and the passive devices were soldered onto the LTCC substrates. The other components were surface-mounted and soldered onto the PWB. Finally, the LTCC front-end modules were BGA mounted on the PWB using high-temperature BGA balls and eutectic solder. The assembly of the

micro-optics will be presented in Sections 4.4.1 and 4.5.2. The implemented transmitter and receiver parts are shown in Figure 38. A separate PWB with optical waveguides on top was placed in between them in order to illustrate the interconnect system during characterisation.

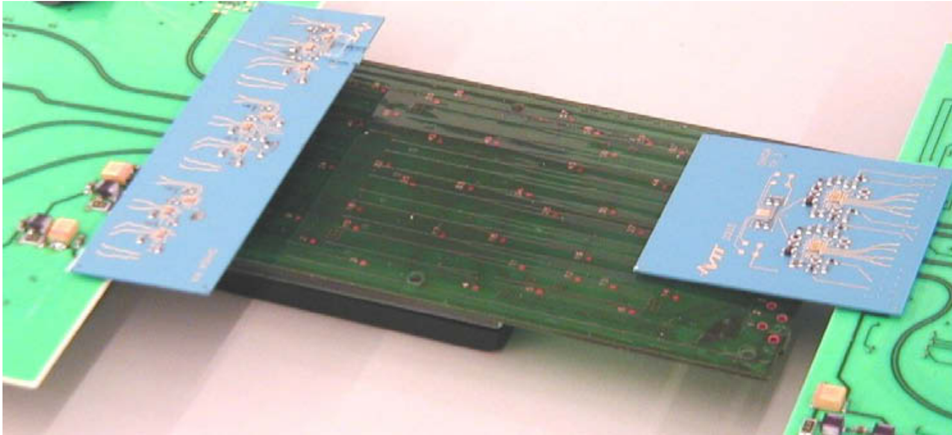

Figure 38. The 4x10 Gb/s transmitter (right) and 3x4x10 Gb/s receiver (left) parts of the test assembly. In addition, a separate PWB with optical waveguides on top is seen in between them.

4.2.4 Optical waveguides

The optical coupling with the different Tx and Rx components was experimentally studied by the use of polymer waveguides, which were fabricated on an FR4 substrate by Teraherz Photonics Inc. (currently Exxelis Inc.). The waveguide and cladding materials were Truemode Backplane™ acrylates by the same company. The refractive indexes of the core and cladding were 1.55 and 1.53 respectively, which corresponds to NA of 0.25. The waveguide cross-sections were approximately rectangular in shape. The dimensions were 40 µm vertical to substrate (height) and 75 µm parallel to surface (width).

The attenuation of the waveguides was measured by the use of the well known ‘cut-back method’, which allows separating the waveguide attenuation from the other optical losses. In practice, the same waveguides were first measured at full length, then cut into shorter lengths and measured again, and so on. The

waveguide substrates were cut using a Disco dicing saw. This resulted in waveguide end facets having a surface roughness of around 170 nm, as measured with a non-contact optical profilometer. In the insertion loss measurement, an output beam from a 62.5/125 µm GI MM fibre was butt-coupled into the waveguide. From the other end of the waveguide, the output power was gathered into a step-index (SI) fibre having a core diameter of 200 µm. The output fibre was further connected to a Newport optical power meter model 2832-C to measure the optical power. The fibre ends were brought into close proximity to the waveguide facets and aligned for the lowest possible loss using a Newport auto-alignment station. The source wavelength was 850 nm, and the launched optical power was measured by butt-coupling the launch and measurement fibres.

The results of the cut-back measurements with three 83 µm-wide waveguides, which were in parallel on the same FR4 substrate, are presented in Figure 39. Straight lines were also fitted to the measured loss values, in order to determine the waveguide attenuation. The variation in the individual loss results was large compared to the waveguide loss difference due to the change in length. This was mainly because of the variation in the coupling efficiency due to the varying quality of the facet surfaces. From the zero-crossing points of the fitted curves, it can be seen that the coupling losses (in and out-coupling in total) were approximately 1 dB. The average of the three line fitting results indicate that the waveguide attenuation was 0.16 ± 0.02 dB/cm.

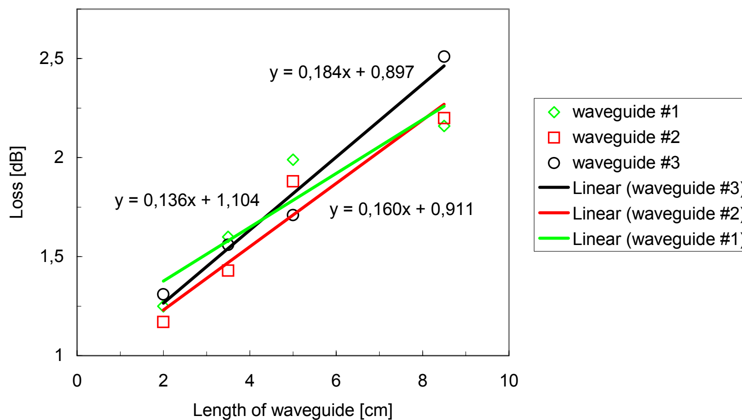

Figure 39. Optical losses of three waveguides measured with cut-back method. Straight lines fitted to the measured losses are also shown.

4.3 Characterisation of butt-coupling

Next, the optical characterisation of the test platform was carried out, starting from the coupling efficiency and the required alignment accuracy of the butt-coupling scheme. The transmitter of the implemented test assembly and the 105 mm-long polymer waveguides, which were presented in the previous chapter, were used. The measurement set-up was similar to the one used in the characterisation of the waveguide attenuation in Section 4.2.4, except that the transmitter was attached to the other arm of the auto-alignment station (instead of the fibre source used before). The position of the waveguide substrate was fixed and the optical output from the other end of the waveguide was collected into a 200 µm-core fibre positioned using the active alignment method.

The smallest coupling loss was almost 6 dB and was achieved when the waveguide was as close as possible to the transmitter. In this case, the separation between the VCSEL and the waveguide end was around 180 µm, defined by the thickness of the LTCC substrate. The attenuation of the 105 mm-long waveguide caused 1.6 dB of the loss. The measured coupling efficiencies versus the misalignment from the maximum efficiency position are presented in Figure 40 and Figure 41. An almost linear decline in the coupling efficiency is observed with increasing transversal misalignment, as well as with increasing separation from the transmitter. The alignment tolerance when the optical power was allowed to drop 1 dB from the maximum value was around ±30 µm in the horizontal and ±25 µm in the vertical direction to the waveguide substrate. The difference between the two directions is mostly explained by the asymmetric shape of the waveguide.

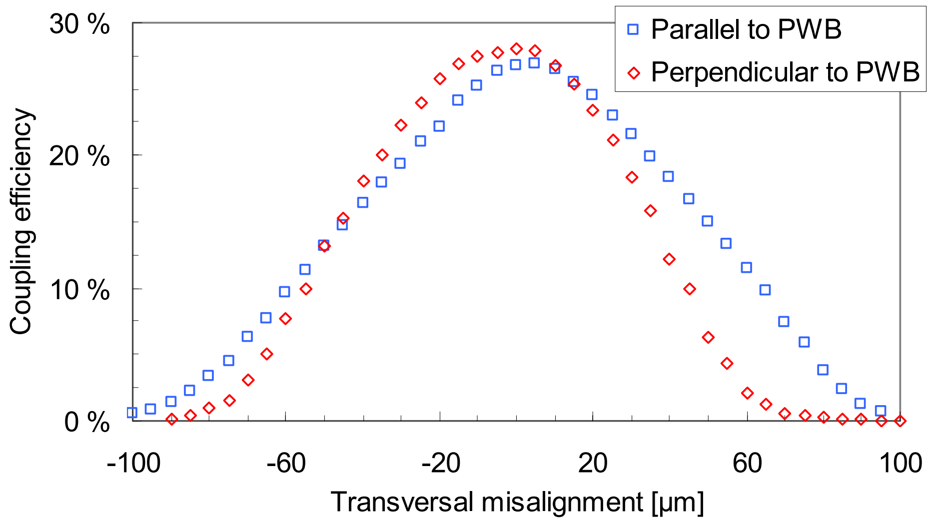

Figure 40. Coupling efficiency from the butt-coupling transmitter to an 83 μm x 40 μm waveguide as a function of transversal misalignment.

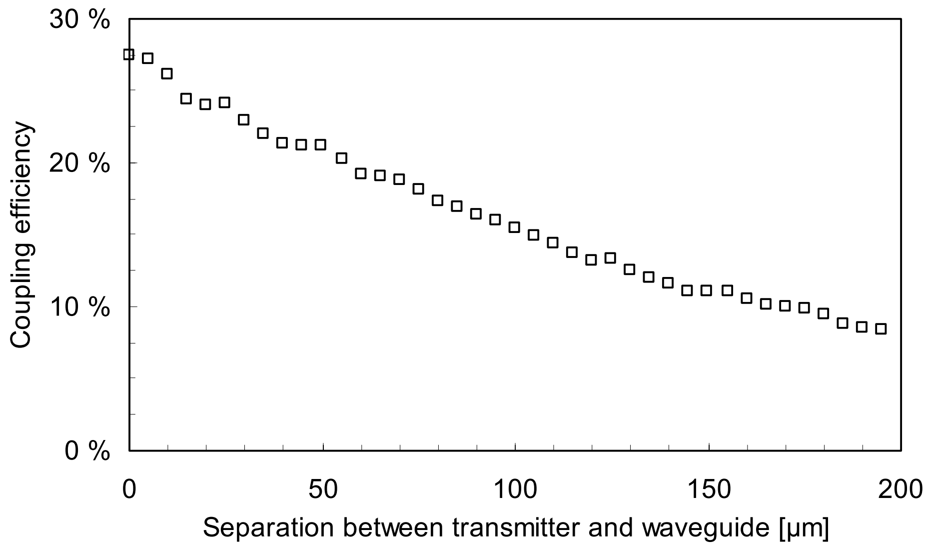

Figure 41. Coupling efficiency from the butt-coupling transmitter to an 83 μm x 40 μm waveguide as a function of separation between them.

4.4 Experiments on ball-lens-based coupling optics

In this section, the implementation and optical characterisation of the test assembly part with ball-lens-based optics is presented. The design of the coupling optics based on ball-lenses on a mirror surface was presented in Section 4.1.3. The ball-lenses were made of BK7 glass by A.W.I. Industries Inc. The ball diameter was 250 µm. First, the mirror was fabricated by grinding a 45° bevel on an edge of a 500-µm-thick glass substrate and subsequently evaporating an aluminium layer on the bevel to ensure a high reflection coefficient.

4.4.1 Assembly

The assembly of the micro-ball-lens transmitter started with the construction of the optical coupling component. Eight ball-lenses were mounted onto the bevel of the glass substrate so that they formed a 2 x 4 ball array and the surfaces of the neighbouring balls were in touch with each other. The balls were attached to the bevel with index-matched adhesive. A photo of the resulted ball-lens-based coupling component suitable for a 4-channel transmitter or receiver is shown in Figure 42.

Figure 42. Micrograph of micro-ball-lenses glued onto an aluminium-coated bevel of a glass substrate.

To mount the optical coupling component (i.e. glass substrate with ball-lenses) to the Tx module, it was clamped to the auto-alignment station with a vacuum gripper tool. The Tx module was attached to a fixed position. First, the lenses

were aligned visually to the through-holes on the Tx module substrate. Next, the position was optimised with the active alignment method of the auto-alignment station. This was carried out by monitoring the output power from the coupling optics with a receiving 62.5 µm fibre, which was mounted onto the other arm of the auto-alignment station. Finally, the position was fixed by gluing the glass substrate to the Tx substrate. Parts of the Tx module with coupling optics are illustrated in Figure 43.

Figure 43. Micrographs of ball-lens-based coupling component mounted on the Tx module substrate having a VCSEL array on the other side; (left) viewed from the rear of the coupling component; (right) side view, where only one ball-lens can be seen.

During the assembly of the coupling component to the transmitter, the needed alignment tolerances of the component were estimated by monitoring the coupling efficiency from the VCSEL to the 62.5 µm fibre through the coupling component. With a –1 dB loss margin to the position with the maximum coupled power, the tolerances were ±4 µm and ±8 µm in the horizontal and vertical directions to the Tx module substrate respectively, and the –3 dB loss margin tolerances were ±7 µm and ±10 µm respectively.

4.4.2 Characterisation of the coupling component

Before mounting the ball-lens-based coupling component onto the Tx module, the component was characterised by using it for coupling light from a 62.5 µm GI fibre (with 0.22 NA) to a similar fibre and measuring the coupled power. The auto-alignment station with the active alignment method was used to place the fibres and the coupling components into the optimal positions. The measured fibre-to-fibre coupling efficiencies are presented in Table 6 from four ball-lens

pairs (i.e. coupling channels) of two different coupling components. For a reference, the measurement was also made in similar geometry but using a mirror without ball-lenses; the resulting fibre-to-fibre coupling efficiency was 1.6%. Because the output aperture of the fibre is much larger than that of a VCSEL and the beam profiles are different (despite approximately the same divergences), no conclusion about the coupling efficiency in the intended application should be drawn from this experiment. Nevertheless, the experiment revealed a quality issue in the coupling components by showing a large variation in the fibre-to-fibre coupling efficiencies (from 11% to 22%) between the eight ball-lens pairs. A potential reason for the variation is that the spreading of the adhesive was not uniform under the lenses and between them; thus there may have been some air bubbles causing reflections. In addition, some minor variations in the positioning of the lenses were also seen.

Table 6. Measured fibre-to-fibre coupling efficiencies using ball-lenses on a mirror as an optical coupling component.

	Fibre-to-fibre coupling efficiency	
Ball-lens pair	Component A	Component B
#1	15%	15%
#2	11%	22%
#3	19%	19%
#4	11%	11%

4.4.3 Characterisation of transmitter-to-waveguide coupling

The coupling efficiency of the assembled ball-lens-based transmitter to a waveguide on PWB was characterised. A 105 mm-long Truemode waveguide having a nominal 67 µm x 40 µm cross-section was used. A similar measurement set-up was used as when characterising the butt-coupled transmitter in Section 4.3.

The measured coupling efficiencies as a function of misalignment in the transversal direction and along the optical axis are presented in Figure 44 and Figure 45 respectively. The lowest coupling losses were around 7 dB. The coupling tolerances for a –1 dB loss budget were ±35 µm when moving in parallel to the waveguide substrate, but only 10 µm or 15 µm when moving perpendicular to the substrate, depending on the direction of the misalignment. The strong asymmetry probably indicates some misalignment in the coupling component, i.e. attaching the balls to the mirror, or a different way of spreading the glue than planned. Along the optical axis (Figure 45), the 1 dB coupling tolerance was 50 µm when reducing the separation between Tx and the waveguide (i.e. moving Tx towards the waveguide) and 110 µm when increasing the separation.

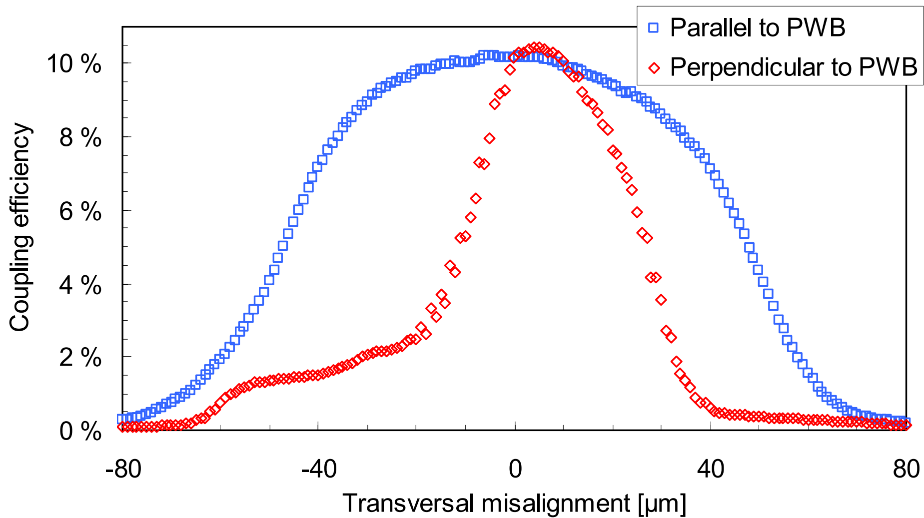

Figure 44. Coupling efficiency of the ball-lens transmitter to a 67 µm x 40 µm waveguide as a function of transversal misalignment to the waveguide.

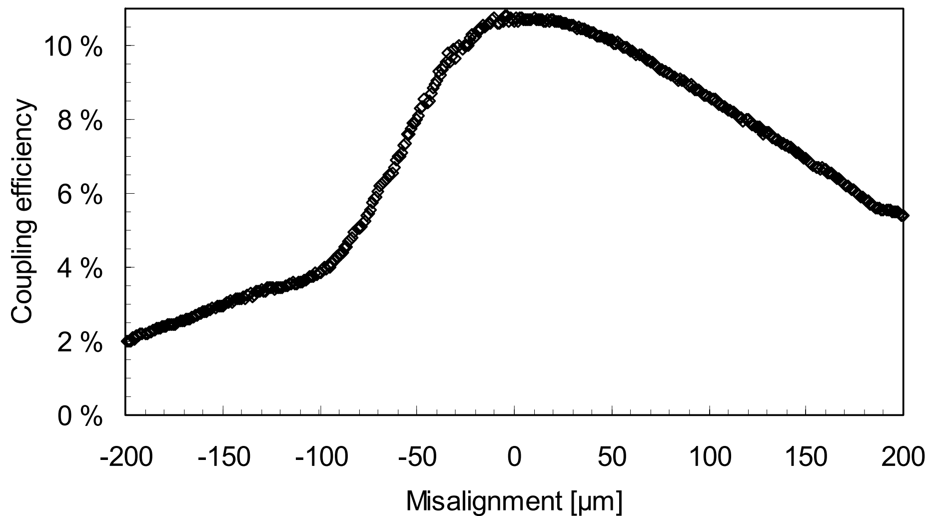

Figure 45. Coupling efficiency of the ball-lens transmitter to a 67 µm x 40 µm waveguide as a function of misalignment in the separation between the transmitter and the waveguide.

4.5 Experiments on microlens-based coupling optics

4.5.1 Microlens array

An important component for parallel optical interconnects is the microlens array. No microlens array with suitable characteristics and specified to survive high temperature could be found for this study. Thus an experiment was carried out to see if the lens changes during reflow. The microlens arrays tested were made by Epigem Limited (UK) of UV-curable acrylate resin, which the supplier claimed exhibited good stability in high temperatures. The material has an upper continuous use temperature of 140 °C, and above this temperature the material softens and may lose some mass due to evaporation of low molecular weight components, but it will not melt (email conversation between Dr. Thomas G. Harvey / Epigem Ltd. and Kimmo Keränen / VTT on 12 March 2004). The lens arrays were patterned from acrylate photopolymer resin on 0.3-mm-thick glass substrates. The specification for the radius of curvature was 266 µm and 250 µm for the lens array pitch and aperture diameter. In the test, the lenses were heat treated in a convection oven using a typical high-temperature reflow profile with

a peak temperature of 260 °C. Visual inspection revealed no changes in the lenses. The shape of the lens' surfaces were measured with an optical profiler (Wyko NT 3300 by Veeco Instruments Inc.). A measured surface profile of a microlens on an array is presented in Figure 46.

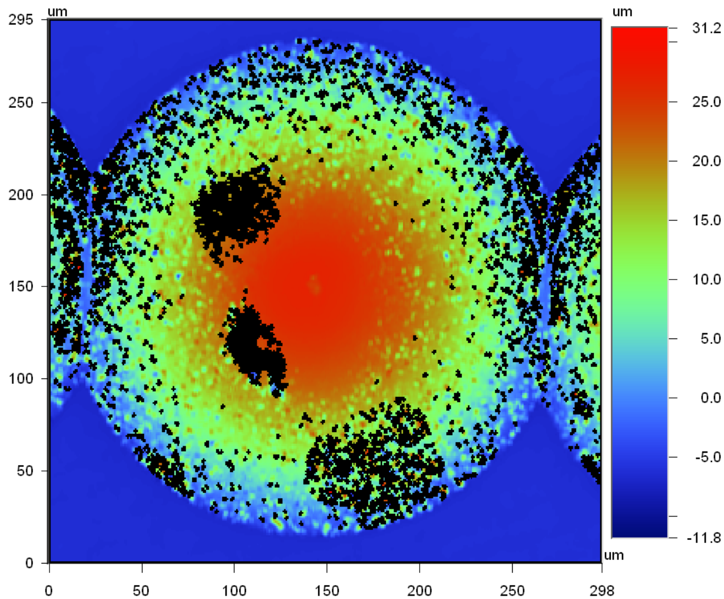

Figure 46. Surface profile of an acrylate microlens by Epigem measured using an optical profiler; data interpolated with a low pass filter.

2D cross-sections of a measured surface profile before and after the heat treatment are shown in Figure 47. This also shows circular arcs, which manually fitted both measurement data. As can be seen, the heat-treated lens has a slightly larger radius than the one not treated, 300 μm versus 285 μm. However, such a small difference can also be due to measurement inaccuracy. Or, since the two profiles were not measured on the same lens, it is possible that the small difference is due to the variation in the microlens manufacturing process, i.e. it already existed before the reflow process.

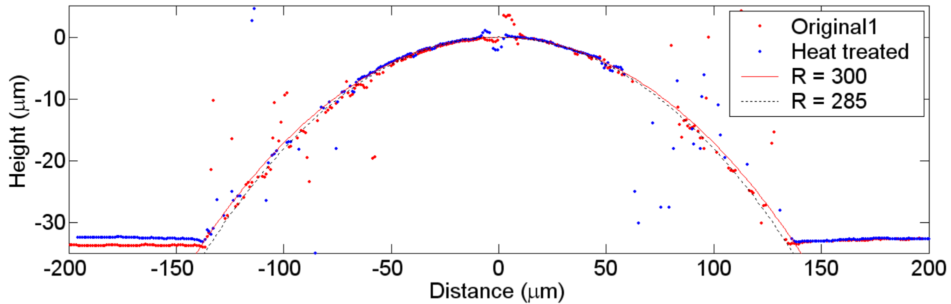

Figure 47. Original and heat-treated (reflow) lens profiles and curves fitted to both data. (The scattering of the measurement results close to the edges of the lens is due to the fact that the optical profiler is not able to follow steep gradients, especially when the surface has low reflectivity, as in this case.)

4.5.2 Assembly

For the test assembly, the double-sided microlens array was realized by joining the bottom surfaces of two microlens substrates. Index-matched adhesive was used. As two microlens arrays by Epigem were joined, the distance between the lens arrays became 0.6 mm. The microlenses were purchased on large substrates including rows of 20 microlenses. After joining the two substrates they were diced into arrays of suitable size for the assembly.

The microlens array stack was actively aligned to the VCSELs. The microlens stack was held with a vacuum gripper on the auto-alignment station and its position was optimised by monitoring the VCSEL-emitted power coupled through the microlens pair to a 62.5 μm fibre, which was attached to the other arm of the auto-alignment station. Finally, the stack was fixed onto the Tx module substrate using UV curable adhesive. A microlens array stack mounted on a transmitter is shown in Figure 48. Before gluing the microlens stack, the transversal alignment tolerances between it and the VCSEL chip were studied by measuring the coupling efficiency into the fibre while scanning both the microlens stack and the fibre in front of the transmitter. The resulting alignment tolerance graph is presented in Figure 49. A –1 dB excess loss is caused with only ±4 μm or ±6 μm misalignment, depending on the direction of misalignment.

Figure 48. A double-sided microlens array on top of the LTCC substrate having a VCSEL array flip-chipped on the other side. The active areas of the VCSELs are seen through the lenses and LTCC via holes.

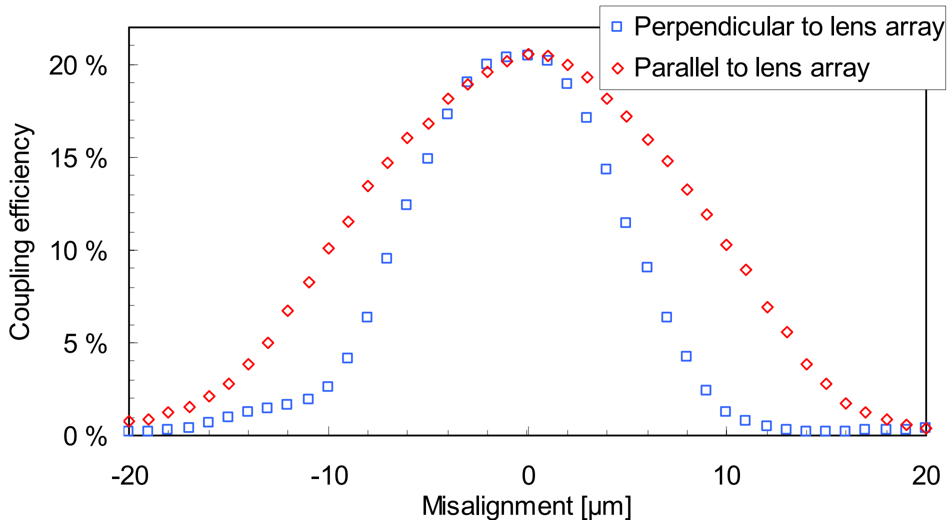

Figure 49. Coupling efficiency from the VCSEL transmitter into a 62.5 µm fibre through double-sided microlens array as a function of transversal misalignment between the transmitter and the microlens array.

On the receiver side, small pieces of blank LTCC substrates were used as spacers to place the microlens array stack at the required distance above the wire-bonded photodiode array chip. The 400 µm-thick spacers were attached with adhesive on the module substrate. Then, the microlens array stack was clamped to the vacuum gripper of the auto-alignment station and placed above the spacers and the PD array. The microlenses were visually aligned to the active areas of the PDs and the position of the stack was fixed with UV-curable

adhesive. The distance between the microlens array and the photodiode surface became 250 µm. The double-sided microlens array assembled above the detector array is presented in Figure 50.

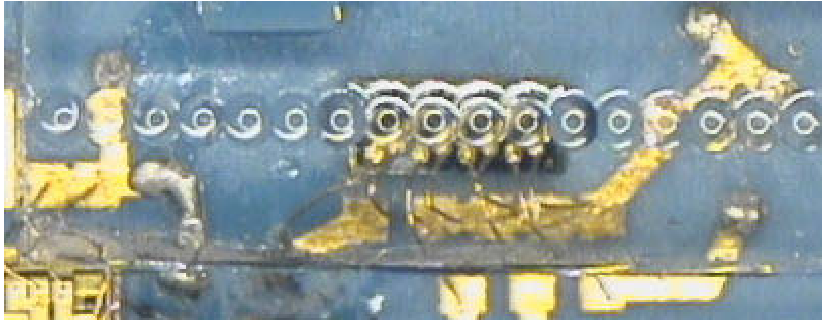

Figure 50. Micrograph of a double-sided microlens array assembled above a photodiode array, which was first bonded onto the Rx module substrate.

Before attaching the microlenses, the alignment tolerance between the microlenses and the detectors were characterized using a 62.5-µm fibre as a source. A smaller than −1 dB increase in loss was measured with the misalignments smaller than ±25 µm in all directions of misalignment.

4.5.3 Characterisation of the transmitter

The coupling efficiency from the double-sided-microlens transmitter to waveguides (by Terahertz Photonics) was characterized as a function of misalignment between the transmitter and the waveguide. First, the position of the transmitter in respect of the waveguide was optimised using a translation stage and monitoring the optical power coupled through the waveguide. The output power from the waveguide was measured by butt-coupling to a fibre with 200 µm core diameter. Four waveguides with core widths varying in the range 50…75 µm were used in the experiment.

The resulting total coupling efficiencies as a function of transmitter misalignment perpendicular and parallel to the optical path, as well as along the optical path, are presented in Figure 51, Figure 52 and Figure 53 respectively. There is no clear trend between the waveguide core width and the absolute

efficiency (although one would perhaps expect the larger waveguide to result in higher maximum efficiency). This is probably because of the varying quality of the waveguide facets. On the other hand, the alignment tolerance curves can be explained by the cross-sectional shape of the waveguide.

By subtracting the other losses in the experiment, the lowest coupling loss between the VCSEL and the waveguide was estimated to be around 7 dB. This is rather low compared to the simulation results, mainly for three reasons: 1) the separation between the VCSELs and the first microlenses was 550 µm, whereas in the optimisations the separation was 400 µm; 2) the divergence of the VCSEL beam was larger than the one used in the simulations; and 3) the shape of the microlenses differed slightly from the spherical surface near the edges of the lens, which was not taken into account in the simulations.

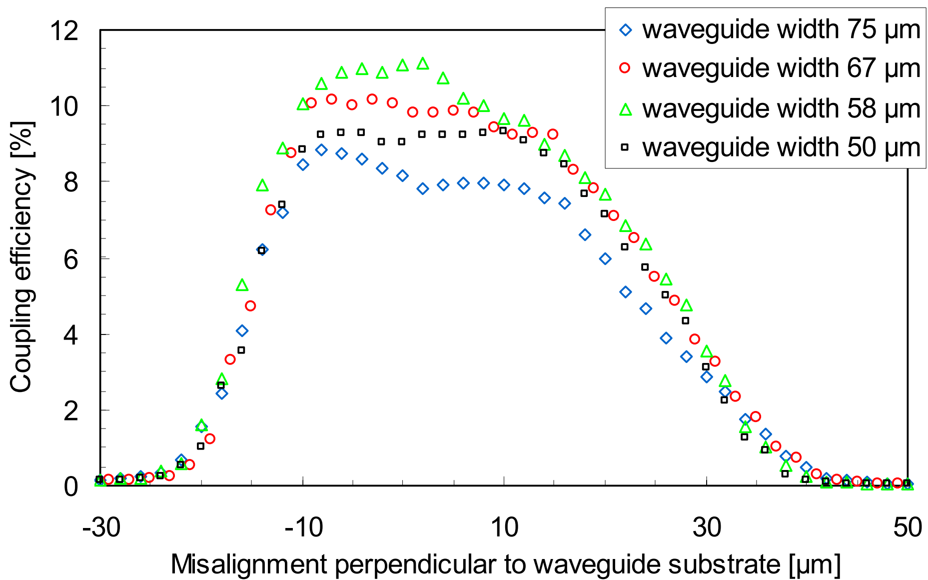

Figure 51. Coupling efficiency of the double-sided microlens-based transmitter to waveguides of different widths as a function of transmitter misalignment perpendicular to the waveguide substrate.

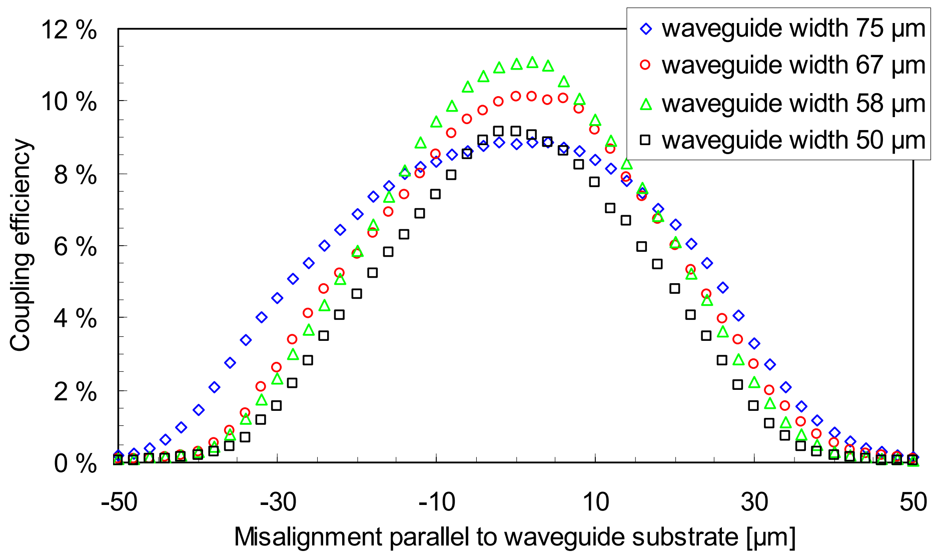

Figure 52. Coupling efficiency of the double-sided microlens-based transmitter to waveguides of different widths as a function of transmitter misalignment parallel to the waveguide substrate.

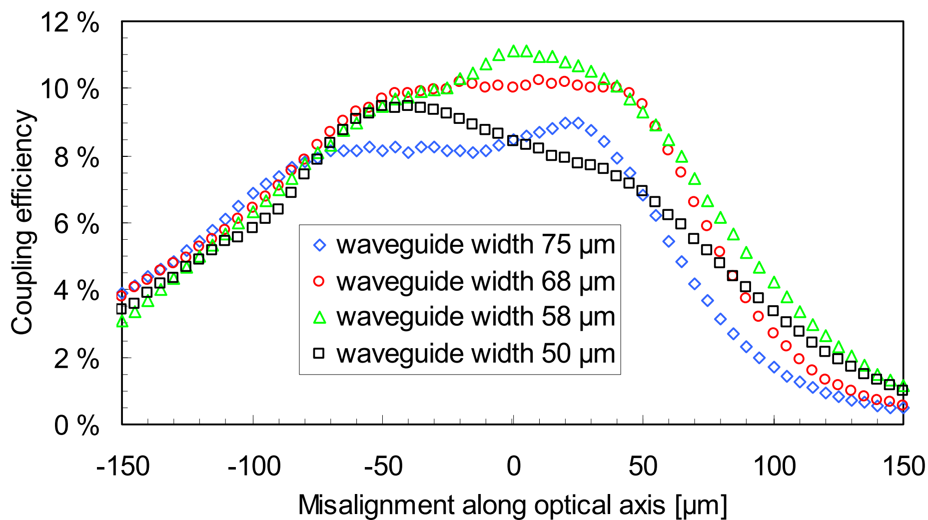

Figure 53. Coupling efficiency of the double-sided microlens-based transmitter to waveguides of different widths as a function of misalignment in the separation between the transmitter and the waveguide.

4.5.4 Characterisation of the coupling efficiency of the receiver

The coupling efficiency from a 67 µm-wide waveguide to a microlens-based receiver was estimated by measuring the signal detect output voltage (RSSI) of the TIA and comparing it to the measured output power from the waveguide and the RSSI conversion ratio specified by the device manufacturer. The minimum attainable coupling loss was 2.5 ± 1.0 dB. Further, the misalignment dependency of the coupling efficiency was studied by moving the receiver in front of the waveguide while monitoring the RSSI voltage. The measured tolerances with misalignments transversal and parallel to the beam are presented in Figure 54 and Figure 55 respectively. The transversal alignment tolerance with almost constant efficiency was measured to be ±20 µm. A –3 dB alignment tolerance is ±30 µm in perpendicular directions and over 350 µm when reducing the separation between the waveguide end and the receiver and over 500 µm when increasing the separation.

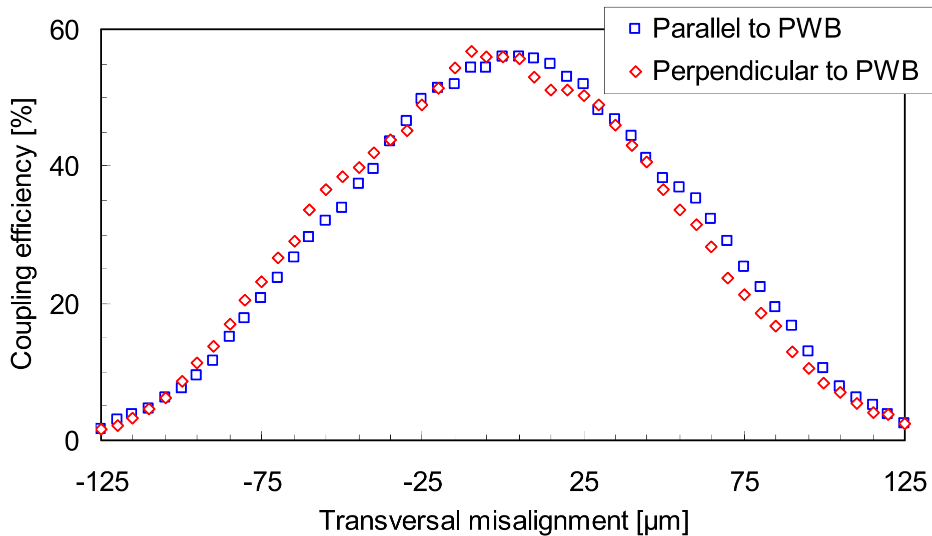

Figure 54. Coupling efficiency from a 67-µm wide waveguide to a double-sided-microlens-based receiver as a function of misalignment transversal to the optical axis.

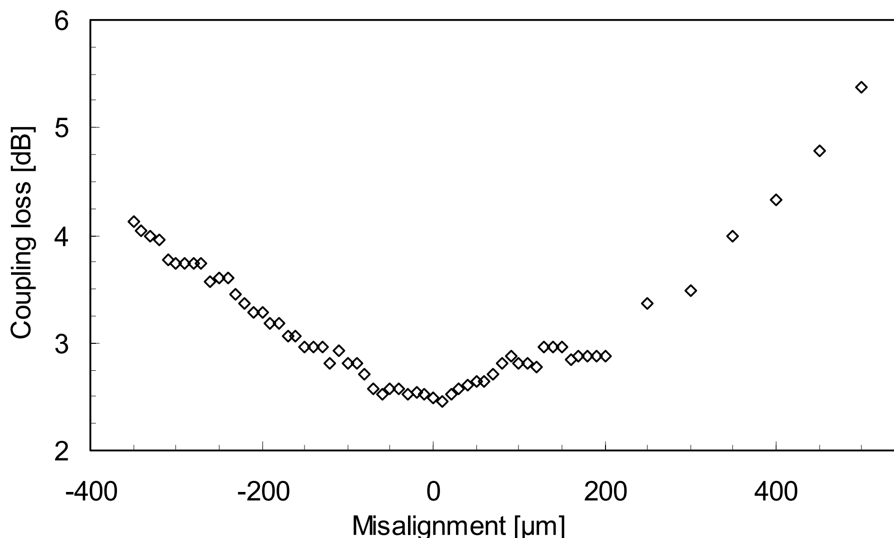

Figure 55. Coupling loss from a 67-µm wide waveguide to a double-sided-microlens-based receiver as a function of misalignment in the separation between the receiver and the waveguide.

4.6 Comparison of coupling schemes

Based on the comparative simulations, the highest nominal coupling efficiency is obtained with microlens arrays. Nevertheless, the shape of the tolerance histogram revealed there are several systems with much lower coupling efficiency, i.e. the variation of total loss was high with these tolerance parameters. The ball-lens system is less sensitive to alignment tolerances than the microlens system, which was also revealed by the experiments. The butt-coupling system was also rather insensitive to misalignments in perpendicular directions. However, it is more sensitive than the others to misalignment along the optical axis.

The measured smallest coupling losses and alignment tolerances of the transmitters based on the three different coupling schemes are summarized in Table 7. The results correspond to coupling into waveguides having 67 x 40 µm cross-sections and 0.25 NA. As mentioned before, the performance of the microlens coupling suffered from the rather large separation between the lens and the

VCSEL. Unfortunately, it is not possible to make a feasible comparison between the presented simulation end experimental results because the calculation results are not directly comparable with the properties that were characterised and also because the simulation models did not exactly match with the implemented ones.

Table 7. Measured coupling losses and alignment tolerances between the transmitter module and a 67 x 40-µm waveguide.

Coupling scheme	Min. loss	–1 dB tolerances [µm]			–3 dB tolerances [µm]		
		Horizon-tal	Verti-cal	Optical axis	Horizon-tal	Verti-cal	Optical axis
Butt-coupling	3 dB	±30	±25	+35	±50	±40	+120
Microlens array	7 dB	±20	±15	–50… +100	±30	±20	–75… +120
Micro ball-lens	7 dB	±40	±20	–50… +100	±50	±25	–5… +200

An additional study was made to get a better idea of the spot size created by the two different coupling optics, i.e. their focusing capability. Their ability to couple between two 62.5 µm GI fibres was measured as a function of transversal misalignment. The receiving fibre was scanned in a plane perpendicular to the beam at a constant distance from the optics, where the maximum coupled power to the fibre was achieved. The micro ball-lens pair that had given the largest coupling efficiency, i.e. pair #2 of component B, was used. The measured power distribution is shown in Figure 56. For comparison, the result from a similar measurement performed with double microlens optics is presented. No mirror was present in the microlens-based optics in this experiment. It is clearly observed that the optics based on ball-lenses creates much a smaller spot size than the one based on microlenses. However, it is also important to note that the fibre output has a much larger aperture and different beam profile than that of a VCSEL.

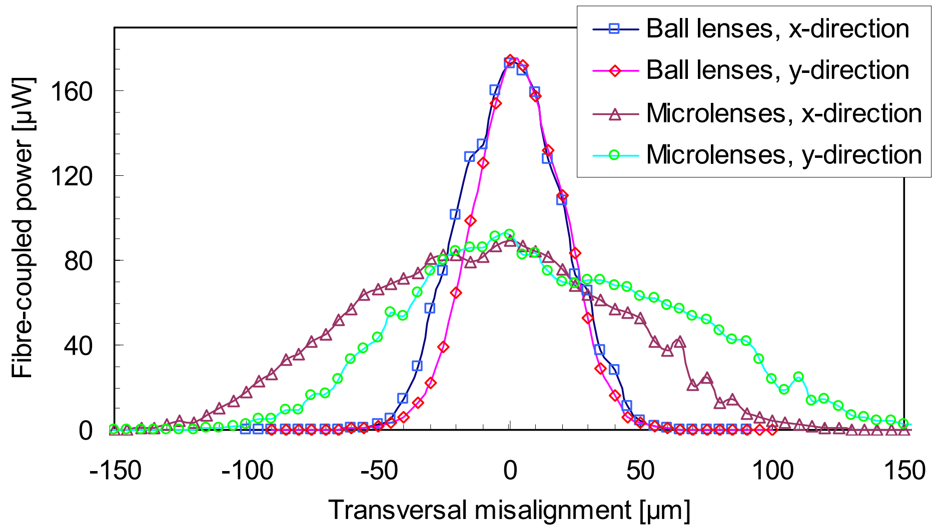

Figure 56. Optical power coupled into a 62.5 µm fibre at focus distance from the transmitter as a function of the transversal misalignment of the fibre. Measurements made with both coupling optics based on a double ball-lens and a mirror and with optics based on a double microlens array.

5. Parallel high bit-rate interconnect integrated on board (Case study II)

This chapter is about the implementation of a multi-channel optical interconnect demonstrator that was fully integrated on a PWB. The presentation includes the design and optimisation of the optical coupling structures, the design of the electronics and packaging, the selection, fabrication and characterisation of the components, and the module and board assembly. The link budget and tolerance analyses are also described. Most of the results presented here were recently published in Karppinen et al. (2006a, 2006b).

5.1 Overview of the demonstrator

The implemented demonstrator (Figure 57) is a 4-channel 10 Gb/s/channel optical link constructed on a standard FR4 PWB. The link consists of 4-channel transmitter (Tx) and receiver (Rx) modules built on LTCC substrates and the optical waveguides processed on the surface of the FR4 board. The length of the straight waveguides between the Tx and Rx modules is 85 mm. The Tx module is based on a VCSEL array chip and a 4-channel driver IC chip, whereas the Rx module is based on a 4-channel PIN detector chip and a 4-channel amplifier IC chip. The modules were BGA-mounted onto the PWB. Microlens arrays and micro-mirrors enable optical coupling from the Tx to the waveguide and from the waveguide to the Rx.

The 10 Gb/s electrical inputs and outputs of the demonstrator are implemented via coaxial card edge connectors and short differential transmission lines to the Tx and Rx modules on the PWB. The somewhat unusual shape of the PWB was selected in order to satisfy three prerequisites: 1) the length of the interconnection, i.e. the waveguide, was to be maximised; 2) no dimension of the board was to exceed 12 cm to be able to fit it into a spinner for spin casting the optical layers; 3) the distance between the coaxial connectors and the Tx/Rx module had to be minimised since 10 Gb/s electrical signal can only be carried a short distance with strip lines on the FR4 board due to the high-frequency dielectric losses.

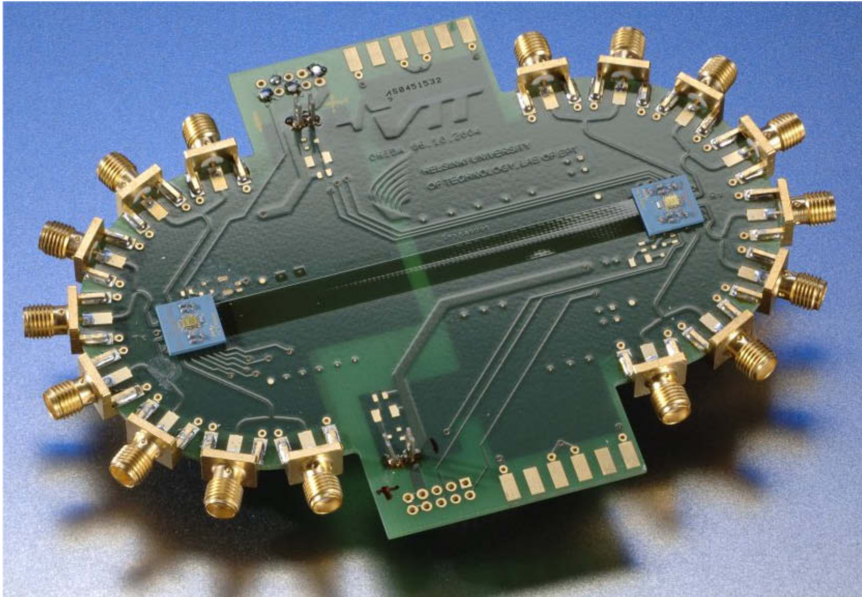

Figure 57. Photo of the 4-channel optical interconnect demonstrator on an FR4 PWB. The optical waveguide layer is on the board between the (blue) transmitter and receiver modules.

The schematic structure of the transmitter and receiver modules and the optical coupling scheme are illustrated in Figure 58. An identical opto-mechanical design was used at both ends of the data link. Bare die devices were used and the through-holes, i.e. 'optical vias', on the LTCC substrate formed an essential part of the module structure and assembly. The coupling between the VCSEL/PD array and the waveguide array is based on two microlens arrays and a mirror. The other lens array was mounted on the LTCC, whereas the other one and the mirror were mounted on the PWB. With this design, an expanded and collimated beam was obtained between the two microlens arrays, i.e. between the module and the board, thus relieving sensitivity to misalignments in the BGA board assembly.

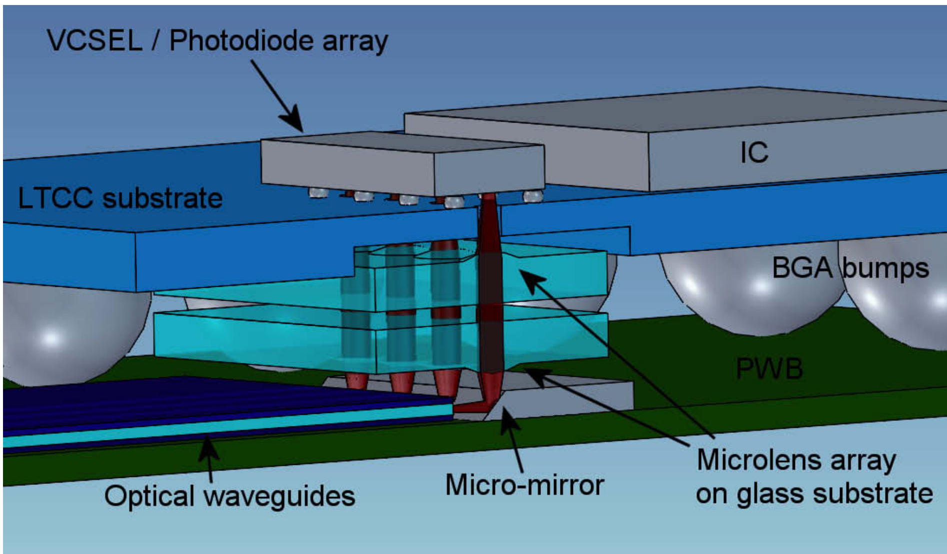

Figure 58. Schematic illustration of the Tx and Rx module packaging and optical coupling structures of the demonstrated interconnect.

5.2 Design

In this section, the selection of components, as well as the optimisation and analysis of the optical design, are presented. The electronics design is briefly described.

5.2.1 Electronics and device selections

The transmitter and receiver modules were built on LTCC multilayer ceramic substrates. The electronics of the transmitter is based on a 4-channel VCSEL driver IC and a monolithic VCSEL emitter array, whereas the receiver is based on a 4-channel receiver IC and a monolithic PIN-photodiode array. In addition to these, only a few discrete capacitors were needed to construct the Tx and Rx electronics. The bandwidth of the active devices enables a maximum of 10 Gb/s/channel data transmission. The layout of the top side of the demonstrator board is depicted in Figure 59. The layouts of the Tx and Rx modules are also shown on the board layout as slightly enlarged.

The monolithic 4-channel VCSEL driver IC (part number PX6414) and receiver IC (part number PX6424) were commercially available devices by Primarion Inc. (which is now part of Zarlink Semiconductor Inc.). Both ICs were manufactured in a SiGe BiCMOS process. The 10 Gb/s differential data inputs operate on CML logic levels. The receiver IC includes both transimpedance and limiting amplifiers for each channel to provide direct CML level differential data outputs. The specified sensitivity of the receiver IC is 20 $\mu A_{peak\text{-}peak}$ for 10^{-12} BER. The supply voltages of the Tx and Rx components are 3.3 V, and the current consumption is around 180 mA for Tx and around 240 mA for Rx, when all channels are enabled (Primarion 2002a, 2002b). The ICs include serial control interfaces, which allow the user to set laser bias and modulation currents separately for each of the four channels and, in the receiver, to adjust the signal detection levels of the channels.

The 4-channel VCSEL array was a monolithic die (part number APA4101040000) made by Avalon Photonics Ltd. (which is now part of Bookham Ltd.). The main specifications are: threshold current 1 mA, output optical power 2.5 mW at 8 mA drive current, differential resistance 50 Ω, modulation bandwidth, emitting wavelength 850 nm, 10 Gbps, and e^{-2}-full-width beam divergence 28 degrees (Avalon Photonics 2003).

The 4-channel photodiode array die (part number LX3045) was made by Microsemi Inc. It is a GaAs-based PIN photodiode with coplanar electronic contact layout to enable 8 Ghz bandwidth and 50 Ω characteristic impedance. The device capacitances are 0.3 pF, the diameters of the circular active areas are 75 μm, and the responsivity is 0.6 A/W at 850 nm (Microsemi 2002).

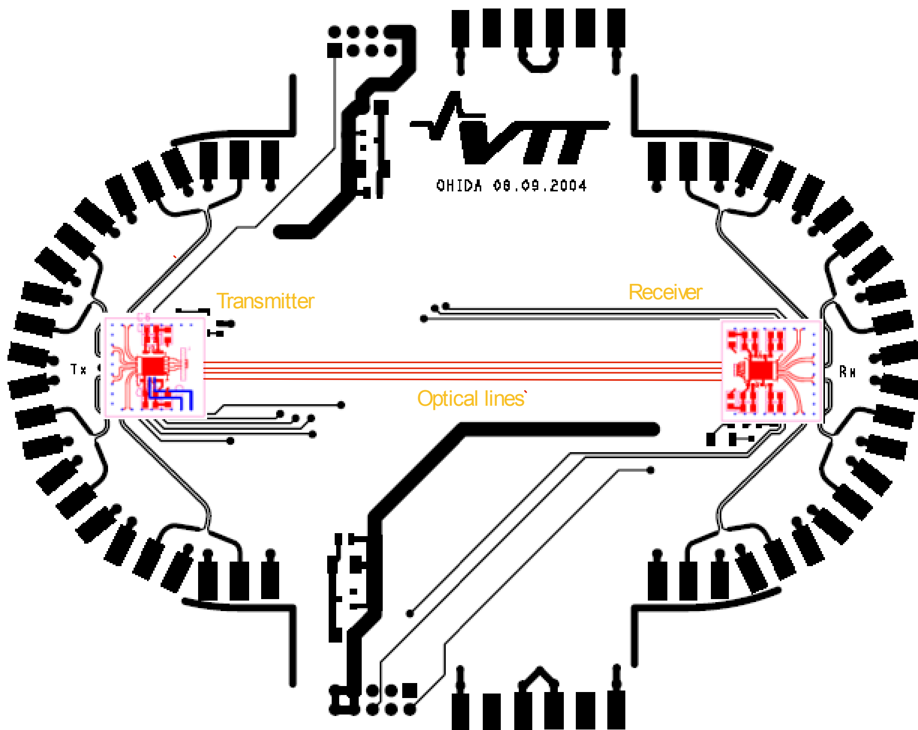

Figure 59. Top-layer conductor layout of the demonstrator. The layouts of the Tx and Rx modules, i.e. the LTCC substrates, are enlarged here (1.5-fold) compared to the layout on the PWB.

5.2.2 Optical coupling components and packaging design

The optical coupling structure between the transmitter and receiver modules and the waveguides was based on double microlens arrays and micro-mirrors, as illustrated in Figure 58. The micro-mirror was a piece of 100-µm-thick glass sheet with one edge forming a 45° mirror facet and coated with aluminium for high reflectivity. Because suitable micro-mirrors were not commercially available, they were fabricated at VTT. The selected microlenses had a high refractive index of 1.82 (at 850 nm), focal length 340 µm, and the radius of curvature was 275 µm. They were fabricated from glass material on a 0.3 mm-thick substrate made of the same glass.

The polymer optical waveguide layer was fabricated as a three-step lithographic pattern transfer process onto the PWB. Each of the three polymer layers was first spin-cast onto the PWB and then photopatterned with chrome mask. The layout of the waveguide layers is illustrated in Figure 60 and Figure 61. Alignment marks for the assembly of the microlens array and the module were included in the core layer mask.

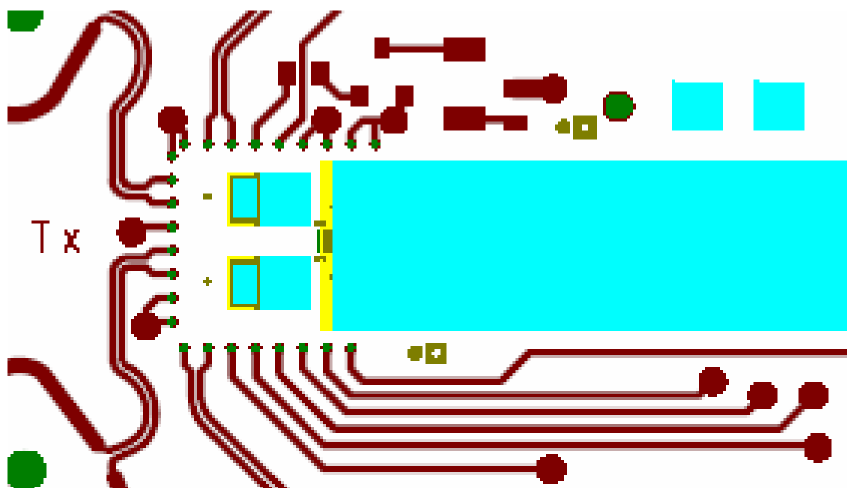

Figure 60. Layout of the optical layers on top of the PWB layout. Only part of layout area around the Tx module is shown. The under-cladding layer is drawn in yellow, core layer in light green, and top-cladding in blue. Brown represents the top layer conductors and green represents the solder mask openings.

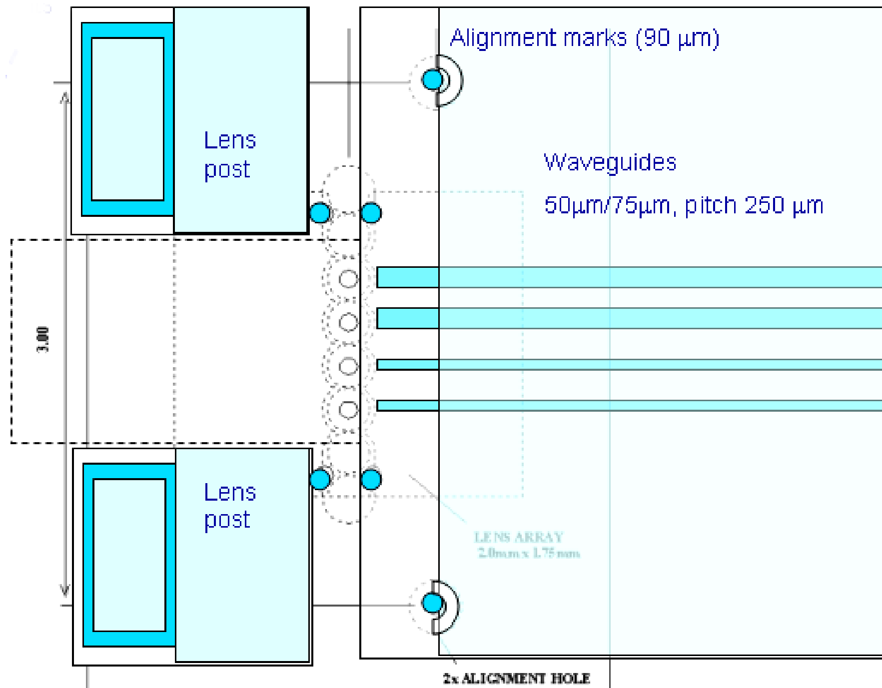

Figure 61. A closer view of the layout of the optical layers on top of the PWB layout. The placing for the micro-mirror, the microlens array, and the two LTCC alignment holes are also illustrated.

The optimised coupling structure and implemented packaging structure are presented in more detail in Figure 62. The coupling optics and the waveguide layer structures were identical at both the Tx end and the Rx end of the link. The mirror was mounted on the PWB in front of the four waveguide end facets. This was enabled by patterning a cavity onto the optical layers. The "lower" microlens array was then mounted above the micro-mirror using the supporting posts, which were also fabricated in the optical waveguide process on the PWB. The optical layer facets served as mechanical stoppers for the mirror component; on two sides its place was defined by the 'lens supporting posts', and the separation between the mirror and the waveguide end facets was defined by the edge of the under-cladding layer.

The other microlens array was mounted into a cavity on the bottom of the LTCC substrate. The 'optical via' holes were used as registration marks to enable alignment with the top-mounted VCSEL/PD array.

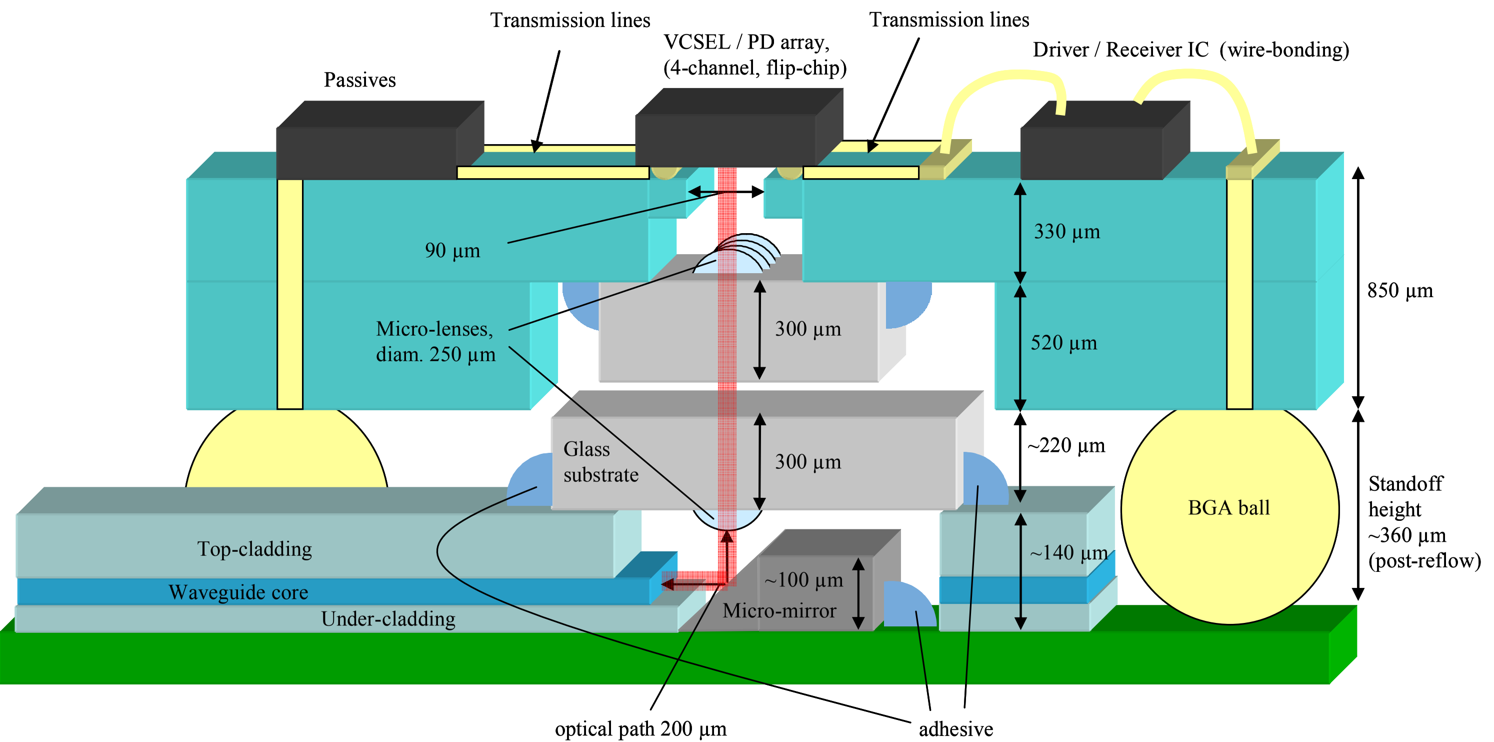

Figure 62. The structure of the transmitter and receiver modules and the optical coupling elements. Some assembly methods and key dimensions are also presented.

In conclusion, the lithographically patterned optical layers and the LTCC substrate were to enable fully passive alignment and assembly of the micro-optical parts. All the optical components were fixed using UV-curable adhesives.

5.2.3 Optimisation of coupling structure

The ray-trace-based sensitive and tolerance analyses to study this kind of coupling scheme were presented in Section 4.1.7. The benefits were compared to a coupling structure with a stacked double microlens array, as well as to a similar coupling but with lower diffractive index microlenses. However, not all the parts were exactly the same in the previous analysis as in the demonstrator – for instance, the VCSEL and its beam divergence was different.

Therefore, before manufacturing, an optimisation of the coupling structure was carried out by the use of a Monte Carlo tolerance analysis, which was based on ray-trace simulations of the complete optical path from the VCSEL to the PD. The estimated mounting tolerances of the components, i.e. input parameters, were the same as used earlier, i.e. they were listed in Table 4. In addition, another tolerance analysis was run with 1.5 times bigger mounting tolerances, i.e. all tolerance parameters were 1.5 times those in Table 4. The main figure of merit in optimising the system to be implemented was to have low sensitivity to misalignments in the predicted alignment tolerance range. However, the total loss should also be rather low when the components are in their nominal positions.

The results obtained with the estimated alignment tolerances are shown in Figure 63, the results with looser tolerances are shown in Figure 64. It is clearly seen that some systems become much worse if the component alignment accuracy is 1.5 times looser than originally expected. On the other hand, some systems are not much affected by this kind of change in the alignment tolerances.

From these simulations, a system that corresponds to parameter set Monte4 and Monte16 in the figures was implemented in the demonstrator. This selection was made, because, in addition to weak sensitivity for misalignments and a rather low minimum low, this system has identical dimensions both at the Tx and Rx end, which would simplify the implementation. The dimensions of the optimized structure are presented in Figure 62.

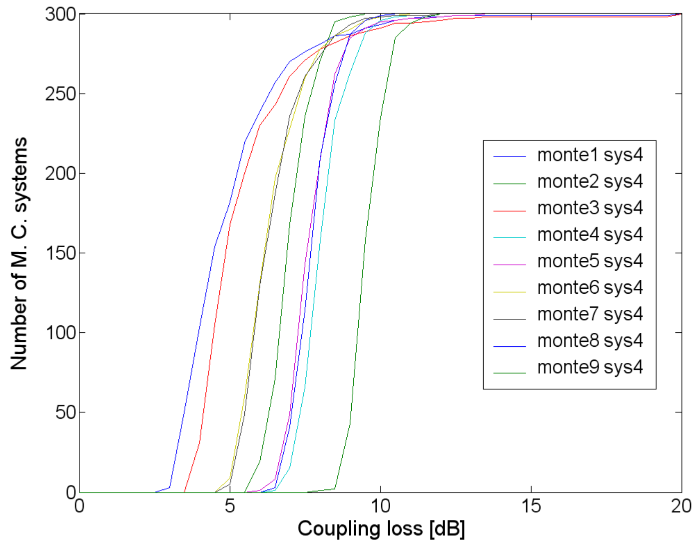

Figure 63. Cumulative path loss histograms from tolerance simulations for the optimisation of the demonstrator coupling structure.

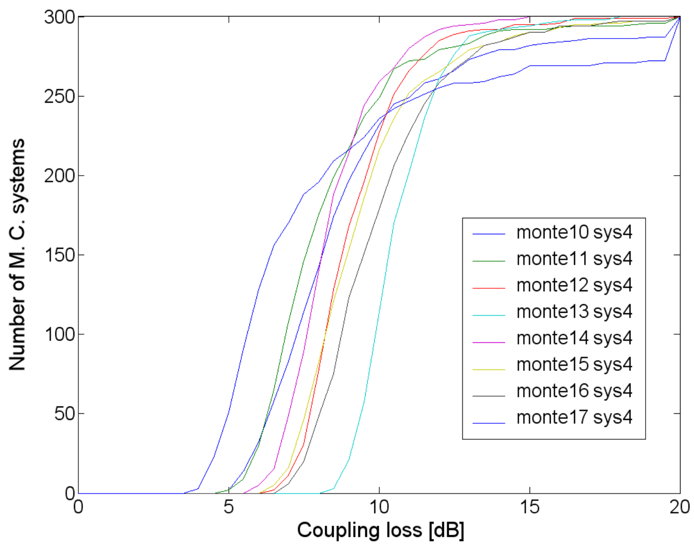

Figure 64. Cumulative path loss histograms from tolerance simulations for the optimisation of the demonstrator coupling structure, but using 1.5 times looser tolerance parameters.

5.2.4 Final tolerance analysis of the implemented structure

A final tolerance analysis of the demonstrator was also performed using the realized placement tolerances. In this case, the system model also included the edge of the under-cladding layer, which blocks part of the optical beam between the waveguide end facet and the micro-mirror. The material attenuation of the waveguide was specified to be 0.55 dB/cm. The simulation included ten thousand Monte Carlo systems in order to get more accurate results than in the optimisation phase. The result of the final Monte Carlo tolerance analysis of the implemented demonstrator is presented in Figure 65. The simulation predicts that the total optical loss is less than 15 dB in 80% of the assembled demonstrators. However, there will be some cases with around 20 dB loss.

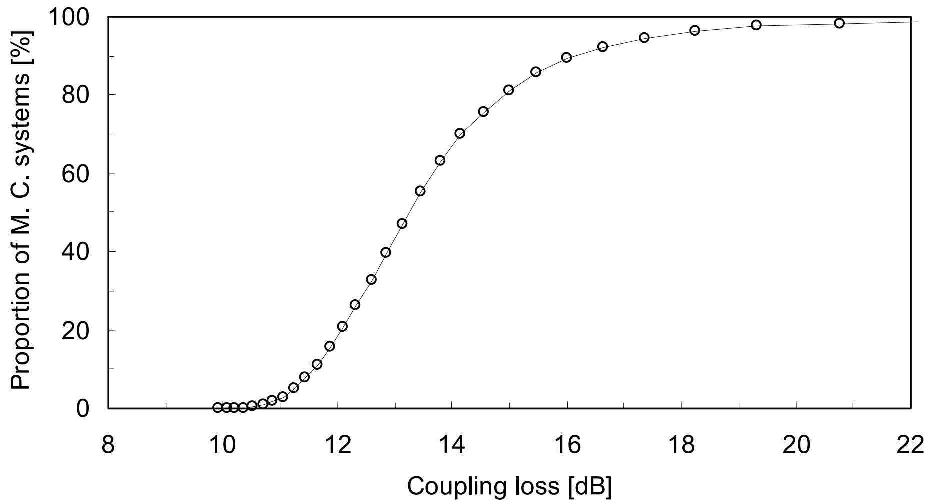

Figure 65. Cumulative distribution of Monte Carlo systems simulated with the parameters of the implemented demonstrator.

According to the device specifications, the maximum feasible peak-to-peak modulation of the transmitter is around 2 mW, and the specified receiver sensitivity is 32 μW with 10^{-12} BER. This results in a 18 dB maximum power margin. Therefore, one can conclude that, according to the simulations and the specified performance of the devices, an assembled demonstrator will operate properly with a probability of circa 95%.

5.3 Manufacturing of components for demonstrator

After optimisation of the demonstrator design, the components were fabricated as described in this section. The work included processing of LTCC module substrates, PWBs with waveguides, and the micro-mirrors. The other components, i.e. the electronic and optoelectronic devices, as well as the microlens arrays, were acquired as commercially available components.

5.3.1 Module substrate manufacturing and characterisation

The LTCC substrates of the transmitter and receiver modules were designed to have a dielectric tape and conductor layer structure as shown in Figure 66 and Table 8. The layer count and the thicknesses of the tape layers were selected so that the depths of the microlens cavity and through-holes, as well as the total substrate thickness, were optimised in the module structure (Figure 62). In addition, the aim of the substrate design was to achieve the best possible mechanical accuracy of the through-holes, of which some were used as both 'optical vias' and alignment marks and some as alignment marks only. The alignment was chosen to be based on the through-holes because they could be processed during the same via punch run as the 'optical via' holes, thus avoiding the misalignments that could be caused between different process steps, such as the alignment during the lamination of the substrate layers.

Two panel versions having slightly different thicknesses of tape layer 1 (see Table 8) were processed. This was because the final BGA standoff height, which affects the separation between the two microlens arrays, was not precisely known at the time of the substrate manufacturing. So the different substrate thicknesses gave two options to adjust the lens separation.

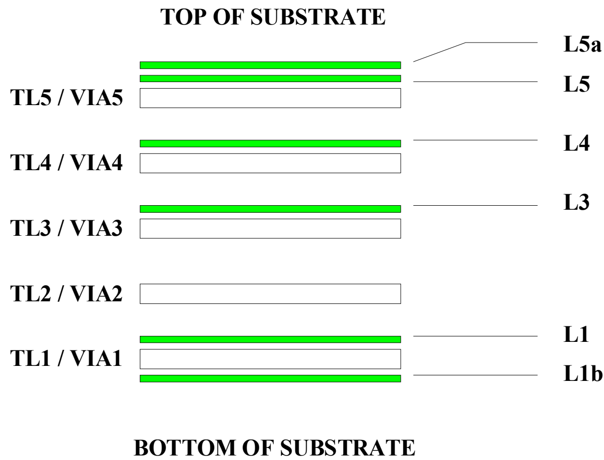

Figure 66. Layer designation of the LTCC substrate of the transmitter and receiver modules.

Table 8. Layer structure of the LTCC substrates.

Layer	Tape thickness original / after sintering	Via diameter (punched)	Conductor designation	Conductor material
5			L5a	Au
5	165 / 130 µm	110 / 150 µm	L5	AgPd
4	114 / 90 µm	150 µm	L4	Ag
3	114 / 90 µm	150 µm	L3	Ag
2++	165 / 130 µm	150 µm		
2+	165 / 130 µm	150 µm		
1	165 / 130 µm 1) 254 / 205 µm 2)	150 µm	L1	Ag
1			L1b	AgPd

1) substrate versions 3 & 5
2) substrate versions 4 & 6

DuPont 951 tape system was selected since it has proven to be suitable for implementing accurate structures for micro-optical alignment (see Section 2.4.4). The dimensions of the Tx and Rx module substrates were 10 mm x 10 mm. Thanks to the identical opto-mechanical designs of the Tx and Rx, both Tx and Rx substrates had the same kind of layer structure and could be fabricated in the same LTCC panel. The substrates were manufactured using VTT’s pilot process line with 11.8 mm x 11.8 mm panel size. Each fabricated LTCC panel included 13 pieces of the transmitter substrates and 12 pieces of the receiver substrates.

All conductor layers were screen printed, and no post-fired process steps were needed. Two manufacturing circles were needed for adjusting the process parameters, such as lamination and sintering conditions, before the (challenging) mechanical tolerance specifications were satisfied across the whole panel. A total of four panels were fabricated, two of which had 165 µm-thick Tape layer 1 and the other two with 254 µm-thick Tape layer 1 (as shown in Table 8). Photographs of the top and bottom of a fabricated panel are shown in Figure 67.

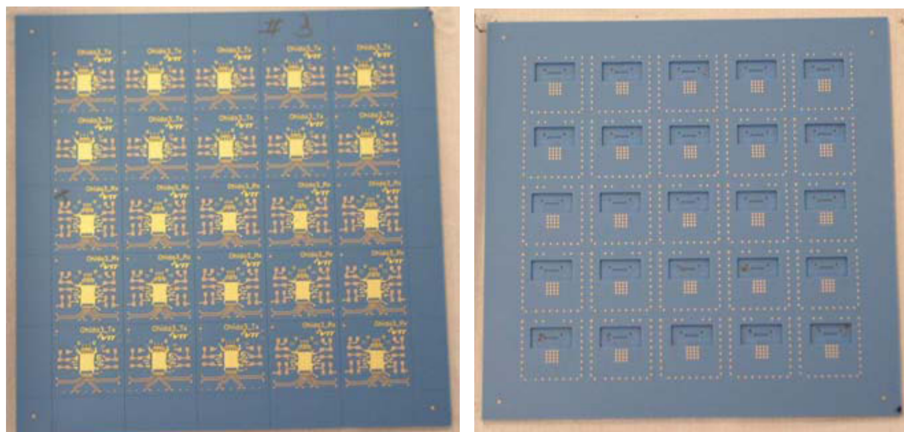

Figure 67. LTCC panel of 13 Tx and 12 Rx module substrates: left) component side (top); right) BGA and microlens side (bottom).

Figure 68 presents a closer look at the bottom of a module substrate. Part of the substrate is cropped out of the picture. Thus only part of the BGA pads can be seen. The registration mark for substrate manufacturing is seen in the upper-left corner. The rectangular cavity for the microlens array is in the centre of the picture, and in the centre of that cavity is an array of four 'optical via' holes. They are surrounded by four other through-holes, which were used as alignment marks during the assembly of the microlens array. The other two through-holes, which are further from the cavity centre, were intended to be utilised in the alignment of the module to the alignment marks on the O/E-PWB during BGA assembly. Below the microlens cavity there is a 4 x 4 array of thermal vias, which were added to improve the heat dissipation from the driver/receiver IC. It was estimated that the cooling of the bare ICs is effective enough due to convection in the laboratory environment. However, if more effective cooling was needed, the pads of the thermal vias could be directly connected to a heat sink or via the PWB using BGA bumps.

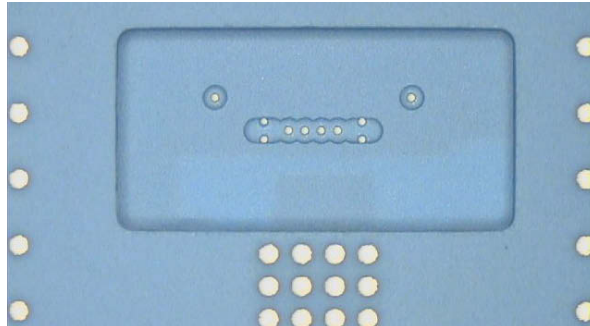

Figure 68. Bottom of the LTCC module substrate (only part of it is shown).

Part of the top of a Tx module substrate is seen in Figure 69. The array of the four ‘optical via’ holes is seen in the centre (as white spots). They are surrounded by the flip-chip contacts for the VCSEL array. The similar through-holes for alignment purposes are also observable. In addition, part of the placement area for the driver IC is seen here with some wire-bonding pads, as well as solder pads for the SMD passives.

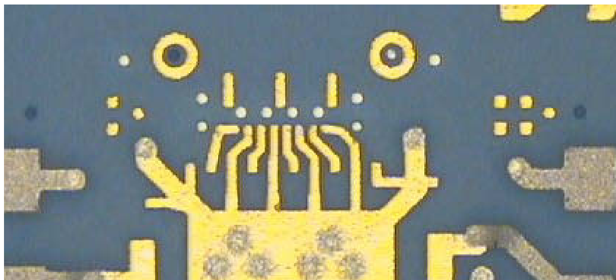

Figure 69. Component side of the Tx module substrate (only part of the module area is shown).

The fabricated panels were characterised using a SmartScope measuring microscope, which typically has ±2 µm measurement accuracy. The flip-chip pads had line widths in the range 70…75 µm. The diameters of the ‘optical vias’ and alignment through-holes varied between 90…95 µm. The diameters of the BGA pads were 270…280 µm and their pitch was 998 µm.

The alignment accuracy between the screen-printed flip-chip pads and the punched through-holes was also studied for all the module substrates in the four panels. Some offset misalignment may be caused as the pads are fabricated in different process steps, and it is critical to keep these errors small in order to avoid causing bad contacts or contacts with the neighbouring pads during the flip-chip bonding. This is because the VCSELs and PDs are aligned using the 'optical via' holes as alignment marks (for the active areas) and, consequently, this also results in adequate alignment between the flip-chip bumps and pads. The measured placements are presented in Figure 70 and the results are in Table 9. The misalignments along the x-axis and y-axis varied between 0…18 µm across the panels, in most cases being only a few microns. This was considered small enough compared to the used stud bump diameter of around 75 µm and to the smallest separations between the flip-chip pads (smallest pitch was 125 µm).

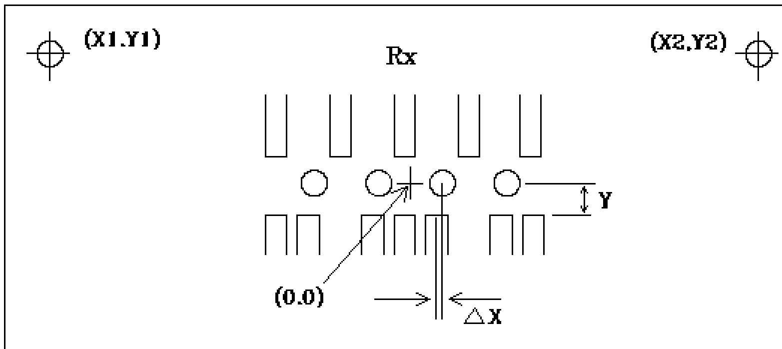

Figure 70. Measurement of the alignment offset of flip-chip pads in respect of the through-holes on the Rx substrates, and the nomination of symbols. A corresponding nomination was used with the Tx substrates.

Table 9. The placements of the contact pads compared to the through-holes measured on all the Tx and Rx substrates of the four panels.

	Y	**ΔX**	**X1**	**Y1**	**X2**	**Y2**
Average [µm]	106.0	6.0	-1496.6	498.7	1495.8	499.3
Std. deviation [µm]	12.8	4.1	1.8	2.0	2.6	1.9

The surfaces of the cavities, to be used for mounting the microlenses on the LTCC, were characterised. An example of a surface profile measured by the use of a non-contact optical profiler is presented in Figure 71. The line scans made (for instance, along the blue and red lines shown in the picture) showed that the unevenness of the microlens cavity bottom surface is in the order of 20…30 µm. From the line scans, the depth of the microlens cavity edges was estimated to be around 480…500 µm for substrate #4. The LTCC thickness variations are probably caused by the layout structure of the inner (i.e. buried) connector layers, as well as the cavities and vias. The bottom surface of the cavity is mostly rather smooth, but there also faster variations of the depth, especially around the edges of the smaller cavity for the 'optical vias', as illustrated by the left picture in Figure 71. This may cause small angular misalignment (tilt) of the assembled microlens array. These surface profile results were also verified by measuring with a stylus profiler, which gave some line scans of the surface.

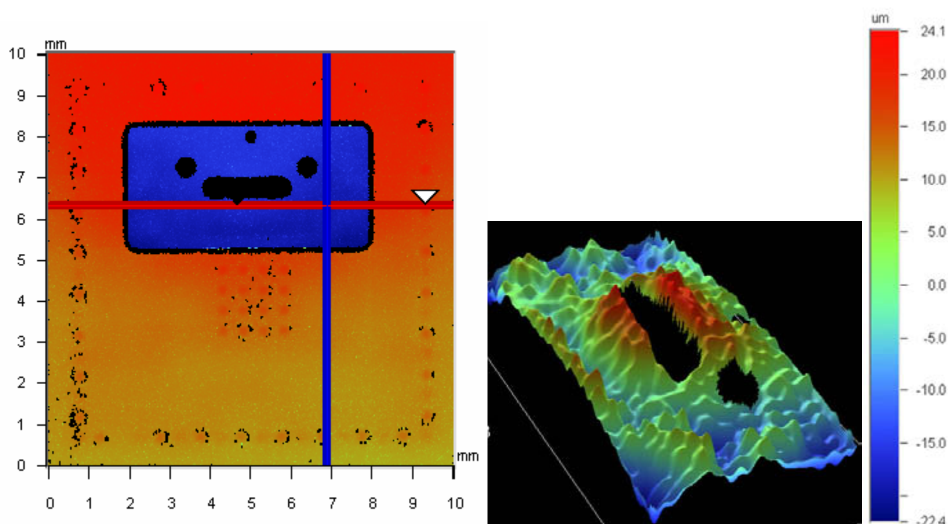

Figure 71. Surface profiles of the module substrate measured by an optical profiler: left) the surface of the whole module substrate (the red and blue lines indicate cross-sections that were studied by plotting line scans); right) a 7 × 3 mm area of the microlens cavity bottom surface around the deeper cavity with 'optical vias'.

The thickness of the substrates and the depth of the microlens cavities were also investigated using a 3D coordinate measuring machine (Mitutoyo Strato 9166),

which has a measurement accuracy of ±1 µm. After determining the level of the LTCC top surface from four reference points, the depth of the cavity bottom was measured from four points. The resulting cavity depths were 502…534 µm and 603…613 µm for substrates #4 and #6 respectively. The variation in the measurement results also indicates the unevenness of the surface. The substrate thicknesses were measured from two points. The results were 850 µm and 852 µm for substrate #4, and 912 µm and 919 µm for substrate #6. The measurement of the cavity depth was needed in order to specify the standoff height of the modules and, thus, the target size of the BGA balls.

5.3.2 Board with optical waveguide layers

The PWBs for the demonstrator were manufactured in the production line of Aspocomp Group Oyj in Salo, Finland. E-glass reinforced epoxy (FR4) was selected as the substrate material. The 1.2 mm-thick 4-layer board had a solder mask layer (halogen-free PSR-4000 GEC50 by Tayio) on top of it. This solder mask defined the edges of the Ni/Au contact pads for the BGA assembly of the Tx and Rx modules.

The polymer optical waveguide layers were fabricated on top of the solder mask of the FR4 PWBs using a three-step spin-coating and lithographic patterning process; first, the under-cladding layer was coated and patterned, followed by the processing of the waveguide core layer and the top-cladding layers respectively. Each of the three polymer layers was first spin-coated onto the PWB and then UV-exposed through a chrome mask and, finally, the layer was developed to remove the unexposed polymer.

The waveguides used in the assembled demonstrator were fabricated from a commercially available photo-definable polymer system: epoxy-based Nano™ SU-8-25 (by MicroChem Corp.) was used as the core material, and its index-matched epoxy (by Micro Resist Technology Gmbh) was used as cladding. SU-8 is negative-acting resist that has been developed with uniform thick layers with a low edge bead in a single coating step. The processing of the optical layers was carried out at the Helsinki University of Technology in a Class 100 clean room environment by the use of a standard IC mask aligner.

Detailed process parameters with further observations are described in (Immonen et al. 2005b).

Of the four waveguides on the demonstrator, two had a nominal width of 50 µm and the other two had a nominal width of 75 µm. The nominal values here refer to the waveguide patterns of the lithography mask. The thickness of the waveguide core layer was measured at several points on two boards and the results varied from 44.5 µm to 46.8 µm. The waveguide array had the same 250-µm pitch as the VCSEL and PD arrays.

Within the optical build-up, a supporting structure was designed for the lenses to be assembled on the PWB. The supporting posts were fabricated in the optical waveguide process. The optical layer facet served as a mechanical stopper for the mirror component, which was placed between the lens supporting posts. Thus the lithographically processed structure enabled fully passive alignment and assembly of the micro-optical parts. A micrograph of the optical waveguides and passive alignment structures on the PWB is shown in Figure 72, imaged from the tilted angle and from above. The surface profile of the same area is presented in Figure 73, and a cross-section photograph of the waveguides is shown in Figure 74.

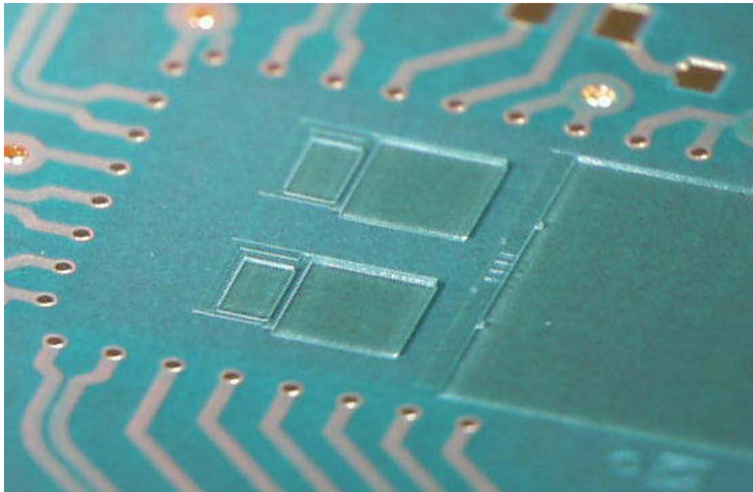

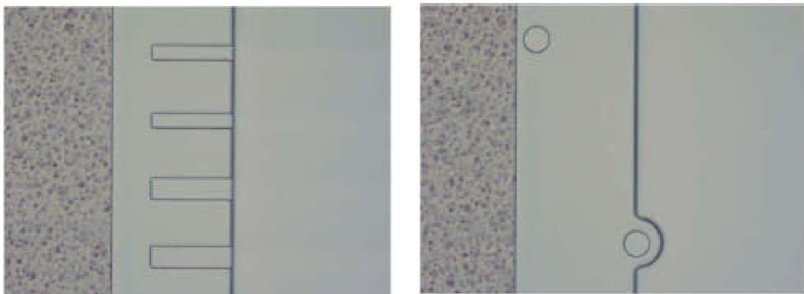

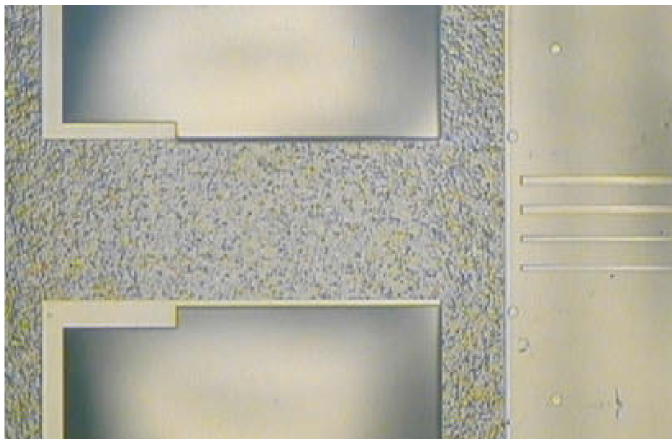

Figure 72. Optical build-up layer on FR4 PWB, the area under the Tx module (before assembly of micro-optics and BGA-mounted transmitter). Four parallel multimode channel waveguides and passive alignment structures and marks for micro-optics are seen. The structure in the lowest micrograph is without the top-cladding layer. (Upper micrographs by Helsinki University of Technology.)

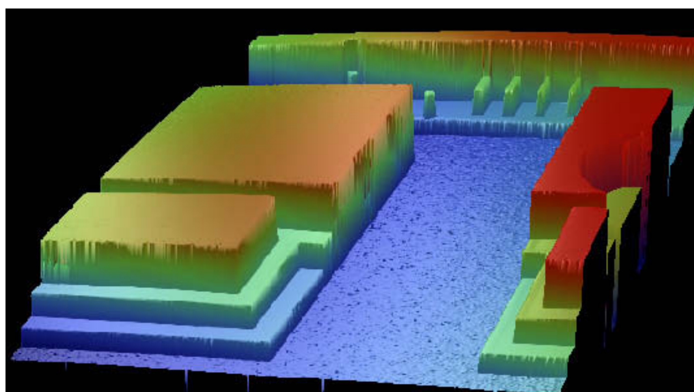

Figure 73. Surface profile of the optical build-up layer measured with an optical profiler.

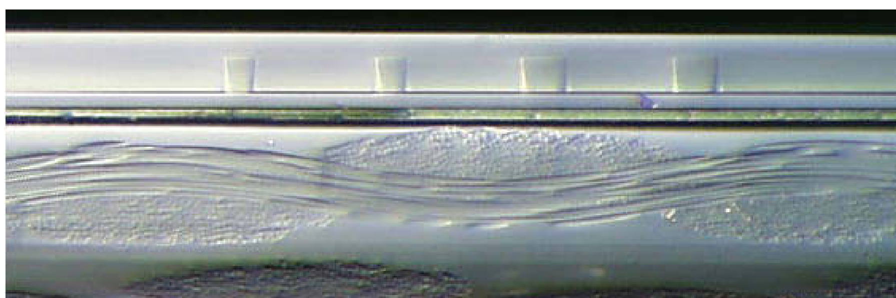

Figure 74. Cross-section of the optical build-up layer on FR4 PWB (micrograph by Helsinki University of Technology).

The attenuation of the waveguides was characterised using the cut-back method at the 850 nm wavelength. The average attenuation was 0.55 dB/cm. The measured wavelength dependence of the attenuation is presented in Figure 75. The measured refractive index was n_{TE} = 1.587 for the waveguide core material and n_{TE} = 1.573 for the cladding composition respectively. Both were measured using the prism coupling method at 830 nm. These resulted in a waveguide NA of 0.21.

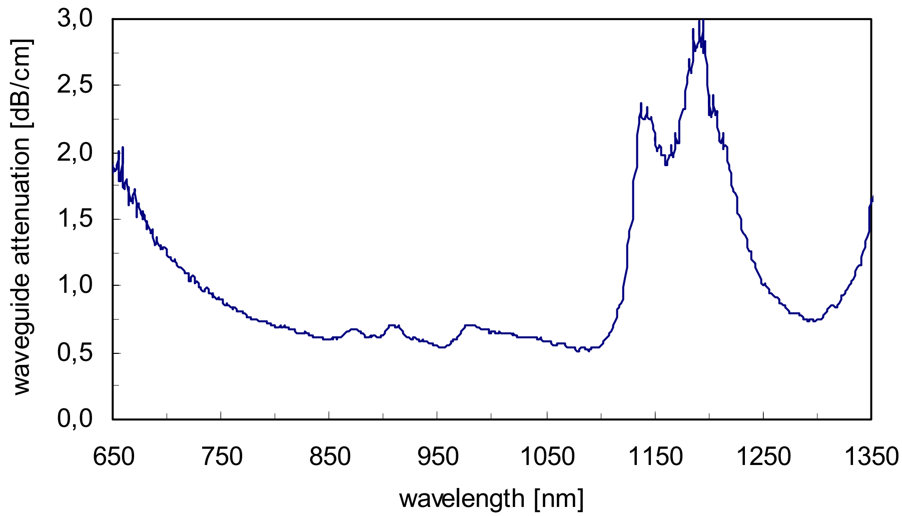

Figure 75. Measured spectral attenuation of SU8 waveguides.

5.3.3 Micro-optical elements

Micro-mirrors for turning the beam through 90° were fabricated (Figure 76) by grinding and polishing one edge of the approximately 100 µm-thick glass substrate in such a way that a 45° bevel was formed. Several substrates were grinded simultaneously by stacking them into a jig, which made it possible to mount them at a 45° angle to the abrasive wheel of the precision lapping and polishing machine (Logitech PM5 Auto-Lap). After polishing, the substrates were placed on adhesive tape and cut into pieces with a dicing saw. In addition, an aluminium coating layer was evaporated on the glass surfaces in order to obtain high reflectivity. A thin layer of chrome was first evaporated on the glass to improve the adhesion of the aluminium.

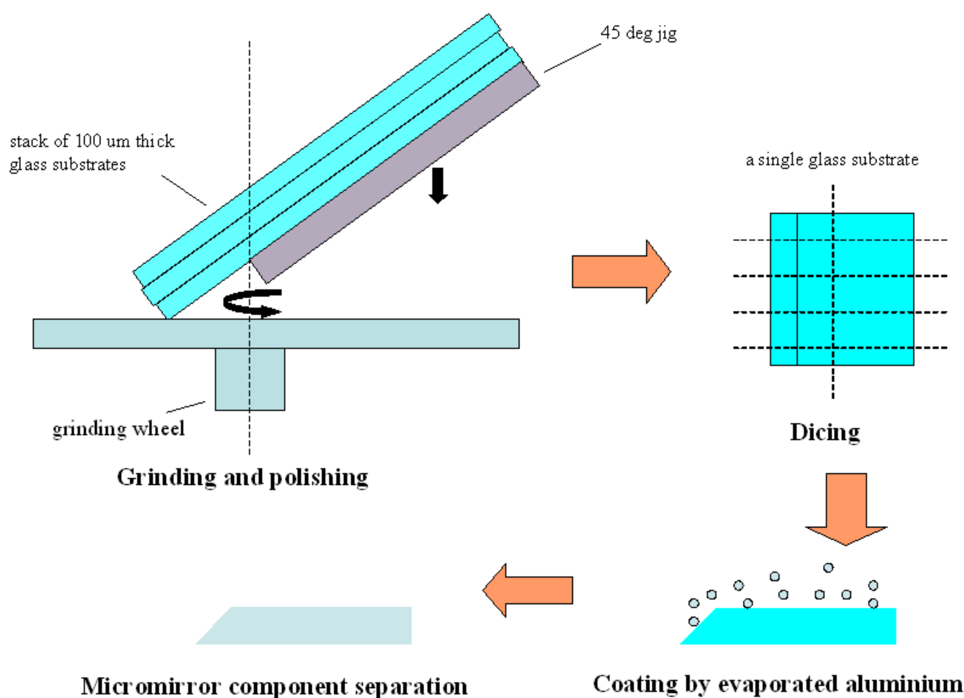

Figure 76. Fabrication process for micro-mirror components.

The refractive microlens arrays used in the demonstrator were made by Advanced Micro-optic Systems GmbH (aμs). The linear arrays of the positive microlenses had been fabricated by contact photolithography and chemical etching of the glass substrates (type S-TIH53 by Ohara Inc.) having a high refractive index of 1.820 at 850 nm. The lens pitch is 250 μm, and the specified lens diameter 235 μm and focal length 340 μm. The specified lens ROC was 275 μm. According to the surface profile measurement with the optical profiler (Figure 77), this appeared to be correct in the central region, but the edges of the lenses have a slightly smaller curvature corresponding to an ROC of 300 μm. Most of the acquired lens arrays were anti-reflection (AR) coated to provide very high transmission at around 850 nm. The thickness of the microlens substrate was 300 μm. Since the T_g of the glass is 624 °C, no deformation was expected during the reflow soldering process. The coefficient of thermal expansion (CTE) of the lens material was specified at 8.8 10^{-6}/°C (in the range –30…+70 °C). Thus the CTE is rather close to the CTE of the LTCC substrate (5.8 10^{-6}/°C for Dupont 951) but only half of CTE of the FR4 board (17 10^{-6}/°C).

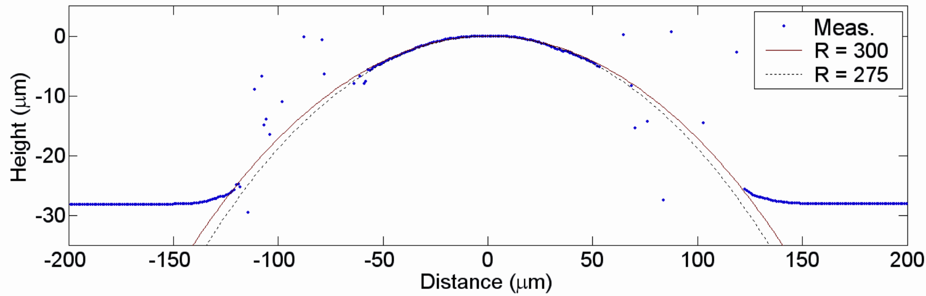

Figure 77. Measured surface profile of a microlens with two fitted curves.

5.4 Assembly

The assembly of the optical interconnect demonstrator is presented here. The assembly process was as follows: first, the electronic components were assembled on the LTCC panels in the order defined by the soldering temperatures. This was followed by the mounting of the micro-optical components onto the O/E-PWB and LTCC substrates. Finally, the Tx and Rx modules were BGA-mounted on the O/E-PWB. This kind of assembly flow is compatible with the industry standard assembly methods, except for the additional steps to mount the optical components. No active optical alignment method was used in any phase. The surface mounting of the microlens arrays and micro-mirrors was designed to be suitable for the use of a die bonder. The components were attached with UV-cured adhesive, which was chosen to be viscose enough not to spread to the optical surfaces. Nevertheless, the alignment of the microlens arrays was carried out using a pneumatic gripper tool controlled by an Automatic Alignment Station (Newport 8100), which provides high resolution displacement control and video microscopes for the alignment purpose. With this equipment it was also possible to study the alignment tolerances of the optical coupling.

5.4.1 Assembly of Tx and Rx electronics

The assembly of the electronic components on the Tx and Rx module substrates was carried out by industrial partners. The surface-mount and chip-on-boards

were made using production equipment by Elcoteq Elektronik GmbH. The components were assembled on the LTCC panels, i.e. before dicing into individual Tx and Rx substrates. The assembly was started by dispensing lead-free SnAgCu bumps onto the BGA pads of the LTCC substrates. The target size of the BGA balls was 320 µm. This was specified by the standoff height of the modules, which was first calculated from the measured microlens cavity depth and the optimised optical design.

Next, the VCSEL and PD array dies were bumped with Au stud bumps using 25 µm-thick Au wire. The bumping was carried out by Fraunhofer-Institut für Zuverlässigkeit und Mikrointegration (IZM) of Germany. Figure 78 shows examples of the bumped devices. Then, the thermo-compression flip-chip bonding of the VCSELs and PDs was carried out by Finetech GmbH using a Fineplacer Lambda bonder, which can achieve better than ±1 µm alignment accuracy. The active areas of the devices were aligned to the 'optical via' holes on the LTCC substrates by visual adjustment during the flip-chip bonding. A micrograph captured from the screen of the flip-bonder during the alignment phase is presented in Figure 79. Special beam-splitter-based optics allows seeing both the device and the substrate on top of each other simultaneously.

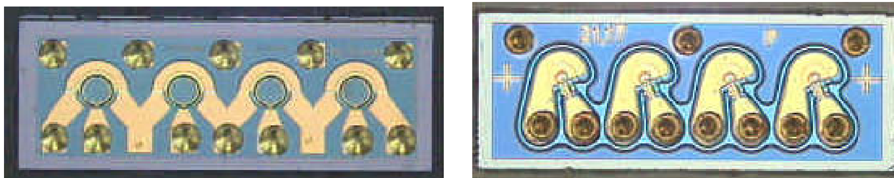

Figure 78. Micrographs of the 4-channel PIN diode (left) and VCSEL (right) array dies equipped with Au stud bumps (photo by Fraunhofer IZM).

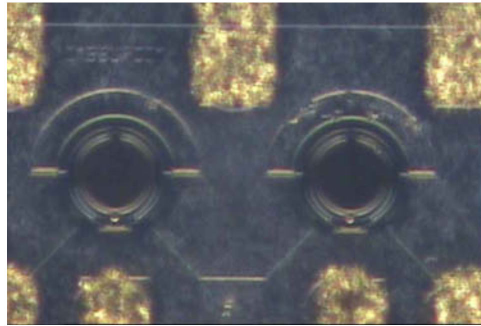

Figure 79. Alignment of the active areas of the detector array to the optical via holes, as seen with the Vision Alignment optics of the flip-chip bonder (photo by Finetech).

Next, the driver and receiver ICs were die bonded onto the LTCC substrates using silver-filled epoxy, followed by thermo-sonic ball bonding with 25 μm-thick Au wires. Finally, the passive components, i.e. capacitors, were mounted using SMD assembly and no-clean solder paste (GLT 6-$Sn_{63}Pb_{37}$), which avoided contamination of the optical surfaces of the VCSELs and PDs. Figure 80 presents photographs of a bonded IC and a VCSEL array from both sides of a Tx module substrate.

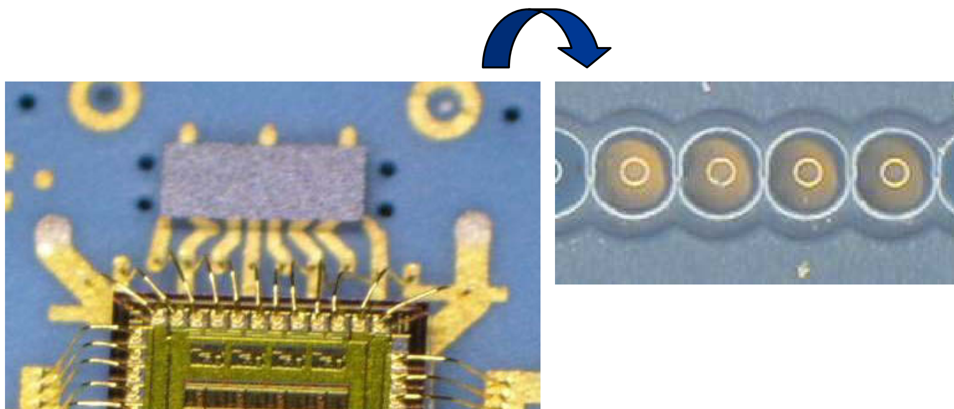

Figure 80. (left) Flip-chipped-mounted VCSEL array and part of a wire-bonded driver IC on Tx module substrate; (right) Active areas of VCSELs seen through the 'optical via' holes from the rear of the LTCC substrate.

When the microlens arrays were assembled on the LTCC substrates it was found that the flip-chipping process was not successful with good yield; the VCSELs and PDs were not always accurately aligned to the through-holes. Thus a few modules, including both transmitters and receivers, were examined with a SmartScope measuring microscope. The misalignment was around ±5…8 µm in both lateral directions in most of the modules, but misalignment values even as high as 20 µm were observed. Such a high misalignment would cause a significant drop in the optical coupling efficiency because the microlens array substrate will be aligned with the through-holes as well. Only the modules with good alignment accuracy were selected for the demonstrator assembly.

In addition to the poor alignment of the flip-chipping, it was noted that the contact resistance between many of the VCSEL chips and the contact pads on the LTCC was relatively high and the mechanical strength of the joint was weak. Probably, the pressure or the temperature in the flip-chipping process had not been high enough and the contact between the solder bumps and the pads on the LTCC failed. The flip-chip pads on the LTCC seemed almost unaffected by the process in the samples in which the VCSEL chips broke off, indicating weak joints between the the bumps and the LTCC pads.

5.4.2 Assembly of microlens array on LTCC

After the assembly of the electronic devices, the microlens array components were mounted onto the cavities of the Tx and Rx module substrates (seen in Figure 68). The microlens array was aligned using the four additional through-holes on the LTCC as alignment marks. A pneumatic gripper tool controlled by the Auto-Alignment Station was used to pick-and-place the component, as shown in Figure 81. The microlens substrate was fixed to the LTCC using UV-curable adhesive.

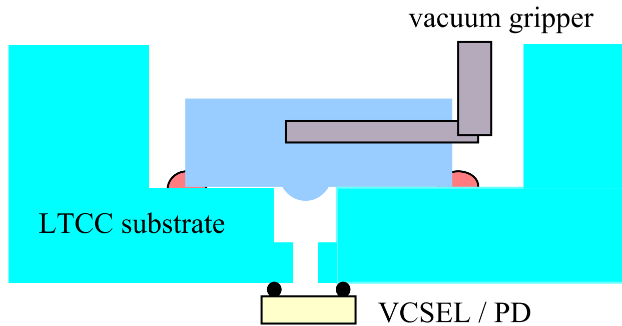

Figure 81. Assembly of the microlens array onto the LTCC.

Figure 82 shows a photo of a microlens array substrate on a Tx LTCC substrate after assembly. It also shows how the microlens array was visually aligned to the four through-holes, which were used as registration marks. In order to accurately see those through-holes with the assembly microscope camera, it was necessary to illuminate the LTCC substrate from the rear (i.e. from the side with the electrical components). For this reason, a special assembly jig made of glass was fabricated and placed on top of the reflecting surface. The through-holes were clearly visible when illuminated from the rear. The lateral (i.e. parallel to the substrate) alignment accuracy achievable with this method was estimated to be better than ±10 µm.

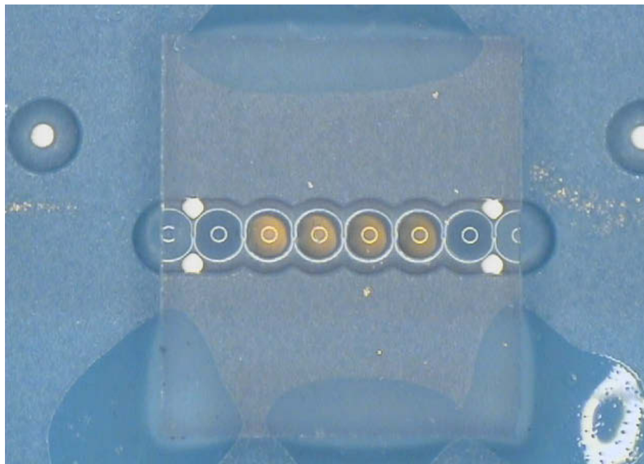

Figure 82. Microlens array assembled on the LTCC substrate of a Tx module. The four active areas of the VCSEL array, which is flip-chip bonded onto the other side of LTCC substrate, shimmer through the microlenses and the 'optical via' holes.

5.4.3 Assembly of micro-optics on O/E-PWB

The micro-mirror and the microlens array were mounted on the FR4 board by the use of alignment structures lithographically patterned on the waveguide layers (as described in Section 5.2.2). Figure 84 shows a photo of a microlens array and a micro-mirror underneath it after assembly on the O/E-PWB. First, a micro-mirror was assembled onto the PWB in the cavity formed by the optical waveguide layers – that is, between the microlens mounting posts and the waveguides. The micro-mirror was assembled using a die bonder with a low-pressure gripper needle and attached with UV-cured adhesive dispensed from a syringe. The distance of the mirror from the waveguide core ends was defined by the edge of the under-cladding layer. Thus, no visual alignment was needed.

Next, the microlens array was mounted on the O/E-PWB above the micro-mirror. Similar methods and tools were used as when mounting the microlens array on the LTCC substrates (in Section 5.4.2). The microlens substrate was again picked with the customised pneumatic gripper tool and brought into contact with the upper-cladding layer, as shown in Figure 83. The alignment marks (rods) that were patterned to the waveguide core layer defined the correct microlens position in the lateral directions. Finally, the microlens substrate was attached to the upper-cladding layer with UV-cured adhesive.

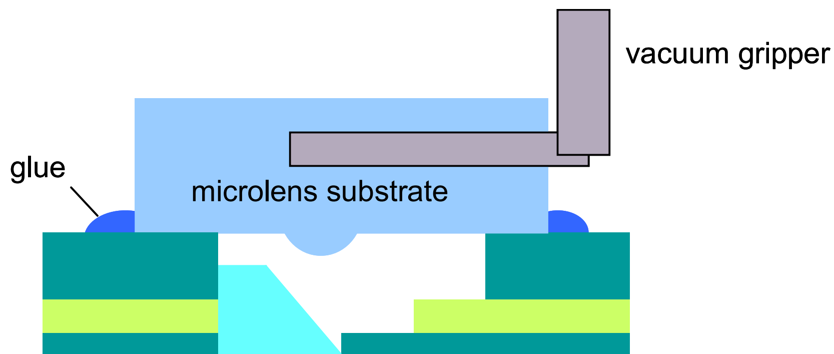

Figure 83. Mounting of microlens array onto O/E-PWB with micro-mirror.

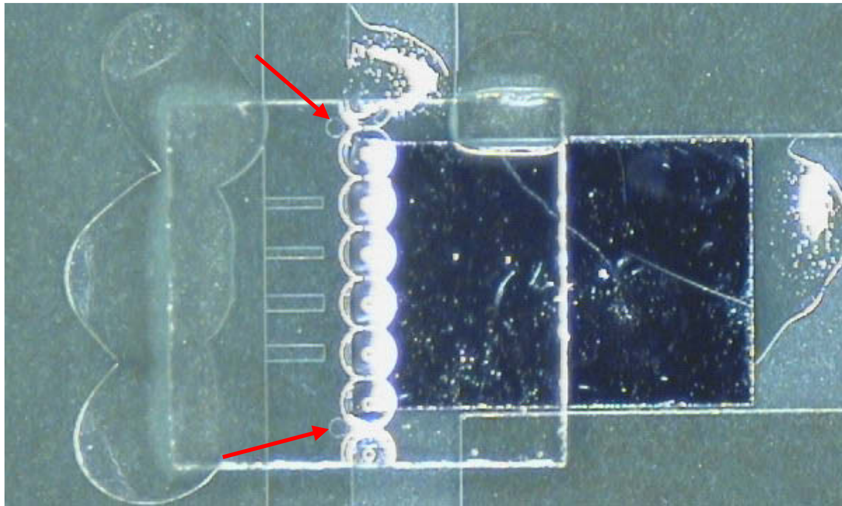

Figure 84. Assembled microlens array and micro-mirror on PWB with optical waveguide layers. The photo-patterned alignment marks (rods) for the microlens assembly are emphasised with red arrows.

5.4.4 BGA assembly of Tx and Rx modules to O/E-PWB

Finally, the Tx and Rx modules were BGA-mounted on the demonstrator O/E-PWB equipped with optical coupling components. The modules were mounted using a flip-chip bonder equipped with a customised pneumatic gripper tool, which was first manufactured in order to get a firm hold of the LTCC module. The special tool was needed because it was not possible to touch the central area of the module due to the electrical components on it. The module was aligned with the O/EPWB using the two through-holes on the LTCC substrate (see Figure 68) and the two rods patterned to the waveguide core layer on the O/E-PWB as alignment marks. These marks could be seen at the same time as the alignment optics of the flip-chip bonder.

A common way to BGA-mount an LTCC module on PWB is reflow soldering in a convection furnace. However, the module may move in the reflow oven during the melting of the solder. Thus, a preliminary test series to study the post-reflow alignment accuracy was carried out with a set of test LTCC modules (without electronics) as well as with four slightly different ball and pad sizes. No-clean

$Sn_{63}Pb_{37}$ solder paste was deposited onto the BGA pads on the FR4 board before assembly. The measured lateral misalignments were in the range of 4…39 µm, with an average of 15 µm.

In the case of the largest misalignment, the excess optical loss would become high. On the other hand, it was not possible to solder during the flip-chip bonder with the standard method because the substrate heat plate of the bonder was not able to heat up the large FR4 board. Therefore, the solder was melted by heating with a fan heater when the module was in the correct position in respect of the PWB at the flip-chip bonder. An Rx module assembled on the demonstrator O/E-PWB in this way is shown in Figure 85. For reliability, the dies, as well as the wire-bonds and flip-chip bonds, should be protected. When applying glob-top material and underfill, care should be taken not block the optical path under the flip-chip mounted VCSEL/PD. Glop-top protection of the dies and bonds was also demonstrated by dispensing the adhesives in such a way that the spreading of the adhesives under the flip-chip mounted device was avoided.

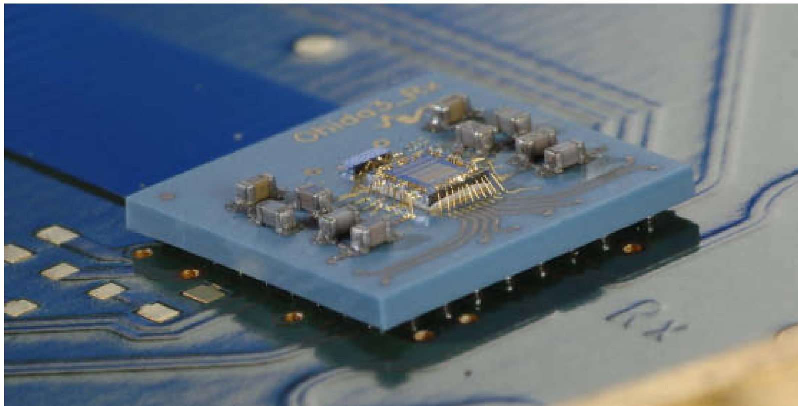

Figure 85. 4 x 10 Gb/s receiver module BGA-mounted on O/E-PWB.

5.5 Characterisation

Next, the characterisation results of the demonstrator and some of its parts are presented. The optical coupling efficiencies and alignment tolerances of the critical parts in the demonstrator were characterised. The high-speed transmission performance was studied by eye-diagram measurements.

5.5.1 Coupling loss due to the micro-mirror

The optical insertion loss of the coupling structure consisting of the micro-mirror in front of the waveguide facets was characterised by the use of a sample and the arrangement illustrated in Figure 86. The sample was one half of the demonstrator board, which was prepared by sawing the board into two pieces and polishing the sawed waveguide facets. This enabled butt-coupling light into the waveguides from a fibre. Only a micro-mirror was assembled on the sample board. The optical power was launched from a 50/125 µm graded-index fibre (NA 0.22) into a selected waveguide. The light reflected upwards from the mirror was collected into a 200 µm-cored step-index fibre (NA 0.22) equipped with fibre-coupling optics. Excess loss caused by the micro-mirror coupling was estimated from the measured losses by subtracting the waveguide loss and the fibre-coupling losses. The latter had been obtained from the reference measurements from similar straight waveguides butt-coupled to fibres at both ends. The excess loss thus calculated includes losses due to the quality (roughness, angle) of the mirror, refraction and scattering from the under-cladding surface, and the possibly poorer quality of the lithographically patterned waveguide facets compared to a sawed and polished facet.

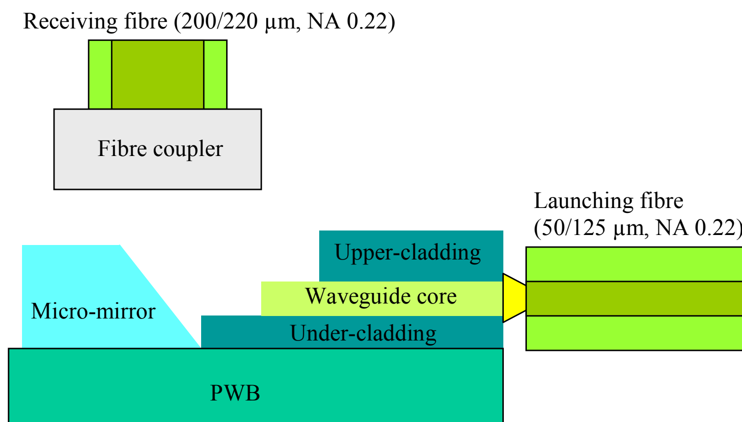

Figure 86. Measurement setup to characterise coupling loss caused by the micro-mirror.

The four waveguides on two sample boards were measured, totalling eight measurement results. The resulting excess losses were between 4.0…6.5 dB,

with an average of 5.1 dB. The variation is partly due to the varying quality of the sawed waveguide facet, which was used at the in-coupling. Part of the excess loss is caused by the edge of the under-cladding layer between the waveguide end facet and the micro-mirror. From the geometry of the structure, it is clear that the under-cladding edge refracts, scatters and reflects part of the optical beam in unwanted directions, thus significantly increasing the total excess loss. Furthermore, the excess loss is probably slightly different in the fully assembled demonstrator since the area and field-of-view of the fibre-coupling optics (NA of lens was 0.5 and focal length 5 mm) are different to the area and field-of-view of the microlens, which couples light onto the detector in the demonstrator.

5.5.2 Coupling efficiency and mounting tolerance of Tx module

The alignment accuracy requirements of the BGA-mounted Tx module were characterised. Figure 87 describes the measurement arrangements. A special DC version of the transmitter without the driver IC was assembled for this purpose. The DC version only had a VCSEL array die flip-chip mounted onto the LTCC substrate, electrical contacts for the VCSEL and a microlens array mounted in the cavity. Individual VCSEL channels could be controlled by external laser driver, i.e. a constant current source.

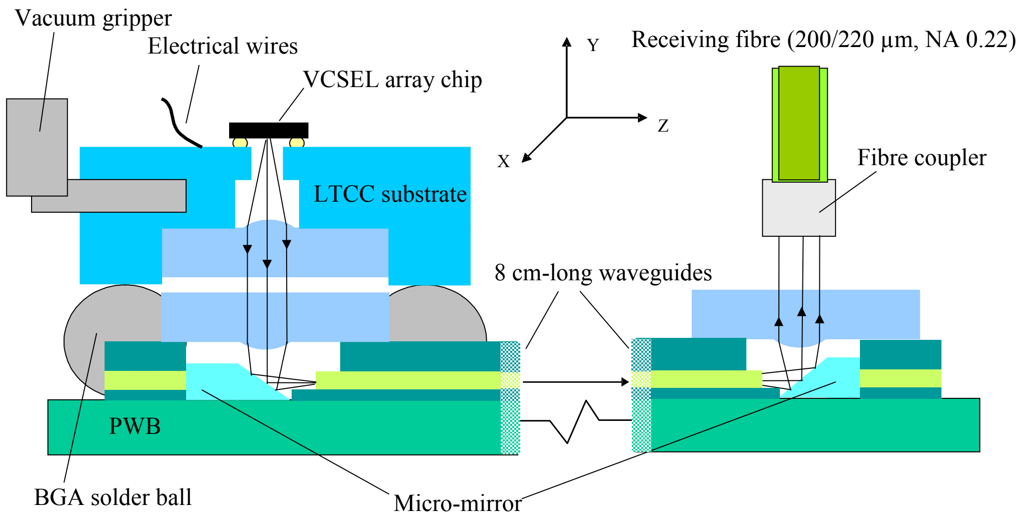

Figure 87. Alignment tolerance of the Tx module measurement setup.

The DC Tx module was attached to a vacuum gripper, and a single VCSEL channel was driven with a 5 mA constant current. The location of the module was scanned in the x, y and z directions while monitoring optical output power from the receiver end with a 200/220 µm fibre having NA 0.22 and equipped with a coupling lens. That is, the Rx module was replaced with the fibre, but the micro-mirror and a microlens array had been assembled on the PWB. Thus the power was transmitted through the whole 83 mm-long SU-8 waveguide, through three microlens arrays, and was reflected from two mirrors.

Figure 88 presents the measured alignment tolerance in transversal misalignment when propagating through a 50 µm-wide waveguide. The characterized transversal tolerances with 1 dB loss margin are ±40 µm in both directions. On the other hand, the -3dB alignment tolerances are ±80 µm or ±90 µm, depending on the direction of misalignment. The smallest total insertion loss of the measurement was 17 dB. A small dip in the coupling efficiency was seen at the 'nominal' position when moving the module parallel to the waveguide axis. This was probably caused by a combination of the edge of the lower-cladding layer and the 'vulcano crated'-shaped VCSEL beam; because of the edge, the whole beam cannot be coupled to the waveguide. Thus the lowest losses are achieved when the module is in positions where one or the other half of the 'volcano crater'-shaped beam is coupled to the waveguide; the loss is slightly increased between those positions.

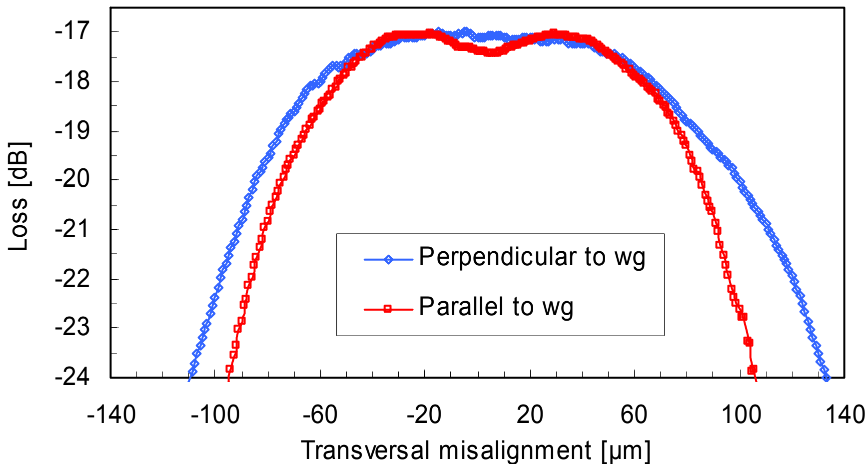

Figure 88. Coupling loss through the full link as a function of Tx module misalignment with a 50 µm-wide waveguide. (Fibre used as a receiver instead of an Rx module.)

Alignment tolerances were similarly characterised for the 75 µm-wide waveguides as well. The measured transversal misalignment dependence of the coupling loss is shown in Figure 89. The tolerances with a 1 dB loss margin are ±40 µm and ±60 µm when moving the module perpendicular and parallel to the waveguides respectively. The measured total insertion loss was 15 dB. A similar dip in coupling efficiency is seen as with the narrower waveguide. This is also due to the aforementioned reason.

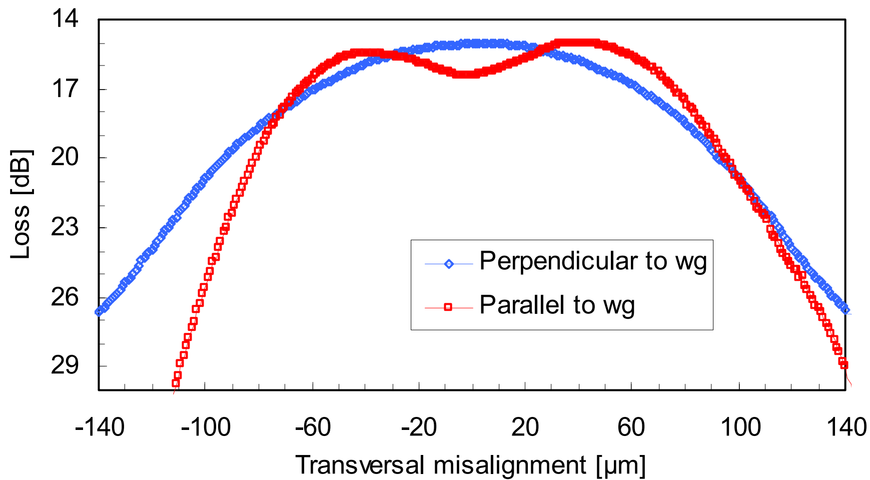

Figure 89. Coupling loss through the full link as a function of Tx module misalignment with a 75 µm-wide waveguide. (Fibre used as a receiver instead of an Rx module.)

In addition, the sensitivity of the coupling efficiency was studied as a function separation between the module and PWB, i.e. the BGA stand-off height or the separation between microlens arrays. When increasing the separation, i.e. lifting the module upwards, the loss increased approximately linearly, but slowly; only a less than 1 dB increase in loss was measured with a 1000 µm excess separation, independent of the waveguide width. This implies that the beam was well collimated between the microlenses.

5.5.3 Summary of the link budget and mounting tolerances

The results of the coupling loss characterisation presented in the previous sections are summarised in Table 10. The measured total insertion loss of the link was around 17 dB when a 200/220 µm-fibre used as a receiver instead of an Rx module. This includes both the losses of the coupling optics and the 4 dB loss due to the attenuation of the SU-8 waveguide. However, the coupling efficiency from the microlens (mounted on the Rx module) to the PD could not be characterised because the sensitivity of the Rx could not be determined.

Table 10. Summary of the measured average losses in the demonstrator link with a 50 µm waveguide. Measured in the case where fibre is used as a receiver instead of an Rx module.

Tx module (VCSEL-to-lens)	~2 dB
Lens-to-mirror-to-waveguide coupling at Tx	~5 dB
Attenuation of the SU-8 waveguide	5 dB
Waveguide-to-mirror-to-lens coupling at Rx	~5 dB
Total	~17 dB

The alignment tolerances for the Tx module with a maximum of <1 dB excess loss are summarised in Table 11. These alignment tolerances for the BGA assembly should be rather easily achievable. For instance, ±20 µm or ±30 µm accuracy was assumed in the tolerance analyses. Although a loose alignment requirement is a ‘good’ result in principle, its relevance is weakened due to the fact that, at the same, the coupling loss is rather large, even in the optimal position.

Table 11. Summary of the measured –1 dB misalignment tolerances for the Tx module in the demonstrator.

Waveguide width	x [µm]	z [µm]	y [µm]
50 µm	±40 µm	±40 µm	> 1000 µm
75 µm	±40 µm	±60 µm	> 1000 µm

5.5.4 Data transmission performance

The data transmission performance of the demonstrator was studied by measuring eye diagrams with an HP83480 Digital Communications Analyzer (DCA) equipped with a receiver unit having a 20 GHz electrical bandwidth. The pseudo-random bit sequences (PRBS) were taken from the Data Pattern Generator (by Anritsu).

First, transmission over 10 cm-long SU-8 waveguides on an FR4 board was studied. A commercial 10 Gb/s 850-nm VCSEL transmitter (New Focus 1780) was used as a source. This has a 50/125-µm GI fibre output, which was butt-coupled to the waveguide. The waveguide output beam was butt-coupled to a similar fibre and the other end of the fibre was connected to a commercial 25 GHz detector module (New Focus 1481-S-50), which was electrically coupled to the DCA via a broadband (0.05…20 GHz) amplifier (New Focus 1421). With the lengths of 2 m and 3 m respectively, the dispersion (2000 MHz/km) of the fibres had negligible effect on the waveforms. An eye diagram of a 10 Gb/s optical signal transmitted through the waveguide is shown in Figure 90. A clear and open eye demonstrated successful high-speed optical transmission on FR4 PWB using waveguides of similar kinds and lengths as in the demonstrator.

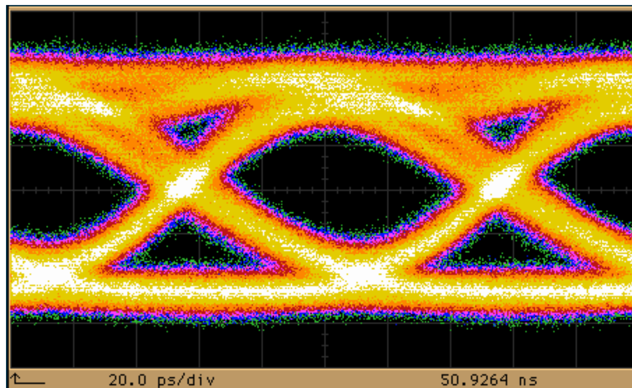

Figure 90. 10 Gb/s eye diagram of transmission through a 10 cm-long SU-8-cored optical polymer waveguide on an FR4 board.

The high-speed operation of the transmitter module was verified by measuring an eye diagram by coupling the output of one channel into a 50/125 µm GI fibre. The Tx was driven with the PRBS signal from the Pattern Generator. The resulting eye patterns at 10 Gb/s and at 4 Gb/s are shown in Figure 91 and Figure 92 respectively. The 10 Gb/s signal was measured with a combination of a New Focus receiver and a broadband amplifier together with DCA (as before) and the 4 Gb/s was measured by feeding the signal to an internal fibre-coupled receiver of the DCA. The internal receiver has an electrical bandwidth of 4 GHz. The 10-Gb/s eye is rather noisy because the fibre-coupled power was a bit too low for the DCA. The coupling loss is high because it was not possible to get the fibre end very close to the VCSEL mounted on the other side of the Tx substrate (with a cavity and 'optical via' structure). On other hand, the 4-Gb/s signal shows a much lower noise level because the internal receiver of the DCA has much higher sensitivity than the New Focus receiver.

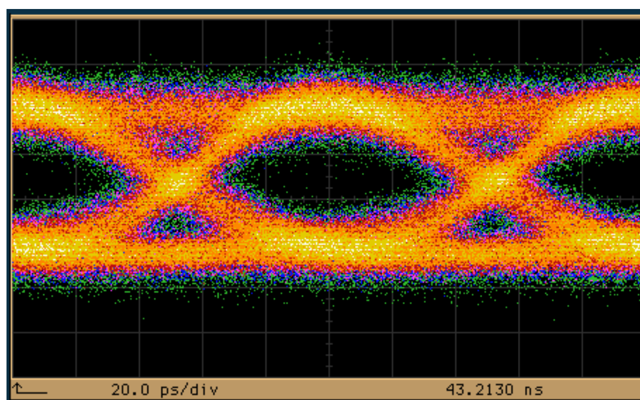

Figure 91. Optical eye diagram measured with a 25 GHz receiver fibre-coupled from the optical output of the Tx module driven by 10 Gb/s PRBS signals.

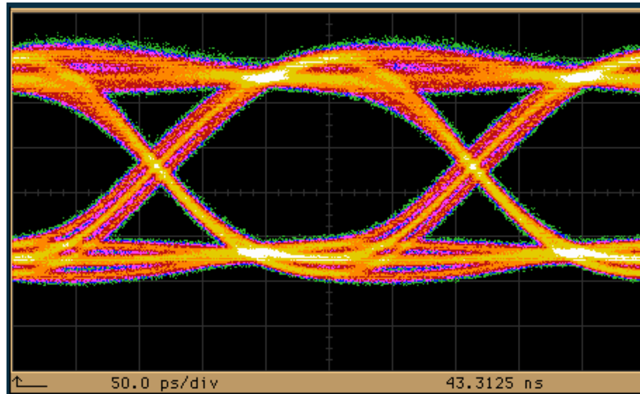

Figure 92. Optical eye diagram measured with a 4 GHz receiver fibre-coupled from the optical output of the Tx module driven by 4 Gb/s PRBS signals.

The high-speed operation of the receiver module was verified by measuring an eye diagram from the electrical output of the board at 10 Gb/s. In this case, a 10 Gb/s optical output from the New Focus VCSEL transmitter was coupled through a 50/125 μm fibre to one of the photodiodes of the Rx. The experiment resulted in a well open eye diagram, as shown in Figure 93. The eye is somewhat noisy because the coupling efficiency from the fibre to the PD is low due to the module substrate structure in between (as in the case of the Tx characterisation above).

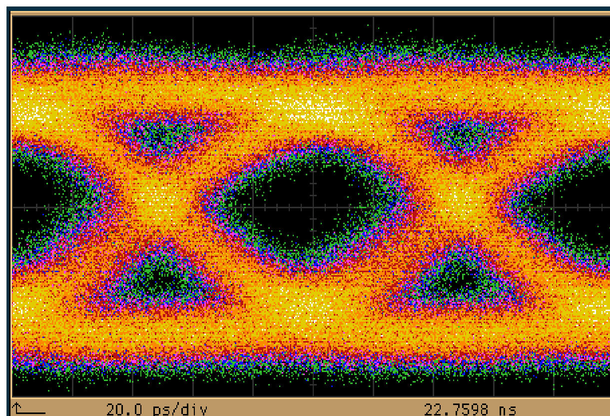

Figure 93. Eye diagram measured from the electrical output of the receiver module with a 10 Gb/s PRBS signal fibre-coupled from the New Focus VCSEL transmitter.

A data transmission eye diagram of the full link was also studied. The transmitter module was driven with a 10 Gb/s PRBS signal from the data pattern generator. The optical output beam from a transmitter channel was coupled to a 50/125 µm GI fibre, and the optical output beam from other end of the fibre was coupled to a photodiode of the receiver module. The measured eye diagram shown in Figure 94 is clearly open, although rather significant jitter is observed.

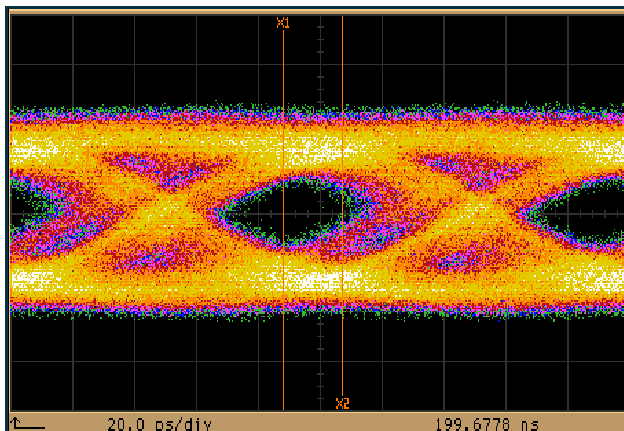

Figure 94. Eye diagram measured from the electrical output of the receiver module with a 10 Gb/s optical input signal from the transmitter module coupled through a GI fibre.

6. Discussion and recommendations

Let us first discuss the results with the integrated demonstrator. As described in Chapter 5, the total optical loss of the implemented link was estimated to be around 19 dB, whereas the calculated power budget of the Tx and Rx was around 17 dB at 10 Gb/s with BER of 10^{-12}. Therefore, the demonstrator should be improved in order to make it fully functional. There are at least two potential ways to reduce the total loss. First, a minor layout change in the under-cladding layer might significantly reduce the coupling loss between the micro-mirror and the waveguide. As stated before, this loss (ca. 5 dB) was mostly caused by the edge of the under-cladding layer blocking part of the beam. Since the registration error between the optical layers was less than 20 µm, it would be possible to pattern the under-cladding edge closer to the waveguide facet, thus increasing the line of sight between the micro-mirror and waveguide facet.

Another way of reducing optical losses would be to change to a lower loss waveguide material; for instance, a recently developed epoxy-based material pair, called Epocore and Epoclad, would give less than 0.15 dB/cm waveguide attenuation (Schröder et al. 2006), resulting in a 4 dB reduction in link loss, and the material would probably be suitable for a similar kind of O/E-PWB fabrication process to that used with SU8. In conclusion, it is probably possible to achieve a total link loss that would enable feasible transmission at 10 Gb/s/channel.

One can also propose other ways to improve the coupling efficiency, such as to pattern a tapered waveguide end that enlarges the width of the waveguide facet, as well as to pattern the waveguide in such a way that the facet becomes slightly curved, thus achieving some cylindrical lens effect. Such structures could be implemented by a minor change to the mask of the core layer. Nevertheless, there would be a trade-off with the tapering: the waveguide should not be enlarged too much to avoid coupling from the adjacent channels, i.e. to avoid optical crosstalk. Alternatively, one could also think about using a more sensitive receiver or higher transmitter power, but in order to reduce total power consumption, device costs and improve link margin, it is more favourable to reduce the losses.

In the optimisation simulations it was seen that there is some trade-off between the highest coupling efficiency and relaxed alignment tolerances. Therefore, in Chapter 4, the tolerance insensitivity of the studied optical designs could have been improved by optimizing the structure based on the loosest tolerances instead of the highest efficiency in the nominal positions. On the other hand, in the integrated demonstrator (Chapter 5) the design was optimised to the system with loosest alignment tolerances, still proving a rather high nominal efficiency.

It is also important to realise that in this work, like in those by many other groups, several compromises had to be made when implementing the actual demonstrators and test devices. This is due to limited time and personnel resources, but, more importantly, due to the fact that it was necessary to rely on components that were available off-the-self or could be fabricated within the project. Since there were no commercial implementations of board-level interconnects, the purchased components used in the work were not originally designed and optimised for this kind of application. Therefore, it is very probable that better performance is achievable. For instance, if custom-manufactured microlens arrays were used instead of off-the-self components, the components could have been equipped with alignment marks, probably allowing more accurate and easier assembly.

Low-cost volume manufacturability is essential to make the interconnection technologies feasible for commercial use. Most of the presented components and assembly techniques are potentially suitable for volume production. Anyway, this is perhaps questionable in the case of the coupling scheme based on micro ball-lenses. A surface-mount assembly of the micro ball-lens component would probably be difficult since the component should be placed in a hole made on the PWB with good quality waveguide end facets. Moreover, due to several small components, the volume production of the component itself would probably be difficult. However, it is probably possible to design an alignment tool, such as a frame, for reproducible gluing of the ball-lenses onto the mirror facet.

What can be said about the accuracy and error sources of the presented measurement results? The results of the coupling tolerance experiments probably slightly over-estimate the effects of individual misalignments because, when characterising a certain misalignment, there are probably also some other,

though small, misalignments that were caused during assembly. This may also be the reason for the small asymmetries seen in some of the characterisation results.

The presented results do not allow drawing a conclusion about which of the studied coupling schemes is the most suitable. In the comparative study, the coupling scheme based on micro ball-lenses was less sensitive to misalignments than micro lenses, but the system is much more difficult to manufacture. The butt-coupling scheme is both simple and has loose alignment tolerances, but the transmitter must be brought close to the end of the waveguide. This might be problematic, because then a subassembly is probably needed. The absolute coupling efficiencies of all the implemented structures were rather small, which also reduces the possibility to draw a clear conclusion from the comparison. This also indicated that better efficiencies should be possible with slightly improved implementations, especially in the micro lens and micro ball-lens schemes. Anyway, the double micro lens scheme is advantageous compared to the others, especially thanks to the expanded beam that allows reduction of the critical alignment tolerances. Therefore, it was also used in the integrated demonstrator, which clearly proved its ability to enhance the optical coupling, extend the separation between components, and loosen the alignment accuracy requirement between the module and the board.

Reliability and environmental issues were not much addressed here. These should, however, be considered when specifying the power margin against temperature variations, tolerances, device and material degradation, etc. Anyway, the thermal effect measurements with VCSELs revealed that, in practical applications, the optical power variations caused by the changing temperature probably have to be accommodated either by automatic power control or by measuring temperature of the VCSEL with a termistor and adjusting the driving currents with this information. These methods are commonly utilised in fibre-optic transceivers for the same reason.

The demonstrated structures are not yet ready for commercialisation, and, based on the work presented on the topic so far (including this work), there does not yet seem to be a board-level interconnect technology that would be commercially feasible for large-volume implementation. It also seems that such technology would only be achieved through a co-operative effort by several

R&D groups (with complementary expertises) in order to simultaneously select and optimise all the sub-technologies needed from optoelectronics devices and micro-optical components in O/E-PWB fabrication, assembly and packaging techniques, design tools, etc. Such work would be easier to initiate and conduct if there was a consensus on a foreseen application expected to have high chances of becoming a commercial success. This foreseen breakthrough application would also define the target specifications for the work. Hopefully, this thesis will bring some information that will encourage initiating such efforts.

7. Summary and conclusions

Technologies to implement waveguide-based high bit-rate parallel optical interconnects on printed wiring boards was presented and demonstrated in this thesis. The aim was to study and develop technologies that would be suitable for volume manufacturing with processes typically used in electronics production, namely surface-mount assembly and board manufacturing. More precisely, the presented technologies can be used in the implementation of a high-speed, point-to-point interconnect between ceramic BGA-packaged ICs or multi-chip-modules on PWB. Both the simulations and the characterisation results suggested that although the implementation of optical interconnects is challenging with today's electronics manufacturing and assembly technologies, the alignment tolerance requirements can be fulfilled with high-end assembly techniques.

No such integration schemes for optoelectronics transmitter and receiver components have been presented before. The implementation of multi-channel high bit-rate transmitters and receivers was based on the use of LTCC packaging substrate technology. LTCC substrates were utilised for the hybrid integration and assembly of photonics devices and micro-optical coupling elements so that the optical alignment was mostly achieved with structures inherent to the LTCC substrate - that is, material-homogeneous integration was used. The accuracy of the through-hole structures and small cavities on LTCC can be in the order of a few micrometers, thus enabling passive optical alignment of the MM waveguides. Furthermore, LTCC enabled dense integration of multi-channel optoelectronic circuits by the use of 10 Gb/s/channel ICs and photonics devices as bare dies.

The designs of the coupling optics for the O/E-PWBs were carried out by the use of ray-trace modelling, including sensitivity and Monte Carlo tolerance analyses of the alignment accuracies. It was shown that an appropriate use of micro-optical elements allows enhancing the coupling efficiency and loosening the component placement accuracy requirements. Also, a 3D opto-mechanical analysis of the whole interconnect path was demonstrated by Monte Carlo tolerance simulations, including the models of the in- and out-coupling optics structures and the waveguide. The design work demonstrated that the modelling methods are suitable optimisation tools for the studied optical systems.

A modular test platform of parallel data links on PWB was implemented in order to study the three different kinds of optical coupling schemes, namely couplings based on microlens arrays, micro ball-lenses and butt-coupling. The platform consisted of three separate units: transmitter, receiver and optical waveguide board. The 10 Gb/s/channel electronics and optics of the transmitters and receivers were integrated on LTCC substrates. The selected optical coupling schemes were optimised and their feasibility was studied by simulations based on ray-tracing. The optical systems were mainly optimized in terms of the highest nominal coupling efficiency, but also aiming at misalignment insensitivity. The nominal coupling efficiencies of both the micro ball-lens and microlens array systems were feasible, but the tolerance analyses suggested that the manufacturing yield would not be sufficient with passive alignments. The presented waveguide-coupling efficiency measurements revealed around ±10 μm alignment tolerances for bare-chip assembly of the VCSELs and photodiodes, as well as around ±15…30 μm alignment tolerances for the proposed surface-mount assembly.

Also, the integration of a waveguide-based parallel optical interconnect on an FR4-based PWB was demonstrated. The demonstrator consisted of 4-channel BGA-mounted transmitter and receiver components as well as four polymer MM waveguides on top of the PWB. The transmitters and receivers built on LTCC substrates included flip-chip-mounted VCSEL or photodiode arrays as well as 4 x 10 Gb/s driver or receiver ICs. Two microlens arrays and a surface-mounted micro-mirror were utilised at both the transmitter end and the receiver end to couple between the optoelectronic device and the waveguide array. A mass-producible method was presented for the fabrication of the micro-mirrors, whereas commercially available optoelectronic components and microlenses were used. The optical alignment was based on the marks and structures fabricated in both the LTCC and optical waveguide processes.

Relaxed surface-mounting placement tolerances were demonstrated with the double microlens array concept. The characterised alignment accuracy requirements of the BGA-mounted components, in transversal misalignment with 1 dB loss margin, were around ±40…60 μm, depending on the direction of the misalignment and the width of the waveguide. As expected, the alignment of the microlenses in respect of the VCSEL/PD devices or waveguide cores must be more accurate, in the order of ±10 μm, which was achievable with the used

mounting methods and the implemented alignment marks and structures. The measured optical coupling loss at the transmitter end was around 7 dB. A significant part of the coupling loss was caused by the edges of the under-cladding layer blocking part of the optical beam between the waveguide end facets and the micro-mirrors. At a speed of 10 Gb/s, the transmitter and receiver modules showed open eye diagrams.

The presented work is an addition to the research work being carried out on the embedded board-level optical interconnects by many other groups, and will perhaps someday lead to commercial utilisation of the technology.

References

Afzalian, A., Flandre, D. 2006. Monolithically integrated 10 Gbit/s photodiode and transimpedance amplifier in thin-film SOI CMOS technology. Electronics Letters, Vol. 42, No. 24, pp. 1420–1421.

Akbulut, M., Chen, C. H., Hargis, M. C., Weiner, A. M., Melloch, M. R., Woodall, J. M. 2001. Digital Communications above 1 Gb/s Using 890-nm Surface-Emitting Light-Emitting Diodes. IEEE Photonics Technology Letters, Vol. 13, No. 1, pp. 85–87.

Alajoki, T. 2004. VCSEL array based transmitter for optical interconnects. Diploma thesis. Oulu, Finland: University of Oulu. 89 p.

Alajoki, T., Hendrickx, N., van Erps, J., Obi, S., Park, S.-H., Karppinen, M., Thienpont, H., van Daele, P., Karioja, P. 2007. Optical Coupling and Optoelectronics Integration Studied on Demonstrator for Optical Interconnects on Board. In: Proceedings of the 16th European Microelectronics and Packaging Conference and Exhibition (EMPC 2007). Oulu, Finland, 17–20 June 2007. Pp. 258–261.

Avalon Photonics. 2003. Nx10 Gb/s multi-mode VCSEL array. Preliminary data sheet. Zurich, Switzerland: Avalon Photonics Ltd. 2 p.

Bakir, M. S., Gaylord, T. K., Ogunsola, O. O., Glytsis, E. N., Meindl, J. D. 2004. Optical transmission of polymer pillars for chip I/O optical interconnections. IEEE Photonics Technology Letters, Vol. 16, No. 1, pp. 117–119.

Biard, J. R., Bonin, E. L., Matzen, W. T., Merryman, J. D. 1964. Optoelectronics as applied to functional electronic blocks. IEEE Proceedings, Vol. 52, No. 12, pp. 1529–1536.

Chang, C.-Y., Yang, S.-Y., Chu, M.-H. 2006. Rapid fabrication of ultraviolet-cured polymer microlens arrays by soft roller stamping process. Microelectronic Engineering, Vol. 84, No. 2, pp. 355–361.

Chen, R. T., Lin, L., Choi, C., Liu, Y. J., Bihari, B., Wu, L., Tang, S., Wickman, R., Picor, B., Hibbs-Brenner, M. K., Bristow, J., Liu, Y. S. 2000. Fully embedded board-level guided-wave optoelectronic interconnects. Proc. of the IEEE, Vol. 88, No. 6, pp. 780–793.

Cheng, J., Shieh, C.-L., Huang, X., Liu, G., Murty, M. V. R., Lin, C. C., Xu, D. X. 2005. Efficient CW lasing and high-speed modulation of 1.3 μm AlGaInAs VCSELs with good high temperature lasing performance. IEEE Photonics Technology Letters, Vol. 17, No. 1, pp. 7–9.

Cook, C., Cunningham, J. E., Hargrove, A., Ger, G. G., Goossen, K. W., Jan, W. Y., Kim, H. H., Krause, R., Manges, M., Momssey, M., Perinpanayagam, M., Persaud, A., Shevchuk, G., Sinyansky, V., Krishnamoorthy, A. V. 2003. A 36-channel parallel optical interconnect module based on Optoelectronics-on-VLSI technology. IEEE Journal of Selected Topics in Quantum Electronics, Vol. 9, No. 2, pp. 387–399.

Eitel, S., Fancey, S. J., Gauggel, H.-P., Gulden, K.-H., Bächtold, W., Taghizadeh, M. R. 2000. Highly Uniform Vertical-Cavity Surface-Emitting Lasers Integrated with Microlens Arrays. IEEE Photonics Technology Letters, Vol. 12, No. 5, pp. 459–461.

van Erps, J., Bogaert, L., Volckaerts, B., Thienpont, H. 2006. Prototyping micro-optical components with integrated out-of-plane coupling structures using deep lithography with protons. In: Thienpont, H., Taghizadeh, M. R., van Daele, P., Mohr, J. (Eds.) Proceedings of SPIE Vol. 6185, Micro-Optics, VCSELs, and Photonic Interconnects II: Fabrication, Packaging, and Integration. 14 p.

Feldman, M. R., Esener, S. C., Guest, C. C., Lee, S. H. 1988. Comparisons between optical and electrical interconnects based on power and speed considerations. Applied Optics, Vol. 27, No. 9, pp. 1742–1751.

Gan, J., Wu, L., Luan, H., Bihari, B., Chen, R. T. 1999. Two-Dimensional 45 Surface-Normal Microcoupler Array for Guided-Wave Optical Clock Distribution. IEEE Photonics Technology Letters, Vol. 11, No. 11, pp. 1452–1454.

Gilleo, M. A., Last, J. T. 1963. Optical coupling – New approach to microcircuit interconnections. Electronics, Vol. 36, No. 47, pp. 23–27.

Gimkiewicz, C., Moser, M., Obi, S., Urban, C., Pedersen, J. S., Thiele, H., Zschokke, C., Gale, M. T. 2004. Wafer-scale replication and testing of micro-optical components for VCSELs. Proc. of SPIE, Vol. 5453, pp. 13–26.

Glebov, A. L., Bhusari, B., Kohl, P., Bakir, M. S., Meindl, J. D., Lee, M. G. 2006. Flexible pillars for displacement compensation in optical chip assembly. IEEE Photonics Technology Letters, Vol. 18, No. 8, pp. 974–976.

Goodman, J. W., Leonberger, F. I., Kung, S.-Y., Athale, R. A. 1984. Optical interconnections for VLSI systems. Proceedings of IEEE, Vol. 72, pp. 850–866.

Griese, E. 1999. Reducing EMC Problems Through an Electrical/Optical Interconnection Technology. IEEE Transactions on Electromagnetic Compatibility, Vol. 41, No. 4, pp. 502–509.

Guo, Y. X., Ong, L. C., Luo, B., Chia, M. Y. W., Karppinen, C., Kautio, K., Mäkinen, J.-T., Ollila, J. 2005. An LTCC optical transceiver for radio-over-fibre. In: 35th European Microwave Conference 2005 – Conference Proceedings. Paris, France, 4–6 Oct. 2005. Pp. 121–123.

Guttman, J., Huber, H., Krumpholz, O. 1999. 19" polymer optical backplane. Proceedings of ECOC '99, 25th European Conference on Optical Communication, Vol. I. Pp. 354–355.

Hecht, E. 1987. Optics. 2nd edition. Addison-Wesley Publishing Company. 676 p. ISBN 0-201-11611-1.

Heikkinen, V., Alajoki, T., Juntunen, E., Karppinen, M., Kautio, K., Mäkinen, J.-T., Ollila, J., Tanskanen, A., Toivonen, J., Casey, R., Scott, S., Pintzka, W., Thériault, S., McKenzie, I. 2007. Fiber-Optic Transceiver Module for High-Speed Intrasatellite Networks. IEEE Journal of Lightwave Technology, Vol. 25, No. 5, pp. 1213–1223.

Hendrickx, N., van Erps, J., van Steenberge, G., Thienpont, H., van Daele, P. 2007. Laser Ablated Micromirrors for Printed Circuit Board Integrated Optical Interconnections. IEEE Photonics Technology Letters, Vol. 19, No. 11, p. 822.

Heyen, J., von Kerssenbrock, T., Chernyakov, A., Heide, P., Jacob, A. F. 2003. Novel LTCC/BGA modules for highly integrated millimeter-wave transceivers. IEEE Transactions on Microwave Theory and Techniques, Vol. 51, No. 12, pp. 2589–2596.

Hikita, M., Tomaru, S., Enbutsu, K., Ooba, N., Yoshimura, R., Usui, M., Yoshida, T., Imamura, S. 1999. Polymeric Optical Waveguide Films for Short-Distance Optical Interconnects. IEEE Journal of Selected Topics in Quantum Electronics, Vol. 5, No. 5, pp. 1237–1242.

Hurm, V., Bronner, W., Benz, W., Kohler, K., Kropp, J.-R., Losch, R., Ludwig, M., Mann, G., Mikulla, M., Rosennveig, J., Schlechtweg, M., Walther, M., Weimann, G. 2002. Large area MSM photodiode array for 0.85 pm wavelength 10 Gbit/s per channel parallel optical links. Electronics Letters, Vol. 38, No. 18, pp. 1051–1052.

IEC. 2001. Safety of laser products – Part 1: Equipment classification, requirements and user's guide. IEC 60825-1:1993+A1:1997+A2:2001. (Edition 1.2.) Geneva, Switzerland: IEC.

Immonen, M., Karppinen, M., Kivilahti, J. K. 2003. Fabrication and Characterization of Optical Polymer Waveguides Embedded on Printed Wiring Boards. In: Proceedings of IEEE Polymers and Adhesives in Microelectronics and Photonics. 21–3 October 2003. Pp. 91–95.

Immonen, M., Wu, J., Kivilahti, J. K. 2005a. Influence of Environmental Stresses on Board-Level Integrated Polymer Optics. In: Proceedings of 55th Electronic Components and Technology Conference (ECTC). Orlando, FL, May 2005. Pp. 1653–1658.

Immonen, M., Karppinen, M., Kivilahti, J. K. 2005b. Investigation of Environmental Reliability of Optical Polymer Waveguides Embedded on Printed Circuit Boards. In: Proceedings of IEEE Conference on Polymers and Adhesives in Microelectronics and Photonics. Wroclaw, Poland, 23–26 Oct. 2005. Pp. 145–151.

Immonen, M., Karppinen, M., Kivilahti, J. 2005c. Fabrication and characterization of polymer optical waveguides with integrated micromirrors for three-dimensional board-level optical interconnects. IEEE Transactions on Electronics Packaging Manufacturing, Vol. 28, No. 4, pp. 304–311.

Immonen, M., Karppinen, M., Kivilahti, J. K. 2007. Investigation of Environmental Reliability of Optical Polymer Waveguides Embedded on Printed Circuit Boards. Microelectronics Reliability, Vol. 47, pp. 363–371.

iNEMI (International Electronics Manufacturing Initiative) Inc. 2004. iNEMI Technology Roadmap 2004.

Ishii, Y., Koike, S., Arai, Y., Ando, Y. 2001. SMT-compatible optical-I/O packaging for chip-level optical interconnects. In: Proceedings of 51st Electronic Components and Technology Conf. (ECTC). Orlando, FL, 29 May 29 – 1 June 2001. Pp. 870–875.

Ishii, Y., Koike, S., Arai, Y., Ando, Y. 2003. SMT-Compatible Large-Tolerance “OptoBump” Interface for Interchip Optical Interconnections. IEEE Transactions on Advanced Packaging, Vol. 26, No. 2, 6 p.

Jelley, K. W., Valliath, G. T., Stafford, J. W. 1992. High-Speed Chip-to-Chip Optical Interconnection. IEEE Photonics Technology Letters, Vol. 4, pp. 1157–1159.

Karioja, P., Keränen, K., Karppinen, M., Kautio, K., Heikkinen, V., Lahti, M., Ollila, J., Mäkinen, J.-T., Kataja, K., Tuominen, J., Jaakola, T., Park, S.-H., Korhonen, P., Alajoki, T., Tanskanen, A., Lenkkeri, J., Heilala, J. 2006. LTCC toolbox for photonics integration. In: Proceedings of Ceramic Interconnect and Ceramic Microsystems Technologies (CICMT 2006). Denver, CO, USA, 24–27 April 2006.

Karppinen, M., Juuso, S., Mäkinen, J.-T., Rajaniemi, H., Karioja, P. 2000. Ray-Tracing Simulations of Free-Space Optical Channels for Impulse Response Studies of Indoor Data Links. In: Proceedings of SPIE, Vol. 3952. Pp. 274–85.

Karppinen, M., Kautio, K., Heikkinen, M., Häkkilä, J., Karioja, P., Jouhti, T., Tervonen, A., Oksanen, M. 2001a. Passively aligned fiber-optic transmitter integrated into LTCC module. In: Proceedings of 51st Electronic Components and Technology Conf. (ECTC). Orlando, FL, 29 May – 1 June 2001. Pp. 20–25.

Karppinen, M., Mäkinen, J.-T., Kemppainen, A., Borenius, M., Karioja, P. 2001b. Free-space optical backplanes based on beacon-like links or on a ring bus. In: Proceedings of SPIE, Vol. 4455. Pp. 88–99.

Karppinen, M., Kataja, K. J., Mäkinen, J.-T., Juuso, S., Rajaniemi, H., Pääkkönen, P., Turunen, J., Rantala, J., Karioja, P. 2002. Wireless infrared data links: Ray-trace simulations of diffuse channels and demonstration of diffractive element for multi-beam transmitters. Optical Engineering, Vol. 41, No. 4, pp. 899–910.

Karppinen, M., Mäkinen, J.-T., Kataja, K., Tanskanen, A., Alajoki, T., Karioja, P., Immonen, M., Kivilahti, J. 2004a. Optical interconnect on printed wiring board. In: Heyler, R. A., Chen, R. T. (Eds.) Proceedings of SPIE, Vol. 5358 – Photonics Packaging and Integration IV. Bellingham, WA: SPIE. Pp. 135–145.

Karppinen, M., Mäkinen, J.-T., Kataja, K., Tanskanen, A., Alajoki, T., Karioja, P., Immonen, M., Kivilahti, J. 2004b. Embedded optical interconnect on printed wiring board. In: Thienpont, H., Choquette, K. D., Taghizadeh, M. R. (Eds.) Proceedings of SPIE, Vol. 5453 – Micro-Optics, VCSELs, and Photonic Interconnect. Bellingham, WA: SPIE. Pp. 150–164.

Karppinen, M., Alajoki, T., Tanskanen, A., Kataja, K., Mäkinen, J.-T., Karioja, P., Immonen, M., Kivilahti, J. 2006a. Parallel optical interconnect between surface-mounted devices on FR4 printed wiring board using embedded waveguides and passive optical alignments. In: Thienpont, H., Taghizadeh, M. R., van Daele, P., Mohr, J. (Eds.) Proceedings of SPIE Vol. 6185, Micro-Optics, VCSELs, and Photonic Interconnects II: Fabrication, Packaging, and Integration. Pp. 190–200.

Karppinen, M., Alajoki, T., Tanskanen, A., Kataja, K., Mäkinen, J.-T., Kautio, K., Karioja, P., Immonen, M., Kivilahti, J. 2006b. Parallel optical interconnect between surface-mounted devices on FR4 printed wiring board using embedded waveguides and passive optical alignments. In: Proceedings of 56th Electronic Components and Technology Conf. (ECTC). San Diego, CA, USA, 30 May – 2 June 2006. Pp. 799–805.

Karppinen, M., Alajoki, T., Karioja, P., Hendrickx, N., van Steenberge, G., van Daele, P., van Erps, J., Debaes, C., Thienpont, H., Obi, S., Immonen, M., Kivilahti, J., Glebov, A. 2007. Integration of optical interconnects on circuit board. In: Proceedings of 13th MicroOptics Conference (MOC'07). Takamatsu, Kagawa, Japan, 28–31 Oct. 2007. Pp. 94–97.

Keiser, G. 2000. Optical Fiber Communications. Third edition. McGraw-Hill Companies. 602 p. ISBN 0-07-232101-6.

Keränen, K., Mäkinen, J.-T., Heilala, J., Väätäinen, O., Kautio, K., Ollila, J., Petäjä, J., Karppinen, M., Heikkinen, V., Karioja, P. 2004. Cost-effective packaging of laser modules using LTCC substrates. In: Heyler, R. A., Chen, R. T. (Eds.) Proceedings of SPIE, Vol. 5358 – Photonics Packaging and Integration IV. Bellingham, WA: SPIE. Pp. 111–121.

Keränen, K., Karppinen, M., Lenkkeri, J., Mäkinen, J.-T., Ollila, J., Karioja, P. 2005. LTCC technology for photonic and millimeter wave module integration. International Journal of Software Engineering and Knowledge Engineering, Vol. 15, No. 2, pp. 215–224.

Keusseyan, R. Sosnowski, J. Doyle, M. Amey, D. Horowitz, S. 2002. A new approach for Opto-Electronic/MEMS packaging. In: Proceedings of 52nd Electronic Components and Technology Conference (ECTC). San Diego, May 2002. Pp. 259–262.

Kim, J.-S., Kim, J.-J. 2004. Fabrication of multimode polymeric waveguides and micromirrors using deep X-ray lithography. IEEE Photonics Technology Letters, Vol. 16, No. 3, pp. 798–800.

Kim, G., Han, X., Chen, R. T. 2000. An 8-Gb/s Optical Backplane Bus Based on Microchannel Interconnects: Design, Fabrication, and Performance Measurements. Journal of Lightwave Technology, Vol. 18, No. 11, pp. 1477–1486.

Koyama, F. 2006. Recent Advances of VCSEL Photonics. Journal of Lightwave Technology, Vol. 24, No. 12, pp. 4502–4513.

Krabe, D., Ebeling, F., Arndt-Staunfenbiel, N., Lang, G., Scheel, W. 2000. New technology for electrical/optical systems on module and board level: The EOCB approach. In: Proc. of 50th Electronic Components and Technology Conf. (ECTC). Las Vegas, NV, 21–24 May 2000. Pp. 970–975.

Krishnamoorthy, A. V., Goossen, K. W. 1998. Optoelectronic-VLSI: Photonics Integrated with VLSI Circuits. IEEE Journal on Selected Topics in Quantum Electronics, Vol. 4, No. 6, pp. 899–912.

Kromer, C., Sialm, G., Berger, C., Morf, T., Schmatz, M.L., Ellinger, F., Erni, D., Bona, G.-L., Jackel, H. 2005. A 100-mW 4x10 Gb/s transceiver in 80-nm CMOS for high-density optical interconnects. IEEE Journal of Solid-State Circuits, Vol. 40, No. 12, pp. 2667–2679.

Kuchta, D. M., Kwark, Y. H., Schuster, C., Baks, C., Haymes, C., Schaub, J., Pepeljugoski, P., Shan, L., John, R., Kucharski, D., Rogers, D., Ritter, M., Jewell, J., Graham, L. A., Schrödinger, K., Schild, A., Rein, H.-M. 2004. 120-Gb/s VCSEL-based parallel-optical interconnect and custom 120-Gb/s testing station. IEEE Journal of Lightwave Technology, Vol. 22, No. 9, pp. 2200–2212.

Kuznia, C., Ahadian, J., Englekirk, M., Wong, M., Richaud, J., Pendleton, M., Pommer, D., Reedy, R. 2003. Ultra-thin silicon-on-sapphire component technology for short reach parallel optical interconnects. In: Proceedings of the IEEE 2003 Custom Integrated Circuits Conference (CICC). San Jose, CA, 21–24 Sept. 2003. Pp. 335–338.

Kühner, T., Schneider, M. 2007. Surface mounted coupling elements for PCB embedded optical interconnects. In: Proceedings of the 16th European Microelectronics and Packaging Conference and Exhibition (EMPC 2007). Oulu, Finland, 17–20 June 2007. Pp. 253–257.

Lehmacher, S., Neyer, A. 2000. Integration of polymer optical waveguides into printed circuit boards. Electronics Letters, Vol. 36, No. 12, pp. 1052–1053.

Lin, C.-K., Tandon, A., Djordjev, K., Corzine, S. W., Tan, M. R. T. 2007. High-speed 985 nm bottom-emitting VCSEL arrays for chip-to-chip parallel optical interconnects. IEEE Journal on Selected Topics in Quantum Electronics, Vol. 13, No. 5, pp. 1332–1339.

Liu, Y. 2002. Heterogeneous Integration of OE Arrays with Si Electronics and Microoptics. IEEE Transactions on Advanced Packaging, Vol. 25, No. 1, pp. 43–49.

Liu, Y. S., Wojnarowski, R. J., Hennessy, W. A., Bristow, J. P., Liu, Y., Peczalski, A., Rowlette, J., Plotts, A., Stack, J., Yardley, J., Eldada, L., Osgood, R. M., Scarmozzino, R., Lee, S. H., Ozgus, V. 1996. Polymer Optical Interconnect Technology (POINT) Optoelectronic Packaging and Interconnect for Board and Backplane Applications. Critical Reviews of Optical Science and Technology. Vol. CR62. SPIE Conference for Optoelectronic Interconnects and Packaging. Jan. 1996. Pp. 405–414.

Luniz, B., Guttmann, J., Huber, H.-P., Moisel, J., Rode, M. 2001. Experimental demonstration of 2.5 Gbit/s transmission with 1-m polymer optical backplane. Electronics Letters, Vol. 37, p. 1079.

McEwan, I., Suyal, N., Li, X., Tooley, F. 2002. A High Performance Optical Photo-Polymer for Planar Lightwave Circuits. In: Proceedings of 2002 IEEE/LEOS Workshop on Fibre and Optical Passive Components. Glasgow, UK, 5–6 June 2002. Pp. 133–139.

Microsemi. 2002. LX3044/45/46, 10.3 Gb/s Coplanar GaAs PIN Photo Diode. Production data sheet. Rev. 1.0, 2002-10-29. Garden Grove, CA, USA: Microsemi, Integrated Products Division. 5 p.

Miller, D. A. B. 1997. Physical reasons for optical interconnection. International Journal of Optoelectronics, Vol. 11, No. 3, pp. 155–168.

Moynihan, M., Sicard, B., Ho, T., Little, L., Pugliano, N., Shelnut, J., Zheng, H. B., Knudsen, P., Lundy, D., Chiarotto, N., Lustig, C., Allen C. 2005. Progress Towards Board-level Optical Interconnect Technology. In: Heyler, R. A., Chen, R. T. (Eds.) Proceedings of SPIE, Vol. 5731 – Photonics Packaging and Integration V. Bellingham, WA: SPIE. Pp. 50–62.

Palen, E. 2007. Low costs optical interconnects. In: Earman, A. M., Chen, R. T. (Eds.) Proceedings of SPIE, Vol. 6478 – Photonics Packaging Integration and interconnects VII. Bellingham, WA: SPIE.

Paraskevopoulos, A., Hensel, H. J., Molzow, W. D., Klein, H., Grote, N., Ledentsov, N. N., Shchukin, V. A., Moller, C., Kovsh, A. R., Livshits, D. A., Krestnikov, I. L., Mikhrin, S. S., Matthijsse, P., Kuyt, G. 2006. Ultra-High-Bandwidth (>35 GHz) Electrooptically-Modulated VCSEL. In: Proceedings of the Optical Fiber Communication Conference, 2006 and the 2006 National Fiber Optic Engineers Conference. 5–10 March 2006. 13 p.

Park, S. H., Park, S. M., Park, H.-H., Park, C. S. 2005. Low-Crosstalk 10-Gb/s Flip-Chip Array Module for Parallel Optical Interconnects. IEEE Photonics Technology Letters, Vol. 17, No. 7, pp. 1516–1518.

Plant, D. V., Kirk, A. G. 2000. Optical Interconnects at the Chip and Board Level: Challenges and Solutions. Proceedings of IEEE, Vol. 88, No. 6, pp. 806–818.

Plant, D. V., Venditti, M. B., Laprise, E., Faucher, J., Razavi, K., Châteauneuf, M., Kirk, A. G., Ahearn, J. S. 2001. 256-Channel Bidirectional Optical Interconnect Using VCSELs and Photodiodes on CMOS. Journal of Lightwave Technology, Vol. 19, No. 8, pp. 1093–1103.

Primarion. 2002a. PX6414, 4x10 Gb/s VCSEL Driver, Advanced information data sheet. Revision 0.91, 9/5/2002. Tempe, AZ, USA: Primarion Inc. 14 p.

Primarion. 2002b. PX6424, 4x10 Gb/s Optical Receiver IC, Advanced information data sheet. Revision 0.9, 9/11/02. Tempe, AZ, USA: Primarion Inc. 13 p.

Robertsson, M. 2004. Mirrors for Polymer Waveguides. International Patent. WO 04/015463, 2004-2-19.

Schares, L., Kash, J. A., Doany, F. E., Schow, C. L., Schuster, C., Kuchta, D. M., Pepeljugoski, P. K., Trewhella, J. M., Baks, C. W., John, R. A., Shan, L., Kwark, Y. H., Budd, R. A., Chiniwalla, P., Libsch, F. R., Rosner, J., Tsang, C. K., Patel, C. S., Schaub, J. D., Dangel, R., Horst, F., Offrein, B. J., Kucharski, D., Guckenberger, D., Hegde, S., Nyikal, H., Lin, C.-K., Tandon, A., Trott, G. R., Nystrom, M., Bour, D. P., Tan, M. R. T., Dolfi, D. W. 2006. Terabus: terabit/ second-class card-level optical interconnect technologies. IEEE Journal of Selected Topics in Quantum Electronics, Vol. 12, No. 5, pp. 1032–1044.

Schild, A., Rein, H.-M., Müllrich, J., Altenhain, L., Blank, J., Schrödinger, K. 2003. High-gain SiGe transimpedance amplifier array for a 12x10 Gb/s parallel optical-fiber link. IEEE J. Solid-State Circuits, Vol. 38, No. 1, pp. 4–12.

Schneider, M., Kühner, T. 2006. Optical interconnects on printed circuit boards using embedded optical fibers. In: Thienpont, H., Taghizadeh, M. R., van Daele, P., Mohr, J. (Eds.) Proceedings of SPIE Vol. 6185, Micro-Optics, VCSELs, and Photonic Interconnects II: Fabrication, Packaging, and Integration.

Schow, C. L., Schares, L., John, R. A., Fischer, L. S., Guckenberger, D. 2006. 25 Gbit/s transimpedance amplifier in 0.13 μm CMOS. Electronics Letters, Vol. 42, No. 21, pp. 1240–1241.

Schröder, H., Bauer, J., Ebling, F., Franke, M., Beier, A., Demmer, P., Süllau, W., Kostelnik, J., Mödinger, R., Pfeiffer, K., Ostrzinskig, U., Griese, E. 2006. Waveguide and packaging technology for optical backplanes and hybrid electrical-optical circuit boards. In: Eldada, L. A., Lee, E.-H. (Eds.) Proceedings of SPIE, Vol. 6124. Optoelectronic Integrated Circuits VIII.

Schubert, E. F., Hunt, N. E. J., Malik, R. J., Micovic, M., Miller, D. L. 1996. Temperature and Modulation Characteristics of Resonant-Cavity Light-Emitting-Diodes. IEEE Journal of Lightwave Technology, Vol. 14, No. 7, pp. 1721–1729.

van Steenberge, G., Geerinck, P., van Put, S., van Koetsem, J., Ottevaere, H., Morlion, D., Thienpont, H., van Daele, P. 2004. MT-compatible laser-ablated interconnections for optical printed circuit boards. IEEE Journal of Lightwave Technology, Vol. 22, No. 9, pp. 2083–2090.

Suzuki, N., Hatakeyama, H., Fukatsu, K., Anan, T., Yashiki, K., Tsuji, M. 2006. 25-Gbps operation of 1.1-um-range InGaAs VCSELs for high-speed optical interconnections. In: Proceedings of the Optical Fiber Communication Conference and the 2006 National Fiber Optic Engineers Conference. Anaheim, USA, 5–10 March 2006. 3 p.

Svensson, C. 2002. Electrical Interconnects Revitalized. IEEE Transactions on Very Large Scale Integration (VLSI) Systems, Vol. 10, No. 6, pp. 777–788.

Thienpont, H., Baukens, V., Ottevaere, H., Volckaerts, B., Tuteleers, P., Vynck, P., Vervaeke, M., Debaes, C., Verschaffelt, G., Hermanne, A., Veretennicoff, I. 2001. Free-space monolithic microoptical modules: A low-cost route for photonic interconnects to Silicon. In: Proceedings of SPIE, Vol. 4455, pp. 231–242.

Tooley, F. A. P. 1996. Challenges in Optically Interconnecting Electronics. IEEE J. Sel. Top. Quantum Electron, Vol. 2, No. 1, pp. 3–13.

Tummala, R. R., Rymaszevski, E. J. 1989. Microelectronics Packaging Handbook. New York: Van Nostrand Reinhold. 1194 p.

Uhlig, S., Robertsson, M. 2006. Limitations to and solutions for optical loss in optical backplanes. Journal of Lightwave Technology, Vol. 24, No. 4, pp. 1710–1724.

Vervaeke, M., Lahti, M., Karppinen, M., Debaes, C., Volckaerts, B., Karioja, P., Thienpont, H. 2006. Packaging a free-space intra-chip optical interconnect module: Monte Carlo tolerance study and assembly results. In: Thienpont, H., Taghizadeh, M. R., van Daele, P., Mohr, J. (Eds.) Proceedings of SPIE, Vol. 6185, Micro-Optics, VCSELs, and Photonic Interconnects II: Fabrication, Packaging, and Integration. Pp. 201–213.

Wittmann, B., Johnck, M., Neyer, A., Mederer, F., King, R., Michalzik, R. 1999. POF-based interconnects for intracomputer applications. IEEE Journal of Selected Topics in Quantum Electronics, Vol. 5, No. 5, pp. 1243–1248.

Zaleta, D., Patra, S., Ozguz, V., Ma, J., Lee, S. H. 1996. Tolerancing of board-level-free-space optical interconnects. Applied Optics, Vol. 35, No. 8, pp. 1317–1327.

Zhao, X., Choa, F. S. 2002. Demonstration of 10-Gb/s Transmissions over a 1.5-km-Long Multimode Fiber Using Equalization Techniques. IEEE Photonics Technology Letters, Vol. 14, No. 8, pp. 1187–1189.

Zhou, M. 2001. Low-loss polymeric materials for passive waveguide components in fiber optical telecommunication. APOC 2001. In: Proceedings of SPIE, Vol. 4580. Pp. 83–93.

Series title, number and report code of publication

VTT Publications 698
VTT-PUBS-698

Author(s)
Karppinen, Mikko

Title

High bit-rate optical interconnects on printed wiring board
Micro-optics and hybrid integration

Abstract

Optical interconnects are foreseen as a potential solution to improve the performance of data transmission on printed wiring boards (PWB). Optical interconnects carry data signals as modulation of optical intensity, for instance through an optical waveguide, thus replacing traditional electrical interconnects.

The aim of the research work was to study and develop board-level optical interconnection technologies that would be suitable for volume manufacturing with typical electronics production processes, such as surface-mount assembly and board manufacturing. More precisely, the work focuses on the hybrid integration of multi-channel optoelectronics transmitters and receivers, which are equipped with micro-optical structures enabling coupling to board-embedded optical waveguides. The presented integration schemes are based on the use of low-temperature co-fired ceramic (LTCC) circuit boards with high-precision alignment structures.

Two experimental set-ups were designed and implemented to study the feasibility of the proposed integration schemes. The first set-up enabled evaluation of three different kinds of optical coupling schemes, which are based on microlenses, micro-ball lenses and butt-coupling respectively. The other demonstrator is a parallel optical interconnect integrated on a standard PWB. The optical coupling is based on microlens arrays and a micro-mirror, which, together with four polymer multimode waveguides on the PWB, form the interconnections between the surface-mounted 4-channel transmitter and receiver components.

The optical performance of the demonstrated structures is studied by modelling and characterisation. With the proposed improvements, the presented technologies are suitable for implementation of high bit-rate interconnections between ceramic-packaged integrated circuits or multi-chip modules on PWB.

ISBN
978-951-38-7127-7 (soft back ed.)
978-951-38-7128-4 (URL: http://www.vtt.fi/publications/index.jsp)

Series title and ISSN	Project number
VTT Publications 1235-0621 (soft back ed.) 1455-0849 (URL: http://www.vtt.fi/publications/index.jsp)	

Date	Language	Pages
October 2008	English	162 p.

Name of project	Commissioned by

Keywords	Publisher
data transmission, optical interconnects, printed wiring boards, micro-optics, multi-channel optoelectronics, optical transmitters, optical receivers, optical waveguides, microlens arrays, micro-mirrors, LTCC, hybrid integration	VTT Technical Research Centre of Finland P.O. Box 1000, FI-02044 VTT, Finland Phone internat. +358 20 722 4520 Fax +358 20 722 4374

Optical interconnects are foreseen as a potential solution to improve the performance of data transmission on printed wiring boards (PWB). Optical interconnects carry data signals as modulation of optical intensity, for instance through an optical waveguide, thus replacing traditional electrical interconnects.

The aim of the research work was to study and develop board-level optical interconnection technologies that would be suitable for volume manufacturing with typical electronics production processes, such as surface-mount assembly and board manufacturing. More precisely, the work focuses on the hybrid integration of multi-channel optoelectronics transmitters and receivers, which are equipped with micro-optical structures enabling coupling to board-embedded optical waveguides. The presented integration schemes are based on the use of low-temperature co-fired ceramic (LTCC) circuit boards with high-precision alignment structures.

Two experimental set-ups were designed and implemented to study the feasibility of the proposed integration schemes. The first set-up enabled evaluation of three different kinds of optical coupling schemes, which are based on microlenses, micro-ball lenses and butt-coupling respectively. The other demonstrator is a parallel optical interconnect integrated on a standard PWB. The optical coupling is based on microlens arrays and a micro-mirror, which, together with four polymer multimode waveguides on the PWB, form the interconnections between the surface-mounted 4-channel transmitter and receiver components.

The optical performance of the demonstrated structures is studied by modelling and characterisation. With the proposed improvements, the presented technologies are suitable for implementation of high bit-rate interconnections between ceramic-packaged integrated circuits or multi-chip modules on PWB.

Julkaisu on saatavana	Publikationen distribueras av	This publication is available from
VTT PL 1000 02044 VTT Puh. 020 722 4520 http://www.vtt.fi	VTT PB 1000 02044 VTT Tel. 020 722 4520 http://www.vtt.fi	VTT P.O. Box 1000 FI-02044 VTT, Finland Phone internat. + 358 20 722 4520 http://www.vtt.fi

ISBN 978-951-38-7127-7 (soft back ed.) ISBN 978-951-38-7128-4 (URL: http://www.vtt.fi/publications/index.jsp)
ISSN 1235-0621 (soft back ed.) ISSN 1455-0849 (URL: http://www.vtt.fi/publications/index.jsp)